BIOMASS GASIFICATION IN A NOVEL 50 kWth INDIRECTLY HEATED BUBBLING FLUIDIZED BED STEAM REFORMER

KINETIC MODEL OPTIMIZATION AND PRELIMINARY EVALUATION OF PRODUCT GAS RECYCLE & PROCESS CONDITIONS FOR METHANOL PRODUCTION

MUKTA PRIYADARSHINI TRIPATHY

TUDelft

BIOMASS GASIFICATION IN A NOVEL 50 kW$_{th}$ INDIRECTLY HEATED BUBBLING FLUIDIZED BED STEAM REFORMER

Kinetic Model Optimization and Preliminary Evaluation of Product Gas Recycle & Process Conditions for Methanol Production

by

Mukta Priyadarshini Tripathy

in partial fulfillment of the requirements for the degree of

Master of Science

in Sustainable Energy Technology

at the Delft University of Technology

to be defended publicly on Monday May 31, 2021 at 4:00 PM

Student number: 4825209

Project duration: September 1, 2020 - May 31, 2021

Thesis Committee: Prof. dr. ir. W. de Jong,   TU Delft, Supervisor

                 Prof. dr. D.J.E.M. Roekaerts,   TU Delft

                 Dr. M. Ramdin,   TU Delft

                 Eng. M. del Grosso,   TU Delft, Supervisor

This thesis is confidential and cannot be made public till May 31, 2023.

An electronic version of this thesis is available at: http://repository.tudelft.nl/.

*TU*Delft

ACKNOWLEDGEMENT

ABSTRACT

Meeting the ever-increasing energy demands in our planet where conventional sources of energy are finite and fast depleting, controlling adverse phenomena like climate change, soil erosion, greenhouse gas emission, ozone layer thinning and pollution will remain profound challenges until widespread adoption of sustainable sources of energy is achieved. The shift to a sustainable energy system cannot be complete without the contribution of biomass energy. Within the ecosystem of biomass energy, gasification is a thermochemical conversion process undertaken to obtain a high-quality product gas by increasing the low energy density of solid biomass. The product gas can be used in power applications or be converted to liquid fuels for transportation.

Gasification is carried out at high temperatures (700-1500°C) by using a gaseous agent under sub stoichiometric conditions [1]. The main non-condensable permanent gases obtained from gasification are CO, H_2, CO_2 and CH_4 [1]. Use of allothermal gasifiers, whose working is based on the separation of combustion and gasification chambers within the gasifier, with heat supply for carrying out endothermic reactions, established via heat carrier or heat exchanger, have shown many advantages compared to the conventional gasifiers [2]. The mix-up of product gas and flue gas is avoided in this type of gasification. Secondly, while using air for biomass combustion, the nitrogen present in air reduces the quality of the end product by not participating in gasification, thus resulting in a diluted product gas. A high-quality product gas can be obtained from allothermal gasifiers without the need for establishing an expensive air separation unit, as required in case of conventional gasifiers [2].

The 50 kW_{th} Indirectly Heated Bubbling Fluidized Bed Steam Reformer (IHBFBSR) at Delft University of Technology (TU Delft) represents a new concept of allothermal gasification technology where heat required for the endothermic gasification reactions is provided by two radiant tube burners placed vertically inside the reactor, one at the top and one at the bottom.

The aim of this research is to optimize and validate the kinetic model developed for the IHBFBSR by a former student, Maarten Kwakkenbos in Aspen Plus®. The optimization is carried out with the help of the several steps, described in the report. The optimized model is then validated by using the results of the gasification tests performed under various operational conditions by PhD candidates Mara del Grosso and Christos Tsekos. The optimized model predicts the gas composition obtained from the IHBFBSR quite well. In addition to the yield of permanent gases, N_2, H_2O and tars concentration in the product gas, along with various gas ratios (CO/H_2, CH_4/H_2, CO/CO_2) from the model are compared with the experimental values and found to be in reasonable agreement. Moreover, key performance indicators such as carbon conversion (CC), cold gas efficiency (CGE) and overall efficiency (OE) are also evaluated from both model and experiments and compared. The error ranges for most of the parameters lie within the reported deviations observed in various gasifier models in literature. After the validation of the model, the possibility of recycling a fraction of the product gas to feed the burners in order to make the set up more sustainable is evaluated. Sensitivity analyses is performed by varying steam to biomass ratios (SB*), primary and secondary air flowrate to evaluate the best process conditions under which product gas obtained from the gasifier, after

subsequent cleaning, can be used for methanol production based on the H_2/CO ratio. The results indicate that a higher SB* and a higher secondary air flowrate can result in a H_2/CO ratio closer to the desired value required for optimum methanol production. From the heat analysis performed for the model, a possibility of increasing the overall efficiency of the process by adding a bypass line in the gasifier setup is suggested to be explored. The master thesis concludes by answering the research questions and recommendations to improve the detailing and accuracy of the model.

LIST OF FIGURES

LIST OF TABLES

ABBREVIATIONS

BP - British Petroleum

GDP - Gross Domestic Product

PV - Photovoltaic

GHG - Greenhouse Gas

IPCC - Intergovernmental Panel on Climate Change

IRENA - International Renewable Energy Agency

IEA - International Energy Agency

TPES - Total Primary Energy Supply

CHP - Combined Heat and Power

FAME - Fatty Acid Methyl Ester

HVO - Hydrogenated Vegetable Oil

CCS - Carbon Capture and Storage

TFC - Total Final Consumption

EV - Electric Vehicle

PBL - Netherlands Environmental Assessment Agency

CE Delft - Energy consultant in Delft

EU - European Union

DME - Dimethyl Ether

SNG - Synthetic Natural Gas

HHV - Higher Heating Value

LHV - Lower Heating Value

DFB - Dual Fluidized Bed

ECN - Energy research Centre of the Netherlands

TNO - Netherlands Organisation for Applied Scientific Research

FERCO - Future Energy Resources Corporation

FICFB - Fast Internally Circulating Fluidized Bed

TU Delft - The Delft University of Technology

P&E - Process and Energy Department of the Delft University of Technology

TU Munich - The Technical University of Munich

TU Wien - The Vienna University of Technology

REPOTEC - Renewable Power Technologies

CSTR - Continuous Stirred Tank Reactor

PFR - Plug Flow Reactor

IHBFBSR - Indirectly Heated Bubbling Fluidized Bed Steam Reformer

CC - Carbon Conversion

CGE - Cold Gas Efficiency

OE - Overall Efficiency

VM - Volatile Matter

FC - Fixed Carbon

ar - As Received basis

db - Dry Basis

daf - Dry Ash free

BFB - Bubbling Fluidized Bed

CFB - Circulating Fluidized Bed

EF - Entrained Flow

ORC - Organic Rankine cycle

odt - oven-dried tonnes

WGS - Water gas Shift reaction

MSR - Methane Steam Reforming

BCL - Battelle's Columbus Laboratory, USA

NREL - National Renewable Energy Laboratory, USA

BtL - Biomass to Liquids

SOFC - Solid Oxide Fuel Cell

MSW - Municipal Solid Waste

HPR - Heat Pipe Reformer

HVC - Waste treatment Company in Alkmaar, Netherlands

OLGA - Oil-Based Gas Washer

VLE - Vapour Liquid equilibrium

EOS - Equation of State

IC - Internal Combustion

RK - Redlich Kwong equation of state

TGA - Thermogravimetric Analysis

GC-FID - Gas Chromatography with Flame Ionization Detector

µ-GC - Micro Gas Chromatography

NDIR - Non-Dispersive Infrared Spectroscopy

GB - Premium Green Biomass

RB - Excellent Red Biomass

PSD - Particle Size Distribution

LHHW - Langmuir Hinshelwood

NCPSD - Non- Conventional Solid with Particle Size Distribution

µ-GC - Micro Gas Chromatography

CIPSD - Conventional Inert Solid with Particle Size Distribution

IC - Internal Combustion

PW - Pyrolytic Water

GE - Global Error

LIST OF SYMBOLS AND THEIR UNITS

SYMBOL	PARAMETER	UNIT
H_i	Heights at Different Points of the IHBFBSR w.r.t starting point of bedzone	[m]
CC	Carbon Conversion	[--]
CGE	Cold Gas Efficiency	[--]
OE	Overall Efficiency	[--]
$m_{c, residue}$	Mass flowrate of carbon in residue	[kg/hr]
$m_{c, feed}$	Mass flowrate of carbon in feed	[kg/hr]
m_i	Mass Flowrate of species i	[kg/hr]
LHV_i	Lower Heating Value of species i	[MJ/kg]
LHV_{fuel}	Lower Heating Value of biomass feed	[MJ/kg]
P_{in}	Power supplied by burners and preheaters in Eq 1.3	[MJ/hr]
Y_i^j	Mass fraction of "i" on a "j" basis	[wt%]
$m_{biomass}^i$	Mass of biomass on an "i" basis	[kg]
Δm	Difference in weight or mass	[--]
λ	Equivalence Ratio	[--]
SB	Steam to Biomass Ratio	[--]
SB*	Steam to Biomass Ratio, with fuel moisture	[--]
TE01-TE07	Thermocouples	[gives temperature readings - °C]
u_g	Interstitial Gas velocity	[m/s]
u_{br}	Bubble velocity	[m/s]
ρ_{real}	Real density of bed material	[kg/m^3]
ρ_{bulk}	Bulk density of bed material	[kg/m^3]
Dp	Mean diameter of bed material particle size	[m]
L_{fixed}	Length of bedzone in fixed regime	[m]
L_{fluid}	Length of bedzone under fluidization	[m]

ϵ_{Fixed}	**Voidage of bed material in fixed regime**	**[--]**
D_{in}	Inner diameter of reactor	[m]
D_{burn}	Diameter of burner in reactor	[m]
$D_{reactor}$	Mean hydraulic diameter of reactor	[m]
V_{fluid}	Volume of the bedzone at fluidization	[l]
V_{CSTR}	Volume of first CSTR (bedzone)	[l]
M_{bed}	Mass of bed material	[kg]
V_{bed}	Volume occupied by bed material	[l]
$A_{Reactor}$	Cross-sectional area of reactor	[m^2]
L_{CSTR1}	Length of first CSTR (bedzone)	[m]
L_{CSTR2}	Length of the second CSTR (gas-bed)	[m]
D	Diameter of cyclone	[mm]
H_t	Cyclone Total Height	[mm]
h	Cyclone Height	[mm]
H_t - h	Length of cone section	[mm]
S	Vortex finder length	[mm]
D_x	Diameter of overflow	[mm]
B_c	Diameter of underflow	[mm]
a	Height of cyclone inlet	[mm]
b	Width of cyclone inlet	[mm]
M_{STEAM}	Steam Mass Flowrate	[kg/hr]
T_{PYR}	Pyrolysis Reactor Temperature	[°C]
T_{CSTR1}	Bedzone Temperature	[°C]
T_{CSTR2}	Gas-Bed Temperature	[°C]
T_{PFR}	Freeboard Temperature	[°C]
M_{AIR1}	Primary Air Mass Flowrate	[kg/hr]
M_{AIR2}	Secondary Air Mass Flowrate	[kg/hr]
M_{N2}	Mass Flowrate of Nitrogen Purge Stream	[kg/hr]

λ_{total}	Total Equivalence Ratio (primary + secondary air)	[--]
P_{GAS}	Outlet Pressure of Product Gas	[mbar]
P_{burner}	Power supplied by the burners in Eq 5.2	[kW]
T	Final Temperature of Reactants	[K]
T_0	Initial Temperature of Reactants	[K]
F_{CH_4}	Molar Flowrate of methane	[kmol/s]
$C_{P,i}$	Calorific value of species i	[kJ/kmol K]
ε_{O2}	Excess percentage of oxygen	[%]
Ea,i	Activation energy	[kJ/kmol]
k_i	Reaction Constant	[depends on order of reaction]
r_i	Reaction Rate	For nth order: $[(m^3/kmol)^{n-1}(m/s)]$
ρ_{char}	Density of char	kg/m^3
R_g	Universal Gas Constant (8.314)	J/ (mol K)

MAIN CHEMICAL SPECIES USED IN THE REPORT

Chemical Species Formula	Name of species
CO	Carbon Monoxide
CO_2	Carbon Dioxide
H_2	Hydrogen
CH_4	Methane
N_2	Nitrogen
H_2O	Steam/Water vapour
NH_3	Ammonia
H_2S	Hydrogen Sulphide
HCl	Hydrogen Chloride
C	Carbon/Char
C_6H_5OH	Phenol
C_6H_6	Benzene
O_2	Oxygen
S	Sulphur
$C_{10}H_8$	Naphthalene
C_2H_4	Ethylene (Ethene)

CONTENTS

CONTENTS

1. INTRODUCTION

1.1 Need for Energy Transition and Biomass as a Sustainable Energy Source

With a current global population of 7.8 billion and an annual growth rate of approximately 1.1%, a daunting challenge for mankind is to ensure proper food, housing, education, energy needs for ourselves in the coming years and to provide a clean environment for our future generations [3]. According to the scenario presented by British Petroleum (BP) in Figure 1, the global energy demand will increase as the population increases, and the rapid expansion of economy and higher standards of living will cause a faster rate of growth in energy demand as compared to the rise in population. As the Earth's resources and conventional sources of energy are limited, these factors need to be tackled effectively to ensure a sustainable future for the mankind.
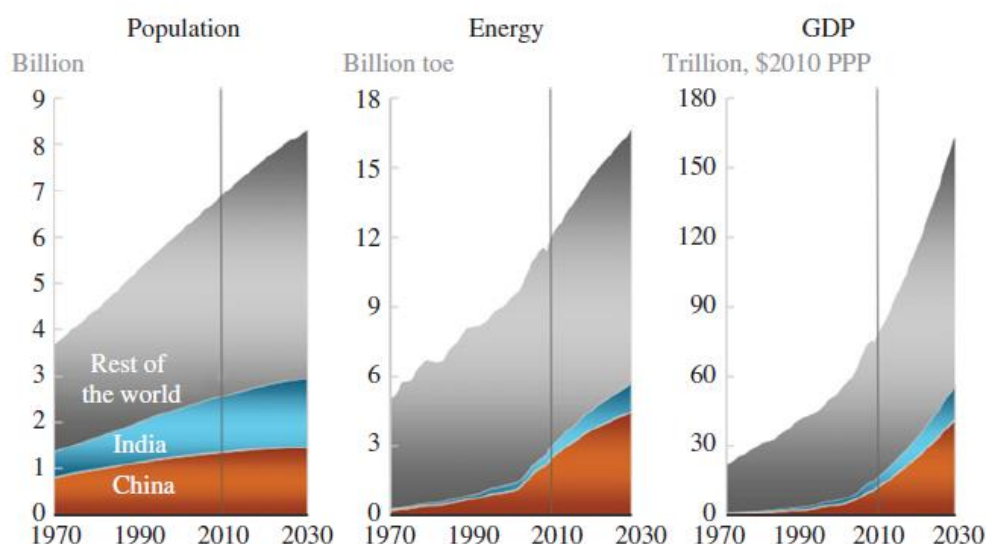
Figure 1: Prospected global growth rates in population, energy demand, and Gross Domestic Product (GDP), adapted from BP [4]

In the past decades, conventional energy sources such as coal and oil have fulfilled the rising energy demand, but increasing CO_2 emissions from fossil fuels and awareness on climate change in recent years gave rise to the use of renewable sources such as solar photovoltaic (PV), wind, hydropower, geothermal and bioenergy. The aim of the Paris Agreement, signed by 195 countries as of 2021, is to put a constraint to the rise of global average temperature below 2°C, with the effort to stay within 1.5°C [5]. The potential adverse impacts of climate change can be tackled by lowering greenhouse gas (GHG) emissions and progressing towards achieving targets such as CO_2 emission targets, as specified by the Intergovernmental Panel on Climate Change (IPCC). Social and economic challenges also need to be handled while working towards these goals. According to a report by the International Renewable Energy Agency (IRENA) in 2017, to limit the rise of global temperature below 2°C in line with the Paris Agreement, the share of renewable energy has to be raised to 65% of the global primary energy supply by 2050 from the share of 13.8 % as of 2018 [6] [7]. This seems challenging to

attain as can be seen by the increase of 1°C of the average global temperature that has already been observed since the pre-industrial period [6]. According to [8], based on historical data, Millar & Friedlingstein analysed and provided a remaining carbon budget estimate of 920 $GtCO_2$ to have a 50% probability of staying below the limit of 1.5°C temperature increase while Kriegler et al. suggested a remaining estimate of $800 GtCO_2$. However, in reality the actual figures may be much lower. Since CO_2 levels have been steadily rising, especially over the past decade, the time available for shifting to sustainable energy use practices resulting in net-zero emission level reduces by two years for every year of delay, as per their study. At the current emission rate of about 30 Gt of CO_2 every year, there remains a time of approximately 25 years, to exceed the estimated remaining carbon budget.
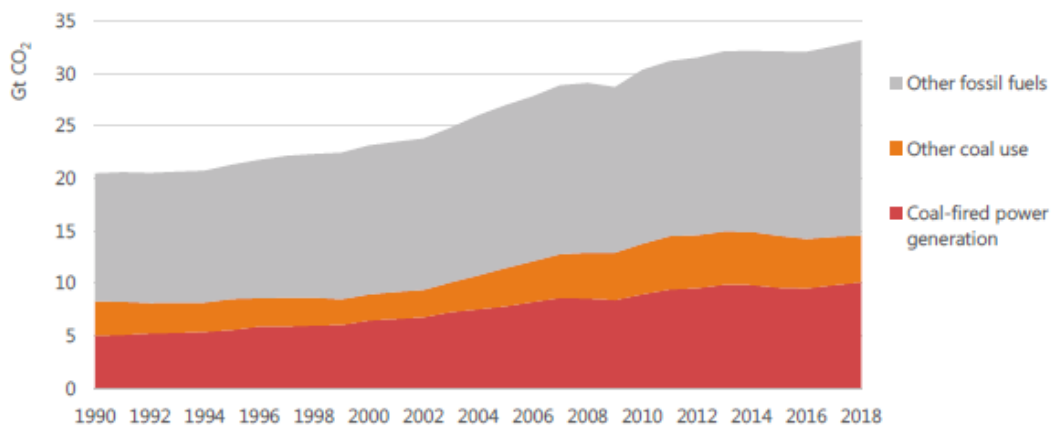
Figure 2: Carbon- dioxide emissions by source, 1990-2018 [9]

As can be seen in Figure 2, year 2018 witnessed a 1.7% increase in CO_2 emissions, with a historic record of 33.1 Gt of CO_2. The International Energy Agency (IEA) analysed and concluded that coal usage was mainly responsible for the rising temperatures and CO_2 emissions, accounting for 30% of the increase in global surface temperatures with respect to pre-industrial levels [9]. Economic development led to an increased energy consumption, accompanied by an increased demand for heating and cooling requirements across different regions in the world due to global warming and unpredictable weather patterns. The major sectors contributing to CO_2 emissions are electricity generation and industrial activities, followed by transportation and residential sectors [6]. Currently fossil fuels play a major role in electricity generation [9]; however, to achieve visible progress in terms of climate change, effort has to be made to increase the share of renewables in electricity generation and other sectors. As of 2018, the share of renewables in electricity generation, heating and transport sectors were 25%, 10% and 3.5%, respectively [9]. For meeting the requirements of the Paris Agreement, it must be targeted that these shares reach 66%, 25% and 19% [9] by 2040 respectively.
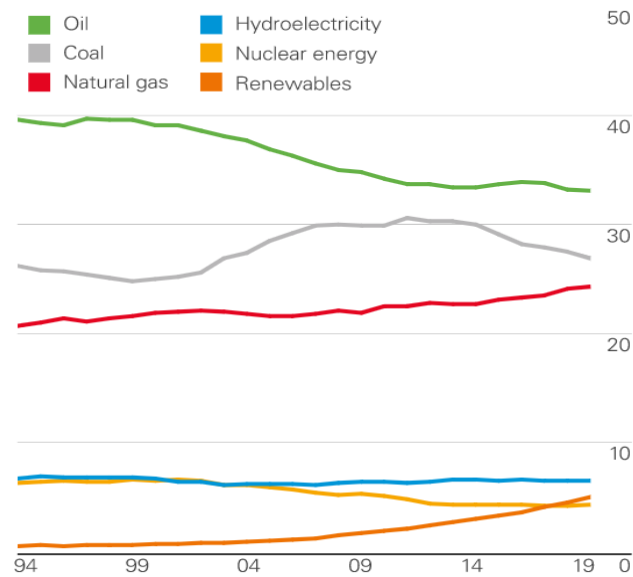
Figure 3 : Shares of global primary energy consumption by fuel from 1994-2019 (percentage) as reported by BP in their yearly statistical review of World Energy, 2020

[10]

Figure 3 shows the global primary energy consumption and the share of each source contributing to the energy mix from 1994-2019. Although the percentage of oil usage seems to be on decreasing trend during this period and the same can be said for coal in the period from 2014-2019, they still together contributed to 60% of the energy consumption in 2019. The share of renewables is rising since 2014 and held 5% share in global energy consumption in 2019. In addition to widespread adaptation of sustainable energy sources, efficiency improvement of energy conversion systems and use of concepts such as carbon capture and storage (CCS) is the need of the hour. Nuclear energy is also helpful in combatting CO_2 emissions; however, usage of nuclear energy poses potential hazards of generating radioactive wastes and dangerous accidents [4].

Biomass is organic matter, derived from living organisms such as plants and animals [11]. The energy from plants and animals can be converted into usable energy through direct (by burning for residential purposes such as cooking or heating) and indirect means (converting to liquid and gaseous fuels which can be used for energy generation or as transportation fuels). Use of biomass as a sustainable energy source presents many advantages such as [4]:

- Ease of availability in the form of stored solar energy in plants.
- Being a more constant energy supply source as compared to the fluctuating nature of solar and wind energy
- Ability to be used along with fossil fuels for energy generation because of its (derivatives') similar composition and physical properties. This will ease the process of energy transition as biomass can be used more effectively compared to other renewable energy sources in present energy conversion systems.
- Harnessing biomass energy is not dependent on use of scarce materials such as gallium/indium and niobium/neodymium for manufacturing of solar cells and wind turbines, respectively.

However, biomass does suffer from the disadvantage of having a low energy density compared to fossil fuels. This is resolved by making use of different conversion routes such as gasification to convert biomass into a usable high energy density gas [4]. A variety of biomass sources comes from forestry products and waste materials such as agricultural residues or industrial or municipal wastes. In addition, microalgae, seaweeds and energy crops too qualify to be used as biomass sources [4].
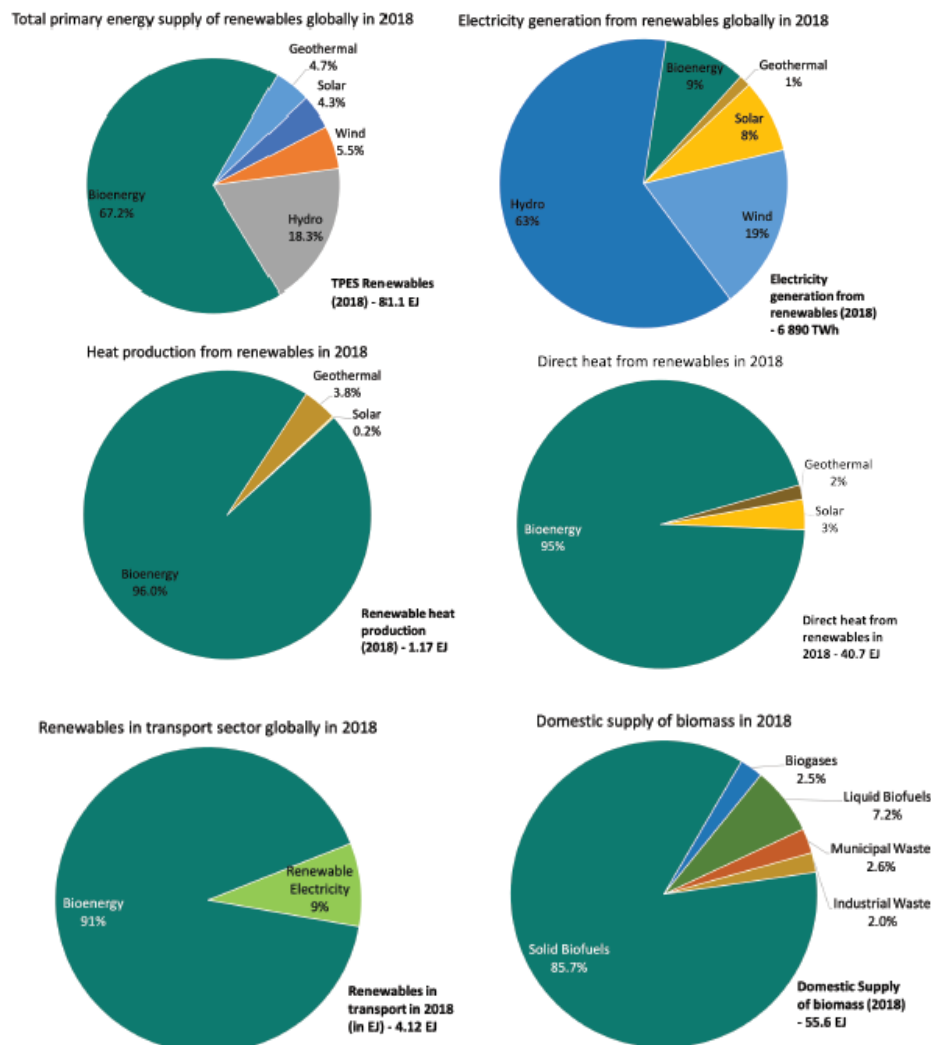
Figure 4: Bioenergy share in the renewable energy contribution to the global total primary energy supply, contribution of bioenergy to various sectors, and sources of bioenergy in energy mix of renewables 2018 [7]

As can be seen in Figure 4, bioenergy had the largest share among renewables in global primary energy supply in 2018 with a contribution of 67.2%. It had the third-largest share in electricity generation and largest share in renewable heat source (both in direct heat applications such as burning biomass for residential, commercial or agricultural purposes and derived heat where heat produced in combined heat and power (CHP) and heat only plants are consumed by end users). Bioenergy also played a dominant role in transportation sector. About 3.58 million people work in bioenergy related fields globally, thus making this field as the second-largest employer among renewable energy sectors [7]. 85.7% of the global domestic supply of biomass in 2018 came from solid biomass sources such as wood pellets, wood chips and sawdust

primarily from forestry residues [7]. Liquid biofuels constituted of bioethanol, FAME biodiesel (Fatty-Acid Methyl Ester), cellulosic ethanol and HVO (Hydrogenated Vegetable Oil) [7]. The main components of biogas are methane and carbon-dioxide [7]. Solid biomass along with industrial and municipal wastes contributed majorly to electricity and heat production sectors. Liquid biofuels saw potential in transportation while biogas was used in all three sectors mentioned above. Even though majority of the contribution among the various bioenergy sources were derived from solid biomass as of 2018, liquid biofuels and biogas have grown at a faster rate since year 2000. On a global supply scale, USA and Brazil were leading in liquid biofuels (69%), while Europe specialised in municipal waste energy (65%) and biogas (50%) in 2018 [7]. Agriculture sector is predicted to have the highest potential for bioenergy utilisation in future [7].
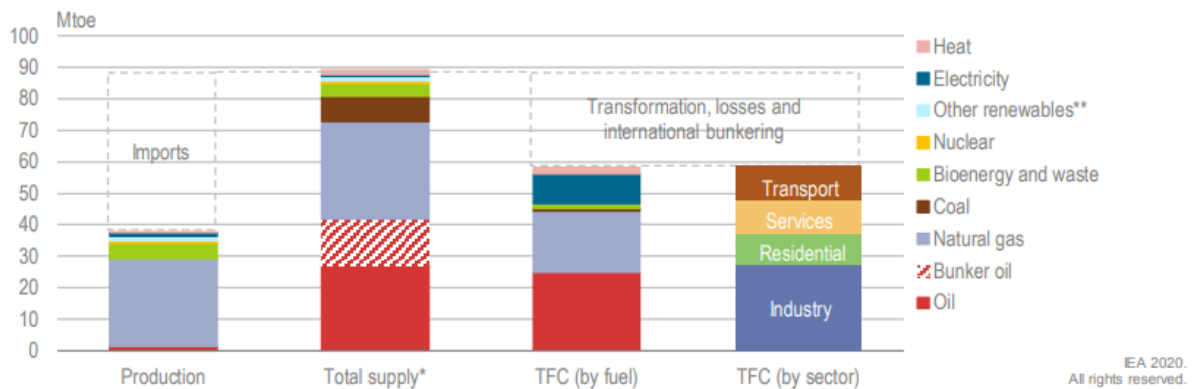
* *Total supply* includes bunker fuels for international aviation and shipping (not part of TPES).
** *Other renewables* includes wind, solar, hydro and geothermal.

Figure 5: The Netherlands Total Energy Supply and Total Final Consumption (TFC) 2018 by fuel and sector [12]

The goal of the 2019 Dutch Climate Act is to bring down GHG emission levels in the Netherlands by 49% in 2030 and 95% in 2050 with respect to 1990 levels. Figure 5 indicates energy production (plus imports), total energy supply and total final consumption (TFC) from different sources and sectors for the year 2018 for Netherlands. It can be seen from Figure 5 that natural gas predominantly contributed to the energy supply (42%) followed by oil (37%) and coal (11%). About half of the rest was contributed by biofuels and the remaining by nuclear, wind, solar, hydropower and geothermal [12]. The total energy supply includes bunker oil (not accounted for in Total Primary Energy Supply -TPES) which is used for international aviation and shipping. Use of natural gas is convenient due to the existence of the Groningen gas field, majorly fulfilling energy use requirements in residential heating, electricity generation and domestic energy production [12]. It can also be seen from Figure 5 that the energy demand is mainly driven by industrial sector. Heating requirements during the winter months also lead to rise in energy demand. The contribution of renewables in the TFC has increased from 4% in 2008 to 7.4% as of 2018 [12]. Bioenergy is the primary source of renewable energy, which is mainly used for heating purposes and as transportation fuels, while wind energy contributes majorly to electricity generation. To meet 2050 goals, the Netherlands is speeding up production and use of clean gases such as hydrogen on large-scale, and looking into CCS options, while making use of digital technologies such as smart meters, electric vehicle (EV) smart charging and implementing projects on demand side response. As of 2018, the GHG emissions were reduced by 15% [12]. However, more robust strategies need to be put

in place; as per analysis conducted in 2019 by the Netherlands Environmental Assessment Agency (PBL), high chances of missing the proposed targets are foreseen.
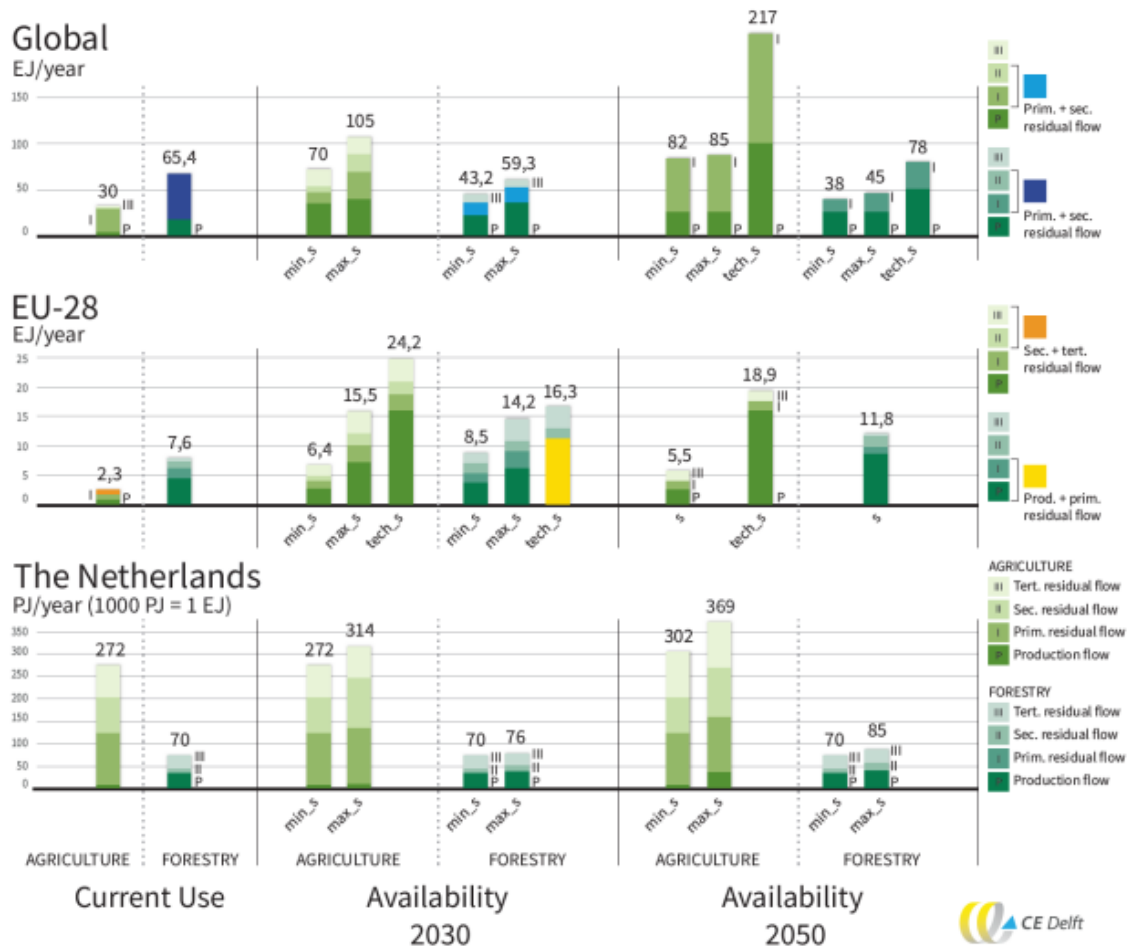
Figure 6: Current use and estimates of biomass availability in European Union (EU), the Netherlands and on global basis for 2030 and 2050 [13]

Figure 6 shows the availability of biomass supply in 2020 (current use) and future estimates of biomass supply in 2030 and 2050 from agriculture and forestry sectors on global scale (EJ/year) as well as for EU (EJ/year) and the Netherlands (PJ/year). These estimates were based on data from literature taken with plausible assumptions. The report was prepared by CE Delft in collaboration with PBL and inputs from various stakeholders. The availability of biomass is calculated based on sum of production of biomass and the primary, secondary and tertiary residual flows resulting from it. The primary, secondary and tertiary residual flows are defined based on where they are generated in the biomass production to use chain. The leftover material generated during production of biomass is referred to as primary residual flows. Examples include plant remains after harvesting in the field. Materials released during biomass processing such as sawdust refers to secondary residual flows. Materials left after consumption is defined as tertiary residual flows. This could include vegetable peels leftover after cooking. The min_s and max_s in Figure 6 represents the minimum and maximum ecological sustainable availability, respectively, taking into account extreme factors such as exclusion of areas having water shortage, or areas with a risk of deforestation and soil erosion. The tech_s represents the technically sustainable availability where the basic constraints such as land use for growing food and fulfilling clothing requirements for rising population are considered. It can be

observed that agriculture shows a higher capability for generating sustainable biomass supply as compared to forestry; however, these estimates are based on assumptions taken behind the above-mentioned factors such as productivity potentials, availability of land use for agricultural purposes, government policies in different countries from where biomass would be sourced, quantity of residual matter to be left on land for soil fertility, water availability in a specific location and use of abandoned or marginal land for growing biomass [13].

1.2 Why Biomass Gasification- Allothermal Gasification

In order to increase to increase the energy density of solid biomass, several conversion routes are applied, one of which is gasification. Gasification is a thermochemical conversion process carried out at high temperatures (700-1500°C) [1]. Herein, using a gaseous agent under sub stoichiometric conditions, a solid or liquid fuel is converted into a product gas, also known as producer gas, syngas or synthesis gas. The gasifying agent can be air, oxygen, carbon-dioxide, steam or a mixture of air and steam [1]. The main non-condensable permanent gases obtained from gasification [14] are carbon monoxide, hydrogen, carbon dioxide and methane. Gasification can be used for heat generation, CHP applications and for production of liquid fuels after tar and solids removal from the producer gas and subsequent gas cleaning steps for ammonia, sulphur species (e.g., H_2S) and CO_2 removal [14]. Liquid fuels such as dimethyl ether (DME), methanol, ethanol, biodiesel and gaseous fuels such as H_2 and synthetic natural gas (SNG) are various products obtained from biomass gasification [1].

The heating value of the product gas is an indicator of the bio-syngas quality as it defines the thermal energy released upon complete combustion of a fuel. It is characterized as higher heating value (HHV) and lower heating value (LHV) [15]. Calculation for HHV and LHV can be differentiated based on the fact that the former is based on inclusion of latent heat of vaporization of water while the latter does not include the same. The calculation for the HHV and LHV is given in Section 2.4. The LHV of the product gas in particular, is influenced by various factors [14]: -

- ➢ Residence time in the gasifier – High residence time promotes CO and CH_4 yield in the final product gas, which could cause a rise in its LHV
- ➢ Type of Biomass – High moisture content can decrease the LHV of the final product gas
- ➢ Operating Temperature –High temperature increases the yield of final product gas and its LHV.
- ➢ Type of gasification agent used – Generally, use of air as gasification agent results in a product gas having low LHV (due to dilution by nitrogen) while other gasification agents such as pure oxygen, hydrogen or steam results in a product gas having high LHV.

Generally, low heating rates and high residence time are the conditions which promote tar cracking, and improve the quality of product gas by increasing the non-condensable gaseous fraction in the product gas [14].

Gasification is a complex process involving multiple endothermic and exothermic homogenous gas-phase and heterogeneous gas-solid reactions. These reactions are presented in Table 15. The endothermic reactions play a significant role in determining the quality and composition of the

product gas. Based on the method of heat supply for carrying out these reactions, gasification process can be classified as autothermal and allothermal [2]. Autothermal gasification relies on the heat produced within the gasifier by various gasification agent (air, oxygen). The heat produced is controlled by the amount and flow of the gasification agent. Allothermal gasification relies on heat transfer by means of heat exchangers, heat pipes or via the circulation of hot solids [2].

Gasifiers operating on allothermal gasification are also called dual fluidized bed (DFB) gasifiers as there are separate chambers for combustion and gasification reactions, which together constitute the gasifier [2]. The heat generated through combustion in the combustion chamber is transferred to the gasification chamber via heat carrier or heat exchanger. As the heat is not generated inside the gasification chamber and transferred indirectly from the combustion chamber, this type of gasification is also commonly known as indirect gasification [2]. Figure 7 shows two methods of heat transfer in allothermal gasification in a DFB gasifier.
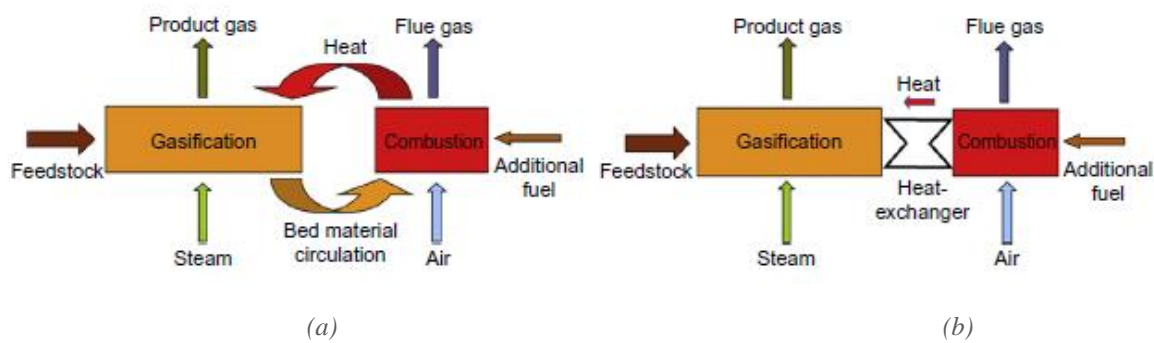
Figure 7: (a) Visualization of allothermal gasification in DFB gasifier by means of bed material circulation (b) by means of heat exchanger(s) [2]

In Figure 7(a), heat transport occurs through circulation of the bed material between the combustion and gasification chamber. The bed material from gasification reactor is circulated and is heated in the combustion chamber (by combustion of biochar produced during gasification) and recycled back to the gasification chamber. In Figure 7(b), the heat transfer takes place via high temperature heat exchanger(s) in the gasifier.

An advantage of separating the gasification and combustion chambers is that the product gas is released from the gasification chamber and flue gas produced upon combustion is released from the combustion chamber, thus avoiding the mix-up of these gases, which is not possible for autothermal gasifiers. Secondly, while using only air for biomass combustion, the nitrogen present in air does not take part in gasification reactions resulting in a more diluted product gas. In an autothermal reactor this can be avoided by using oxygen-enriched air or pure oxygen. However, this requires setting up an air separation equipment which is costly and energy intensive. Use of allothermal gasifiers can facilitate the production of a high-quality synthesis gas without the need for establishing an air separation unit [2]. Different indirectly heated gasifiers, described in detail in Section 2.9 are already operational: the Milena gasifier, developed by Energy research Centre of the Netherlands (ECN, now part of TNO - Netherlands Organisation for Applied Scientific Research), the SilvaGas gasifier, developed by Future

Energy Resources Corporation FERCO, the Heat Pipe Reformer (HPR), developed by the Technical University of Munich (TU Munich) and the Fast Internally Circulating Fluidized Bed (FICFB) gasifier developed by the Vienna University of Technology (TU Wien) in collaboration with the Renewable Power Technologies (REPOTEC).

Currently, the Process & Energy Department (P&E) of the Delft University of Technology (TU Delft) is working on the commissioning of a novel 50 kW$_{th}$ Indirectly Heated Bubbling Fluidized Bed Steam Reformer (IHBFBSR), designed and built together with the Dutch company Petrogas Gas-Systems. The IHBFBSR represents a new concept of allothermal gasification technology where the heat needed for the endothermic gasification reactions is provided by two radiant tube burners placed vertically inside the reactor, one at the top and one at the bottom. This configuration, where the heat is transferred from inside to outside, is expected to result in low heat loss compared to the above mentioned already operational allothermal gasifiers where, usually, heat is transferred from outside to inside. Figure 8 shows a simple visualization of the IHBFBSR setup.
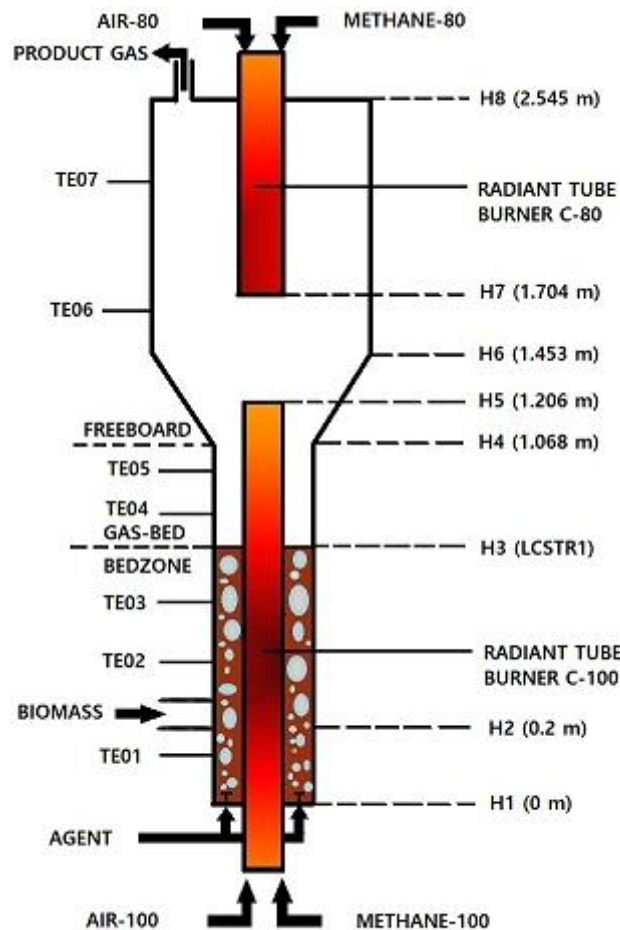
Figure 8: IHBFBSR Visualisation with the Bedzone, Gas-Bed, Freeboard and two Radiant Tube Burners with thermocouples TE01 to TE07

The values of the reactor diameter corresponding to the different H_i values representing the heights of the gasifier at different points with respect to the starting point of the bedzone as seen in Figure 8 are specified in Section 4.1.6.

1.3 Aim of the work, Research Questions and Methodology

The aim of this study is to optimize and validate a kinetic model of the IHBFBSR developed by the former student Kwakkenbos [16]. Moreover, it also focuses on the preliminary evaluation of best process conditions in order to obtain a product gas that, after subsequent gas cleaning, can be used for production of methanol, and explore the possibility of product gas recycle to the burners to make the gasifier set up sustainable. The kinetic model of the IHBFBSR is built in the flowsheeting software (package) Aspen Plus®, which is well-known to have integrated tools for process design, process optimization and economic evaluation.

Gasification is a complex process involving multiple steps defined by various chemical reactions and heat and mass transfer mechanisms. Building a model to simulate this complex chemical process can be helpful in many ways. A model can be used to [17]:

➢ Determine the optimal process conditions for manufacturing a specific product such as methanol or SNG by gasification. Various parameters such as the type of feedstock used, geometry/configuration of the gasifier setup, the choice of gasification agent and the operating conditions can affect the quality of the final product. Conducting experiments without adequate information on the optimal operating conditions for manufacturing a desired product can be time-consuming and expensive. The average operating temperatures for the IHBFBSR lie between 700°C-850°C. The higher the temperatures, the more resources are needed and the more time-consuming the entire process becomes. Based on the results generated by a validated model, conditions required for getting a desired product can be pre-decided; as a result, fewer experiments need to be conducted.
➢ Understand the reactor performance under various operating conditions, which could be further used for process optimization and improving overall efficiency.
➢ Providing information about process scale up.
➢ Determine and understand process limitations to avoid extreme or hazardous operating conditions for the setup, thus ensuring safety while performing experiments.
➢ Perform an economic evaluation of the setup which can be used for financial assistance during scale-up or for determining the cost of incorporating an additional equipment in the setup.

The main research questions of this study can be stated as follows:

➢ **Does the optimized model predict the results of the product gas composition obtained from the IHBFBSR under various operating parameters with respect to the yield of permanent gases, N_2, tars, H_2O concentration in product gas, various gas ratios CO/CO_2, H_2/CO, CH_4/H_2 and other key performance parameters such as carbon conversion (CC), cold gas efficiency (CGE) and overall efficiency (OE) with reasonable accuracy?**

➢ **Can the model be used as a basis for evaluating the best process conditions under which the product gas obtained from the IHBFBSR, can be used for downstream applications, which in this study is the production of methanol?**

➢ **Can the model be used for predicting the possibility of making the current IHBFBSR setup more sustainable by recycling a part of the product gas to produce heat that needs to be provided for the endothermic gasification reactions?**

➢ **Does the model provide any insight for improvements that can be implemented in the current gasifier setup?**

The methodology adopted to answer the above-mentioned research questions is via adaptation of an existing gasifier model by:

➢ Enhanced characterization by performing the particle size distribution (PSD) experiments for biomass and biochar.
➢ Implementation of the PSD for biomass and biochar in the model, along with PSD for ash generated during biomass pyrolysis, performed by a former student.
➢ Addition of a second preheater for heating the gasification agent – air is heated in the first preheater and steam is heated in the second preheater.
➢ Modifying the nitrogen purge flows in the model to resemble the actual gasifier setup.
➢ Using a cyclone separator in the model as it is present in the physical setup of IHBFBSR and observing the variation of PSD for char and ash at the inlet and outlet depending on efficiency of cyclone separator in separating these two components.
➢ Accounting for the mass loss during pyrolysis experiments performed in the CDS Analytical Pyroprobe 5000 apparatus in the Fortran Code in Aspen Plus® through normalization of gas, solid and liquid fractions obtained as pyrolysis products.
➢ Using phenol as model tar to represent tar formation during pyrolysis and introducing phenol decomposition to benzene and naphthalene in the gasifier
➢ Modifying the gasifier setup in the model by dividing it into three sections in the model: bedzone/oxidation-bed, gas-bed and freeboard. The bedzone and gas-bed are modelled by two continuous stirred tank reactor (CSTR) blocks and the freeboard is modelled by an RPlug or plug flow reactor (PFR) block. The first CSTR hosts all oxidation reactions, the second CSTR hosts the phenol cracking and reforming reactions, followed by oxidation and reforming reactions in the PFR.
➢ Introducing a secondary air stream to the freeboard region, to be able to validate the model with results from gasification tests conducted with secondary air supply to the freeboard

The model is then validated by using the results of the first air-steam gasification tests performed under various operational conditions by PhD candidates Del Grosso and Tsekos. The validation is performed with respect to the yield of permanent non-condensable gases, nitrogen, and water vapour in the product gas, as well as tars production and various gas ratios (CO/H_2, CH_4/H_2, CO/CO_2). Moreover, carbon conversion (CC), cold gas efficiency (CGE) and overall efficiency (OE), presented in Eq. 1.1, 1.2 and 1.3, respectively, will be evaluated [1]. CC shows the amount of carbon particles (solid char) in the biomass that is converted into the product gas. CGE represents the ratio of chemical energy contained in the product gas to the chemical energy of the feed. OE is defined as the ratio of the chemical energy released in the

product gas by the combined energy of the feed and the heat power introduced in the gasifier setup. Multiplying the values obtained in Eq 1.1, 1.2 and 1.3 by 100 gives the values of CC, CGE and OE in percentage.

A high CC, CGE and OE results in a better-quality synthesis gas.

$$CC = \sum_{i=1}^{n} 1 - \left(\frac{m_{C,residue}}{m_{C,feed}}\right) \qquad \text{(Eq 1.1)}$$

$$CGE = \sum_{i=1}^{n} \left(\frac{m_i LHV_i}{m_{fuel} LHV_{fuel}}\right) \qquad \text{(Eq 1.2)}$$

$$OE = \sum_{i=1}^{n} \left(\frac{m_i LHV_i}{m_{fuel} LHV_{fuel} + P_{in}}\right) \qquad \text{(Eq 1.3)}$$

Here $m_{C,\ residue}$ and $m_{C,\ feed}$ represent the mass flow rate of carbon in the residue and feed, respectively in kg/hr, m_i represents the mass flow rate of component species i in the product gas in kg/hr. LHV_i corresponds to the lower heating value of component species i in the product gas in MJ/kg. LHV_{fuel} represents the lower heating value of the biomass feed in MJ/kg. Mass flow rate of fuel is denoted by m_{fuel}. P_{in} denotes the heat power supplied to the IHBFBSR in MJ/hr.

After the validation of the model and the comparison and analysis of the difference in experimental and model results in terms of absolute and relative errors, the following analysis will be performed:

> ➢ Consideration of the effect of using a fraction of the product gas produced to feed the burners in order to make the set up more sustainable
> ➢ Perform sensitivity analyses to determine the best process conditions under which product gas obtained from gasifier, after subsequent cleaning, can be used for methanol production.
> ➢ Perform a heat and mass balance for the test for which the above two analysis will be carried out

1.4 Thesis Outline

This section describes the outline of this thesis work. The thesis is divided into 6 chapters.

Chapter 1 gives an introduction on the need for an energy transition to sustainable sources and the contribution of biomass energy to this change. It also gives an overview on the working principle of allothermal gasification and its potential advantages in giving a better-quality product. The aim of this study is to optimize and validate the kinetic model of the IHBFBSR, an allothermal gasifier setup at TU Delft, developed in Aspen Plus®, following which study on product gas recycle to burners and preliminary evaluation of best process conditions for methanol production is carried out.

Chapter 2 gives an overview on the structure of biomass and various aspects related to biomass gasification. It includes a description of proximate and ultimate analysis, calculation of LHV and HHV, different conversion routes for biomass, an overview of two most important

parameters used in biomass gasification: equivalence ratio (λ) and steam to biomass ratio (SB* or SB) and a description of fluidized bed gasifiers. Various allothermal gasifier setups in commercial use have been studied and a comparison has been done for their efficiencies and process parameters with respect to the IHBFBSR. To understand how biomass gasification is simulated in Aspen Plus®, five gasifier models developed in Aspen Plus® based on kinetic approach have been presented in Appendix C.

Chapter 3 gives an overview of the experimental setup of the IHBFBSR and a description of the materials used in the gasification experiments and for performing the PSD for biomass and biochar.

Chapter 4 gives a description of the optimization procedure followed in Aspen Plus® to improve the kinetic model of the IHBFBSR. This section also compares the differences between the reference model and the optimized model.

Chapter 5 presents the results obtained from the model in terms of permanent gases yield, N_2, H_2O, tars concentration in the product gas and various gas ratios: CO/CO_2, H_2/CO, CH_4/H_2 and key performance indicators: CC, CGE and OE and compares them with results obtained from the first air-steam gasification tests conducted in the IHBFBSR. The deviations between the experimental values and the values obtained from the model are presented in terms of absolute and relative errors. Possible causes explaining the deviations have been stated. This chapter also presents the preliminary analysis of the best process conditions for methanol production, based on the H_2/CO ratio and evaluates the possibility of product gas recycle to the burners to make the set up more sustainable by eliminating the need for natural gas consumption for heat generation.

Chapter 6 presents the conclusions by answering the four research questions formulated in Section 1.3. Scope for improvement in the model is discussed through the recommendations provided in this chapter.

2. LITERATURE STUDY

2.1 Formation of Biomass

Biomass is organic matter formed during the decomposition process of nonfossilized and biodegradable organic materials [11]. During the process of photosynthesis, plants break down water obtained from the ground into protons and electrons that convert carbon dioxide from the atmosphere into glucose, in the presence of solar energy and chlorophyll. The reaction taking place during photosynthesis can be represented by equation 2.1 [11]: -

$$Plant + CO_2 + H_2O + Sunlight \xrightarrow{Chlorophyll} CH_mO_n + O_2 - 480\ KJ/mol \qquad \text{(Eq 2.1)}$$
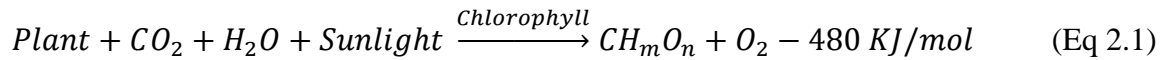
2.2 Structure of Biomass

Biomass consists of organic, inorganic and fluid matter associated with both the organic and inorganic matter [18]. One of the most important components of woody biomass found in plants is the cell wall which provides strength to the plant structure by holding the fibres together and is also responsible for transportation of water to different cells and tissues in plants. The cell wall is primarily made up of cellulose, hemicellulose and lignin [18].

The most abundantly found biopolymer species is cellulose, which is a homopolysaccharide $(C_6H_{10}O_5)_n$ made of glucose C_6 sugar units. It constitutes 40-50% dry weight for most biomass materials and up to 90% dry weight in cotton [11]. A super crystalline structure followed by high degree of polymerization and a high molecular weight, is characteristic of cellulose species. Linearly coupled D-glucopyranoside units connected by β-glycosidic linkages in a 1:4 ratio symbolizes the cellulose structure. The decomposition of cellulose occurs at temperature range within 240°C-350°C [19]. Figure 9 shows a cellobiose unit consisting of two glucose units. The OH-bonds result in a super crystalline structure.
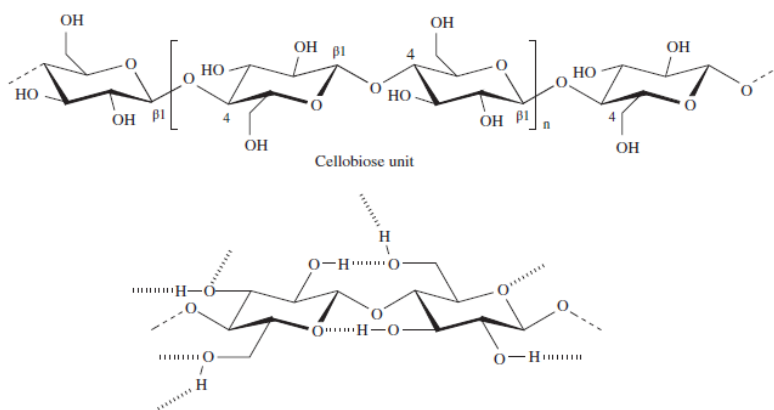
Figure 9: Cellulose structure with inter and intramolecular hydrogen bonding bridges [18]

Hemicelluloses are heteropolysaccharides comprising of C_5 and C_6 sugars. These are represented by the generic formula $(C_5H_8O_4)_n$. Low molecular weight, low degree of

polymerization and weak intramolecular bonds resulting in an amorphous structure is characteristic of hemicellulose species. It constitutes about a quarter of dry wood, around 28% of softwoods and 35% of hardwoods by weight [18]. The main monosaccharides forming the hemicellulose structure is glucose, mannose, galactose, xylose and arabinose [19]. The structure of these monosaccharide constituents is shown in Figure 10. The decomposition of hemicellulose occurs at 200°C-260°C [19]. Figure 11 shows an example of a specific hemicellulose structure.
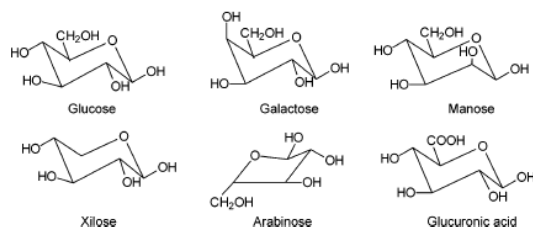
Figure 10: Monosaccharide constituents of hemicellulose [19]
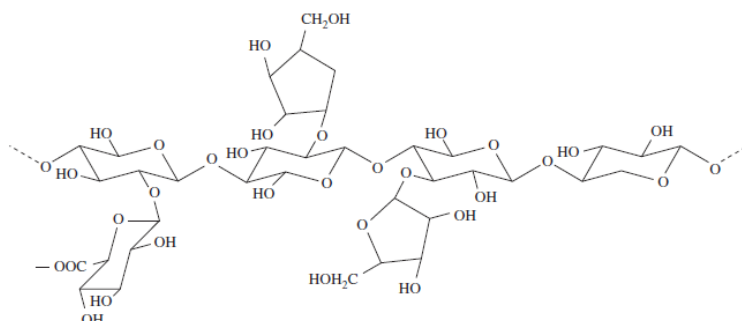
Figure 11: Glucuronoarabinoxylan β-(1,4)-D-xylan hemicellulose structure [18]

Lignin is amorphous three-dimensional polymer consisting of polyphenolic substances. Commonly, phenylpropane units such as p-coumaryl, coniferyl and sinapyl alcohol units are found in lignin structure as shown in Figure 12 [19]. Softwoods constitute 25-35% of lignin and hardwood is made of 18-25% of lignin by dry weight, with variation among different lignin species [11]. The decomposition of lignin takes place at a temperature of 280°C-500°C [19]. A typical lignin structure is shown in Figure 12.
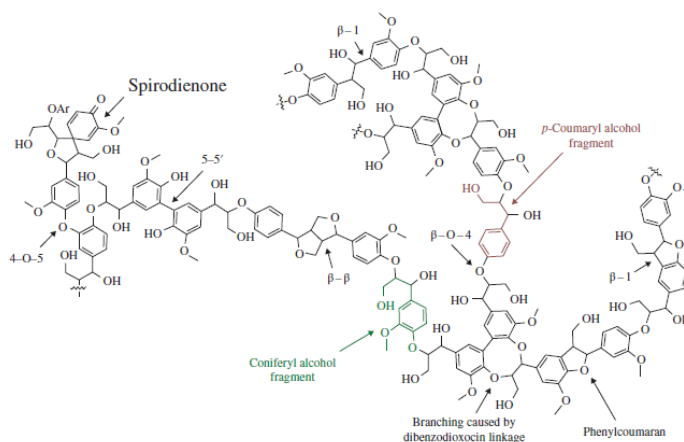
Figure 12: Example of Lignin structure [18]

In addition to cellulose, hemicellulose and lignin, plant biomass is made up of other organic and inorganic components. Oils, fats, starch and proteins form the minor organic constituents found in plant biomass [18]. The inorganic constituents are made up of primary and secondary macronutrients (N, S, P, K, Ca, Mg, S, Fe, C) and micronutrients (Mn, Zn, B, Mo, Cl, Na, Co, V, Ni, Se, Al, Si) and ash [18]. These macro and micronutrients play an integral role in chlorophyll synthesis and serve as source of proteins and amino acids for carrying out various functions.

2.3 Proximate and Ultimate Analysis

Biomass feed can be described by its proximate and ultimate analysis conducted by certain experimental apparatus.

PROXIMATE ANALYSIS

Proximate Analysis is performed to determine the percentages of moisture content, volatile matter (VM), fixed carbon (FC) and ash content of a fuel [18]:

➢ Moisture

The free moisture retained on the surface (surface moisture) and the moisture filling up the pores in the microscopic cell structure (inherent/pore moisture) together constitute the total moisture present in a fuel. It is determined by measuring the weight lost by placing a biomass sample in an oven at 105°C for 24 hours. Eq. 2.2 is used to calculate the moisture content of a fuel on an as received basis [18]. The superscripts ar and db refer to the basis considered: as received and dry basis, respectively.

$$Y^{ar}_{moist} = \frac{m^{ar}_{biomass} - m^{db}_{biomass}}{m^{ar}_{biomass}} \qquad \text{(Eq 2.2)}$$

➢ VM

The vapor released upon heating a fuel which contains both condensable and non-condensable matter constitutes the volatile matter content of biomass [11]. VM on dry basis (db) is quantified by the weight lost upon heating biomass (db) to a temperature of 550°C in an inert environment. Equation 2.3 [18] is used to calculate VM content of biomass sample on dry basis (db).

$$Y^{db}_{VM} = \frac{\Delta m}{m^{db}_{biomass}} \qquad \text{(Eq 2.3)}$$

➢ Ash

The inorganic solid, which remains after complete combustion of biomass is referred to ash. Ash constitutes varying amounts of different elements: Si, Al, Fe, Ca, Mg, Ti, Na and K [11]. Continued heating of biochar produced during VM determination to a temperature of 815°C gives the ash percentage. Equation 2.4 is used to represent the ash content of a fuel on dry basis (db) [18].

$$Y^{db}_{ash} = \frac{m_{ash}}{m^{db}_{biomass}} \qquad \text{(Eq 2.4)}$$

> ➢ Fixed Carbon

The solid carbon remaining after devolatilization process is referred to as fixed carbon [11]. Fixed carbon on dry basis (db) is measured by subtracting the volatile matter and ash content from biomass feed after devolatilization. The calculation for FC (db) is shown in Eq 2.5. If it is reported on an as received (ar) basis, the moisture content also needs to be subtracted along with VM (ar) and ash (ar) content.

$$Y_{FC}^{db} = 1 - Y_{VM}^{db} - Y_{ash}^{db} \qquad \text{(Eq 2.5)}$$

ULTIMATE ANALYSIS

The flue gas generated from combustion of a biomass sample is analysed to determine carbon, hydrogen, nitrogen, sulphur, ash and oxygen values on a dry basis (db) by weight. Ultimate analysis gives an idea about the chemical composition of biomass sample.

The proximate and ultimate analysis of some types of coal and biomass fuel are listed in Table 1. The proximate and ultimate analysis values are reported on a dry basis (db). Hence, the sum of VM, FC and ash equals 100% for proximate analysis and values of C, H, O, N, S and ash equals 100% for ultimate analysis.

Table 1: Proximate and Ultimate Analysis of Different Fuel Types

Fuel Type	Lignite	Anthracite	Bituminous Coal	Pinewood	Wheat Straw	Corn Straw	Wet Sewage sludge
Proximate Analysis (wt%)							
Moisture (ar)	36.9	4.5	5.3	7.6	6.3	4.6	84.2
VM (db)	39.5	8	37.6	80.3	84.9	82.7	41.5
FC (db)	44	85.7	58	18.85	10.9	13.5	5.9
Ash (db)	16.5	6.3	4.4	0.85	4.2	3.8	52.6
Ultimate Analysis (wt% db)							
C	59.3	86	79.1	49.2	43.4	43.3	20
H	3.6	3.4	4.9	5.8	5.9	5.7	1.8
O	19.4	2.3	9.6	43.9	45.8	46.4	12.6
N	0.9	1.3	1.4	0.2	0.6	0.8	4
S	0.3	0.7	0.6	0.05	0.1	0.0	9
	[20]	[20]	[20]	[21]	[22]	[22]	[23]

A high moisture content contributes negatively to the heating value of a fuel as energy is required for evaporation of moisture. A higher VM and higher FC content in a fuel leads to higher heating value. Molecules present in ash tend to agglomerate during gasification process at high temperatures, which and can negatively impact the performance [18].

From Table 1, it can be seen that all three types of coal have higher FC content as compared to biomass. Lignite is classified as a low rank coal because of lower FC content and high VM and anthracite with high FC content and low VM is classified as a high rank coal [20]. However, all biomass types have significantly higher VM as compared to coal. The ash content is lower

for biomass with exception of wet sewage sludge. The range of values for carbon and oxygen for biomass lie between 40-50% on dry basis (db) with the exception of wet sewage sludge. Coal exhibits a higher carbon content and a lower oxygen content as compared to biomass. The hydrogen content of biomass and coal typically lies in the range of 2-6% on dry basis (db). Biomass and coal show very low percentages of nitrogen and sulphur with exception of wet sewage sludge and coal being slightly higher.

2.4 Calculation of HHV and LHV

The significance of heating value in determining the quality of product gas and the performance of a gasification process was discussed in Section 1.2.

LHV is obtained by subtracting the latent heat of vaporization of water from HHV. Equation 2.6 shows the calculation of LHV on dry basis (db) from HHV on dry basis (db) [18].

$$LHV^{db} = HHV^{db} - 2.4 * 8.9 Y_H^{db} \qquad \text{(Eq 2.6)}$$

Here 2.4 MJ/kg refers the latent heat of vaporization of water and 8.9 kg/kg is the stoichiometric ratio of amount of water formed per kg of hydrogen.

The HHV can be determined experimentally using a bomb calorimeter or from the ultimate analysis of a fuel using an empirical relation [18]. An example of empirical relation is reported in equation 2.7.

$$HHV^{db} = 34.91 Y_C + 117.83 Y_H + 10.05 Y_S - 1.51 Y_N - 10.34 Y_0 - 2.11 Y_{Ash} \quad \text{(Eq 2.7)}$$

A higher percentage of carbon, hydrogen and sulphur is observed to contribute positively to HHV while nitrogen, oxygen and ash contribute negatively to the HHV.

Table 2 shows the gravimetric HHV and volumetric HHV calculated from bulk density values found in literature for different fuels.

Table 2: Gravimetric (MJ/kg) and Volumetric HHV (MJ/m^3) on dry basis - (calculated from bulk density values) of different fuels

Fuel Type	Lignite	Anthracite	Bituminous Coal	Pinewood	Wheat Straw	Corn Straw	Wet Sewage sludge
HHV (MJ/kg) (db)							
	23	35.3	35.5	19.4	17.4	15.7	2
	[20]	[20]	[20]	[21]	[22]	[22]	[24]
Average bulk density (kg/m^3)							
	720	1506	720	480	178.5	117	1030
	[25]	[26]	[25]	[27]	[28]	[29]	[30]
HHV (MJ/m^3) (db)							
	16560	53161.8	25560	9312	3105.9	1836.9	2060

It can be observed that generally biomass has lower gravimetric and volumetric HHV as compared to coal and other fossil fuel types. To be able to efficiently store, transport and use biomass as a fuel, an effort is made to look at various biomass conversion routes aimed at converting biomass to products with high heating value.

2.5 Biomass Conversion Routes

The various routes adopted for biomass conversion technologies are presented in Figure 13 below [31] [32]. These methods can be selected based on the feasibility of the technology and desired output.
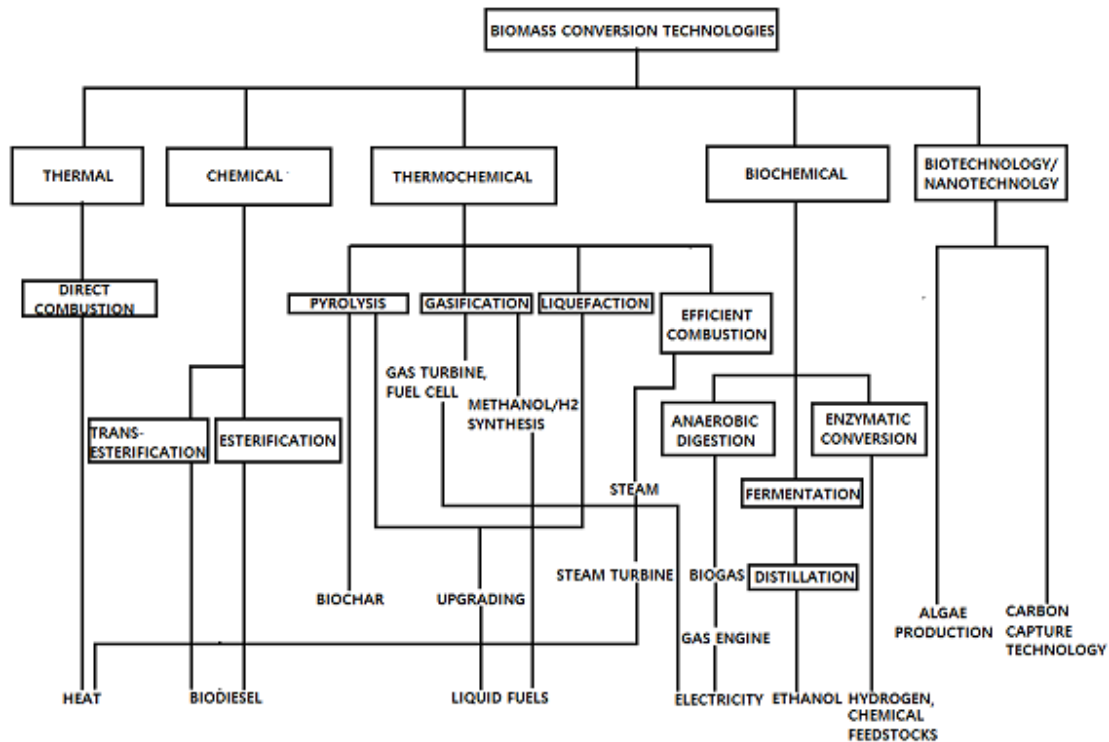
Figure 13: Various routes adopted for biomass conversion [32] [31]

The thermochemical and biochemical methods are most commonly studied for biomass conversion. Thermochemical routes hold the advantage of being able to accept a wider variety of feedstocks compared to biochemical methods such as fermentation or hydrolysis which require pre-treatment and are suitable only for specific feedstocks. This can increase the choice of low-cost feed selection, which when coupled with an efficient conversion process can result in high-quality product gas with minimal emissions [33]. Moreover, biochemical methods are characterised by biological conversion resulting in limited productivity due to longer reaction time and high susceptibility to changes in ambient temperature [34]. However, biochemical methods do hold the advantage of low processing temperatures and high selectivity of the products [34]. The biochemical and other methods are not discussed in detail since this study is based on gasification which is a thermochemical process. Gasification proves to be an energy intensive process, but with a relatively less duration required for process completion, cost-effective and a mature technology [1].

The comparison of the temperatures and pressures employed for different thermochemical biomass conversion technologies is shown in Table 3.

Table 3: Temperature and Pressure employed for various Biomass Thermochemical Conversion Routes [35] [1]

Conversion Process	Temperature (°C)	Pressure (MPa)
Combustion	700-1400	>0.1
Pyrolysis	380-530	0.1-0.5
Gasification	700-1500	0.1-7
Liquefaction	250-330	5-20

2.6 Biomass Gasification Process

Gasification process can be considered to be a series of four main steps involving: -

- Biomass Pre-Heating and Drying

As stated in Section 2.3, a high moisture content reduces the heating value of a fuel. The process of drying requires energy to be supplied to biomass feed to enable moisture evaporation from biomass sample as steam. Drying takes place at a temperature of 100°C [36].

- Pyrolysis

Devolatilization or vaporization of the volatile matter of biomass occurs during this step of gasification. The temperatures for pyrolysis lie in the range of 380-530°C [35]. This process takes place in the absence of oxygen where the biomass feed is heated up to the pyrolysis temperature and kept at that temperature for specific period of time [36].

Pyrolysis of biomass results in formation of: -

- ➢ Vapours: Heavy condensable vapours and lighter non-condensable low-molecular weight gases including H_2, CO, CO_2, CH_4, C_2H_4 and higher hydrocarbon gases [36].
- ➢ Liquid bio-oil/tar which is dark-brown and viscous in nature [37] produced from the cellulose, hemicellulose and lignin components of biomass. All organic components with a molecular weight above benzene are defined as tar [38]. Apart from tars, pyrolytic water is also produced as a part of the liquid fraction. During low temperature gasification, blocking and fouling issues occur in the equipment due to condensation of tars. This is a major hindrance for effective utilisation of syngas. Tar reduction is implemented by primary (by changing the operating parameters such as higher temperature to facilitate internal tar cracking in the gasifier or by using catalysts) or secondary (cleaning the product gas obtained from gasifier) treatment methods [39].
- ➢ Solid char consisting of carbon (85%) along with minor amounts of oxygen and hydrogen, along with inorganic ash present in biomass [36].

Pyrolysis take place in two steps: primary and secondary pyrolysis. Formation of both condensable and non-condensable vapours and solid primary char occurs during primary pyrolysis. This step is followed by secondary pyrolysis which involves further cracking of vapours into secondary char, tar and non-condensable gases at higher temperatures [36].

The conversion of biomass into solid, liquid and gaseous fraction upon devolatilization depends on various factors such as heating rate, final pyrolysis temperature, equipment design and the composition of biomass feed [36].

Since this step refers to devolatilization, it plays a relatively crucial role in biomass gasification as compared to coal gasification due to higher volatile matter content in biomass (70% dry) compared to coal (30% dry) [33].

- Gasification

Gasification takes place at temperatures in the range of 700-1500°C [1]. In this step, the pyrolysis products react among each other and with the gasification agent to give more products. This consists of tar cracking reactions, char heterogenous reactions with CO_2 and H_2O to produce CO and H_2 and homogenous gas phase reactions [33]. The reactions considered for the gasifier model in our study is listed in Table 15. The gasification agent commonly used to carry out these reactions include air, steam or a mixture of air and steam [1]. The selection of the gasification agent can play a major role in deciding the heating value of the product gas. The heating value of the product gas obtained from using different gasification agents is given in Table 4. Heat needed for the endothermic gasification reactions is provided through partial combustion of a fraction of the feedstock with oxygen. Some external sources, such as hot bed material, superheated steam or heat generation from burning of biochar are also commonly used for heat supply [33].The gasification step can be considered to be a set of oxidation and reduction reactions. The oxidation reactions are mainly the reactions of pyrolysis products with oxygen producing CO_2 and H_2O. The Boudouard reaction (reaction of char with CO_2), water-gas shift (WGS) reaction (reaction of CO with steam) and reactions of other components with steam and methanation reaction (reaction of char with hydrogen) constitute the reduction reactions [40]. For our study, an inert bed material is used, but gasification can also be performed in the presence of specific catalysts. Dolomite, calcined olivine, potassium carbonate and Ni-based catalysts are commonly used [41] [42]. Use of catalyst is adopted for primary treatment of tars and to reach chemical equilibrium during gasification at lower temperatures [41] .

Table 4: Heating Value of Product Gas based on Gasifying Agent [43]

Gasifying Agent	Heating Value of Product Gas (MJ/Nm^3)
Air	4-7
Pure Oxygen	12-28
Steam	10-18

The gasification of char with oxygen, water, carbon-dioxide, and hydrogen is shown in Eq 2.8. Factors such as choice of the gasification medium and reactivity potentials influence the rates of these reactions [11].

$$R_{C+O_2} >> R_{C+H_2O} > R_{C+CO_2} >> R_{C+H_2}$$

(Eq 2.8)

The rate of char-oxygen reaction is the highest followed by char-steam reaction which is 3-5 orders less than char-oxygen reaction. This reaction rate is followed by the Boudouard reaction which is 2-5 orders slower than char-steam reaction rate. Methanation reaction is the slowest and hence not considered for our model [11].

- Gas Cleaning and Upgrading

The product gas obtained from the gasifier undergoes several gas cleaning procedures such as removal of dust, chlorine, sulphur and CO_2, along with tar reduction technologies depending on the type of end product to be manufactured. The end product can be liquid fuels such as ethanol, methanol, DME or gaseous fuels such as hydrogen, methane, SNG. The final product can also be used in power applications such as fuel cells, internal combustion (IC) engines and gas turbines [1].

The biomass gasification steps can be summarised in Figure 14.
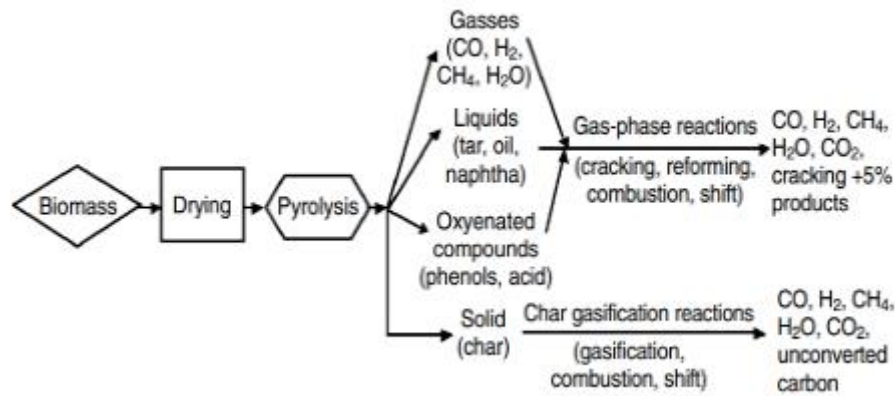
Figure 14: Illustration of Steps involved in Biomass Gasification [40]

2.7 Gasification Process Parameters

There are various process parameters that are considered in gasification such as temperature, pressure, residence time, selection of catalysts, type of fluidization regime and selection of bed material in addition to the type of biomass which affect the composition and quality of the end product. This section focuses on two of the most important process parameters of gasification: equivalence ratio λ and steam to biomass ratio (SB or SB*).

EQUIVALENCE RATIO

The equivalence ratio decides the classification of thermochemical process as combustion, pyrolysis or gasification. It is defined as the ratio between the actual amount of oxygen supplied by the fuel input divided by the stoichiometric oxygen required for complete combustion by fuel input. This is represented by λ in Eq 2.9 [1].

$$\lambda = \frac{supplied\ oxygen/fuel\ input\ (daf)}{stoichiometric\ oxygen/fuel\ input(daf)} \qquad \text{(Eq 2.9)}$$

Oxygen is supplied at stoichiometric ratio for combustion. For pyrolysis and gasification, the supplied oxygen is less than the stoichiometric amount required for complete combustion of the fuel. Since pyrolysis takes place in the absence of oxygen and gasification with limited amount of oxygen, λ is 0 for pyrolysis and lies between 0 and 1 for gasification [43]. The values of λ depending on the type of thermochemical process are given in Table 5.

Table 5: Values for λ pertaining to combustion, gasification and pyrolysis [43]

Thermochemical Process	λ [-]
Combustion	λ = 1
Gasification	0 < λ < 1
Pyrolysis	λ = 0

The typical values of λ required for gasification, range from 0.2 to 0.4 [43]. Beyond this range, gasification might result in a low heating value of product gas due to incomplete char conversion (λ < 0.2) or combustion products CO_2 and H_2O forming predominantly, rather than CO and H_2 (λ > 0.4) [43]. It should be noted that at lower values of λ, less oxygen is available for combustion reactions, thus generating less heat for carrying out the endothermic gasification reactions, and also to compensate for heat loss in reactor walls [1].
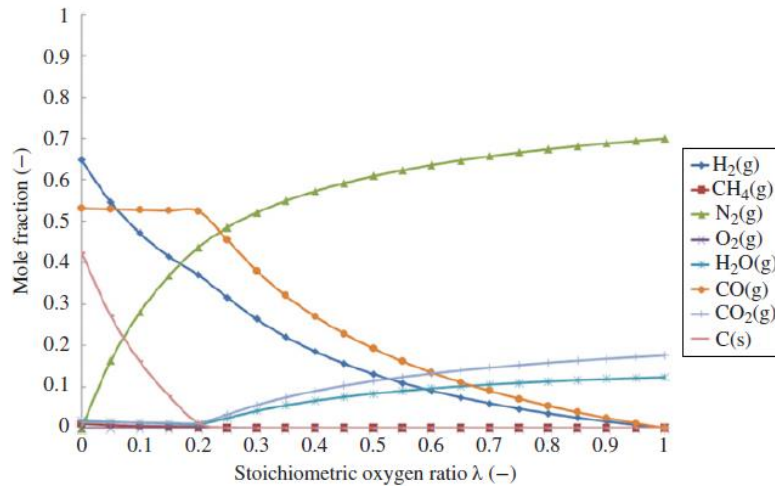
Figure 15: Chemical equilibrium calculations illustrating the Yield of Gasification Products at Varied Values of λ at T=850°C and P= 0.1 MPa [1]

Figure 15 represents the chemical equilibrium calculations illustrating the effect of varying λ on the yield of gasification products with operating temperature and pressure set to 850°C and 0.1 MPa, respectively. A value of 1 on the x-axis represents the stoichiometric ratio needed for combustion. It can be observed from the graphs that by decreasing the value of λ below 1, CO_2 and H_2O which are the main products of combustion decrease in yield, while H_2 and CO which are the main products of gasification increase in yield. At values of λ< 0.2, the amount of solid carbon increases. This is defined as the carbon limit. By decreasing the value of λ below 0.2, not enough oxygen is available for complete carbon conversion, hence char does not get converted to CO, leading to a decrease or a steady value of CO [1].

STEAM TO BIOMASS RATIO

The steam to biomass ratio (SB or SB*) is an important process parameter to be considered during steam gasification. It can be described by formulas given in Eq 2.10 and 2.11 [1].

$$SB = \frac{Steam\ supply\ flow\ rate}{Fuel\ input\ flowrate} \qquad \text{(Eq 2.10)}$$

$$SB^* = \frac{(Steam\ supply\ flowrate + fuel\ moisture)}{Fuel\ input\ flowrate} \qquad \text{(Eq 2.11)}$$

Figure 16 shows the effect of the variation of SB in the range between 0.5 and 1 on the product gas composition for a bubbling fluidized bed gasifier (BFB). An increasing effect on H_2 yield is observed as a function of increasing SB. CO is found to decrease and CO_2 and CH_4 remain more or less constant with slight increase along with increasing SB in [44].
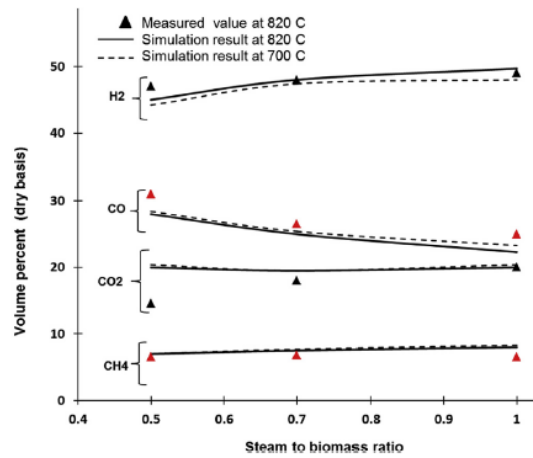
Figure 16: Effect of SB on the composition of product gas at T= 820°C and P=1.05 bar in a BFB [44]

2.8 Types of Gasifiers - Fluidized Bed Gasifiers

According to the transport process/ gas-solid contact mode, gasifiers can be classified as [43]:

- Fixed Bed Gasifier: Updraft, Downdraft and Cross-Draft
- Fluidized Bed Gasifier: Bubbling, Circulating and Dual-Connected
- Entrained Flow Gasifier

These various types of gasifiers are used for different capacities, as can be seen in Figure 17. Based on thermal input, fixed/moving bed gasifiers can be classified as low-capacity gasifiers used in the range of $10kW_{th}$ to $10MW_{th}$, fluidized beds as intermediate capacity gasifiers in the range of $5MW_{th}$ to $100MW_{th}$, and entrained flow (EF) reactors as high-capacity gasifiers used for ranges higher $50MW_{th}$ as seen in Figure 17 [11]. Since the study is focussed on fluidized bed gasifier, this section only describes fluidized bed gasifiers in detail.
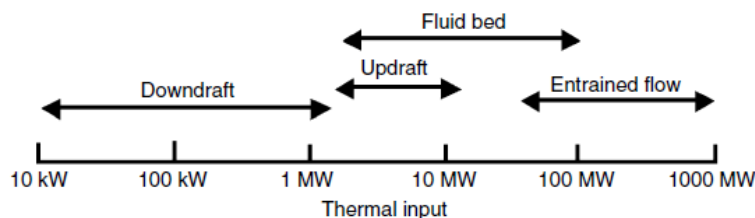
Figure 17: Capacity of different gasifier types based on thermal input [43]

FLUIDIZED BED GASIFIERS

In a fluidized bed gasifier, the gasification agent is passed through a semi-suspended inert granular solid bed material at suitable velocity resulting in uniform mixing conditions and efficient heat and mass transfer. The name is derived from the fact that the gasification agent

and the inert solid bed material together behave like a fluid. The most commonly used bed materials are silica sand and alumina [14]. This design can be used for all fuel types and is particularly useful for biomass gasification. However, downsides to this gasifier design include possible bed sintering and formation of eutectics due to interaction of bed material with ash and other compounds such as chlorine present in biomass along with gas cleaning and pre-treatment necessities for different types of biomass [45]. The operating temperature and pressure for fluidized bed are in the range of 700-900°C and 0-7 MPa, respectively [1]. Bubbling fluidized bed (BFB) and circulating fluidized bed (CFB) gasifiers are the two main types of fluidized bed gasifiers. These are differentiated based on different range of velocities at which the gasification agent is passed through the bed material, as specified in Section 2.8.2.

2.8.1 Overview of Fluidization Regimes in Fluidized Bed Gasifiers and Description of Geldart Chart

To improve fluidization for large and irregularly shaped biomass particles and to facilitate effective heat and mass transfer, catalysts such as dolomite, olivine, potassium carbonate are used as bed material in fluidized bed gasifiers [41]. For determining different parameters related to fluidization, such as minimum fluidization velocity and pressure drop experienced during fluidization, various equations such as Wen and Yu, Ergun and Carman-Kozeny equations are used [46].
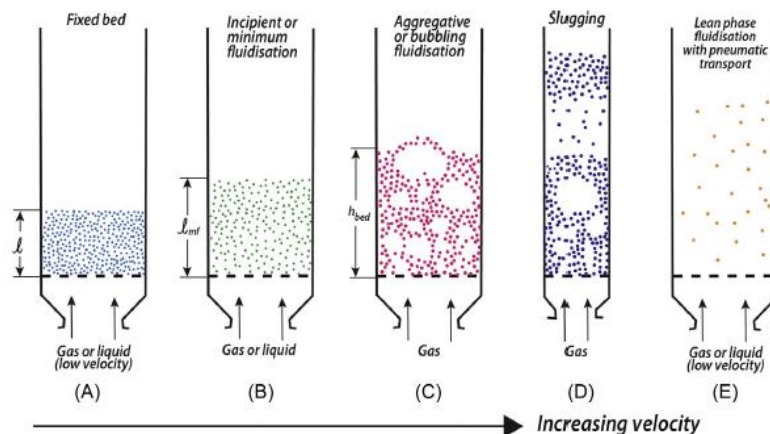
Figure 18: Various Fluidization regimes developed in fluidized bed reactors [46]

Figure 18 represents the various fluidization regimes developed in a fluidized bed reactor under varying velocities of the gasifying agent. At low velocities, the bed is fixed, hence maintaining its stability with drag force and gravitational force acting as equal and opposite forces. As the velocity is increased, the particles tend to rearrange. The velocity at which the drag force just exceeds the gravitational force is defined as the minimum fluidization velocity. As the velocity increases further, the bed starts to expand and there is an increase in the space between the particles which is referred to as voidage. The particles start moving as if they are suspended in the reactor. There is a regular expansion of bed material for a specific range of gas velocities. This regime is referred to as particulate expansion. Higher velocities give rise to the dense/emulsion phase and the lean/bubble phase within the gasifier. This is denoted by the third diagram in Figure 18 known as the aggregative or bubbling fluidization phase. The bubbling regime can be categorised as fast and slow bubbling regime depending on the size of the particles and the upward rising velocity of the gasification agent referred to as the interstitial

gas velocity. Fast bubbling regime is common for beds with finer particles while large-sized bed materials give rise to a slow bubbling regime. The slow bubbling regime is also characterised by large interstitial gas velocity as high velocities are required to fluidize bed material [47].

$$\text{Fast Bubbling Regime: } u_g < u_{br} \qquad \text{(Eq 2.12)}$$

$$\text{Slow Bubbling Regime: } u_g > u_{br} \qquad \text{(Eq 2.13)}$$

In Eq 2.12 and 2.13, u_g and u_{br} denote interstitial gas velocity and rising bubble velocity in m/s, respectively. At higher velocities, the bed resembles a boiling liquid with the dense phase corresponding to the liquid and the lean phase corresponding to the vapor fraction. At even higher velocities, a slugging regime occurs with alternate slugs of gas and fluidised solids. Further increase in velocity leads to a turbulent regime, characterised by regions of varying concentration of solids and loss of identity of the bubbles. The velocity at which the bed completely disappears is defined as the terminal velocity of solids. In this case, there is a need to continuously recycle the bed material to avoid mass loss due to complete entrainment of solids. This phase is characterised by pneumatic transport of solids, also known as fast fluidization. The transition between these phases is dependent on the particle size and density of the solid bed material. Overall, the transition between these phases is not always well-defined and in reality, they could co-exist with each other [46].
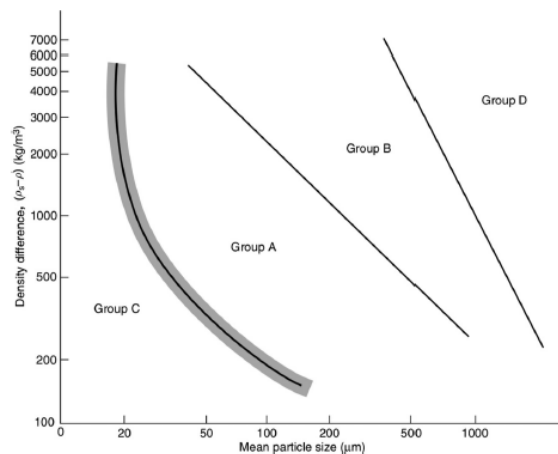
Figure 19: Geldart Chart for different groups of solids [46]

Based on different criteria, Geldart classified solids into four different categories and represented them on a particle size-particle density chart, which is given in Figure 19. The different classes of solids are [46]:

- **Group A**: The solids falling in Group A have a typical particle size ranging between 30-100 μm. Group A solids are characterised by small particle size and low density ($\rho < 1400$ kg/m^3).
- **Group B**: Typical particle size ranges lie between 100-800 μm and densities in the range of 2000-4000 kg/m^3 [45]. Bubbles are formed above the minimum fluidization velocity. An example of solid in Group B is sand. The two types of bed material used for the gasification tests in this study: F054 and F046 corundum also belong to Group B.

- **Group C**: Group C particles have small particle size in the range of 20 µm. Examples include flour, fine silica. Fine powders forming channels, which are difficult to fluidise fall into this category.
- **Group D**: These are characterised by large sized and highly dense particles having a particle size in the order of 1000 µm. Spouted beds fall into this category. Examples also include wheat. Due to the large particle size and high density, these beds are difficult to fluidize.

In general, fine, low-density particles fluidize more easily and evenly compared to large highly-dense particles; however very fine particles also have strong Van-der Waals forces of attraction in between their particles which could be a hindrance for fluidization. In terms of shape, spherical-shaped particles are found to fluidize more easily than others. Bed material showing non-uniformity in terms of particle size show a more uniform fluidization pattern compared to a bed containing particles having same size [46]. Overall, Geldart B particles are the most suitable for fluidized bed gasifiers as they fluidize in a homogenous manner, and result in bubble formation soon after the minimum fluidization velocity is exceeded [45].

2.8.2 Bubbling Fluidized Bed (BFB), Circulating Fluidized Bed (CFB) and Dual Fluidized Bed (DFB)
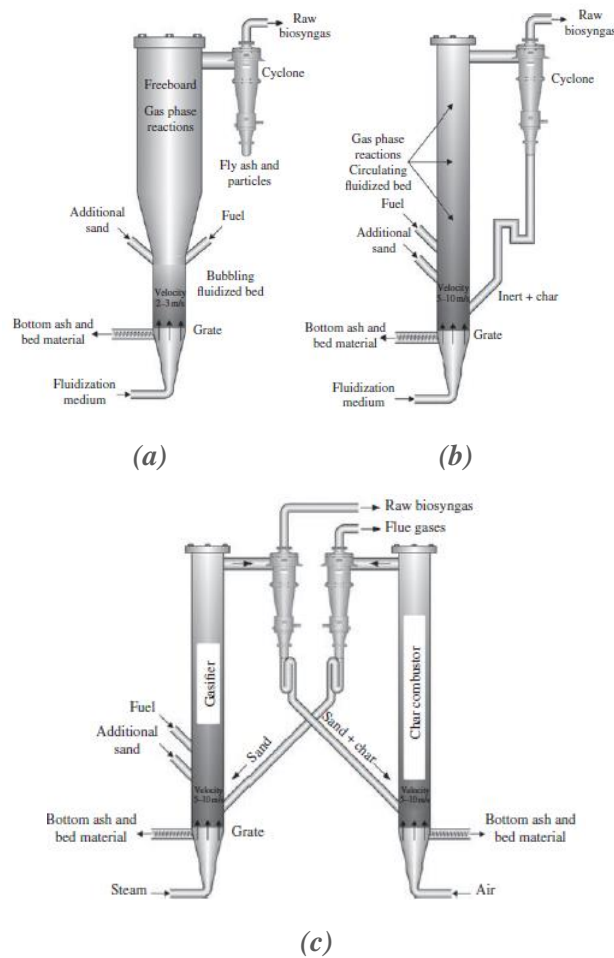
Figure 20: a) BFB, (b) CFB, (c) DFB gasifier [1]

Figure 20 illustrates the various types of fluidized bed gasifiers.

In a BFB, the gasifying agent is introduced with velocities in the range of 0.5 m/s to 2m/s which lie within the minimum fluidization velocity and the maximum terminal velocity [1]. The CFB operates with the same principle as that of BFB, except with velocities higher than terminal velocities (3.5-5.5 m/s) [1] . Such high velocities result in entrainment of large quantity of solids. These solids are separated by cyclone separators and have to be recycled back to the gasifier to avoid mass loss.

A dual fluidized bed gasifier (DFB), also known as twin bed gasifier, operates on the principle of allothermal gasification involving two separate chambers for gasification and combustion. The heat produced from combustion is transferred through heat pipes, heat exchangers or by circulation of bed material/char as discussed in Section 1.2 [2]. However, for biomass gasification, often an external source of heat such as a burner is required for carrying out the gasification reactions, due to low amounts of fixed carbon in biomass compared to coal or other fossil fuels. Thus, the heat generated by combusting biochar is not enough for the process [11].

Examples of DFB in commercial use are the 8 MW_{th} FICFB (fast internal fluidised bed gasifier) in Gussing Austria, the 40 MW_{th} Silva Gas Gasifier in USA and the 20 MW_{th} BFB manufactured by Carbona in Skive, Denmark [33] .

Even though fixed bed and EF gasifiers have not been discussed in detail, an insight into the advantages and disadvantages of each type of reactor can be obtained from Appendix A.

2.9 Commercial Examples of Allothermal Gasifiers

The IHBFBSR setup at TU Delft is an allothermal gasifier. Other allothermal gasifiers in commercial use have been studied to understand the differences in the working principle of these gasifiers and to compare the IHBFBSR to these gasifiers in terms of process conditions, carbon conversion and cold gas or energy efficiency.

2.9.1 Repotec/TU Wien Gasifier (Austria)

The gasifier is a fast internally circulating fluidized bed reactor (FICFB), developed by the TU Wien (TUV) in partnership with REPOTEC manufacturer in Gussing, Austria. This gasifier comprises of two separate chambers for gasification and combustion. Steam, used as gasification agent is supplied to the gasification chamber. The heat necessary for the gasification process is produced by heating biochar and bed material [33]. Calcined olivine is usually used as catalytic bed material [42]. Heat transfer is achieved by circulation of bed material between the two chambers. The gasifier yields a nitrogen-free hydrogen-rich product gas which is released from the gasification chamber [33]. The end product obtained has a calorific value of 12-15 MJ/Nm^3 (on dry basis, db) [48]. Gasification and combustion take place at 900°C and 1000°C, respectively [33]. The gasifier has been tested using wood chips as the main feedstock. This process is carried out at atmospheric pressure [33]. The overall efficiency reached is 81.3% [33] with a carbon conversion of 90% [49].

The initial pilot plants included a 10 kW and a 100 kW plant at TU Wien, following which an 8 MW input CHP plant with gas engine was built at Gussing, Austria in 2002 [33]. The successful implementation of the first commercial scale plant led to the development of a similar 8.5 MW plant in Oberwart, Austria in 2008 with ORC (Organic Rankine Cycle for better electrical efficiency). This was followed by the development of 14 MW input plant with

ORC in Senden, Germany in 2011 and a 32 MW input bio-SNG plant in Goteborg, Sweden in 2013 [50]. The scale up of this gasifier technology was planned in 2012 with building of a 50MW input hydrogen production technology in Vienna, Austria [51]. A schematic representation of the FICFB gasifier is shown in Figure 21.
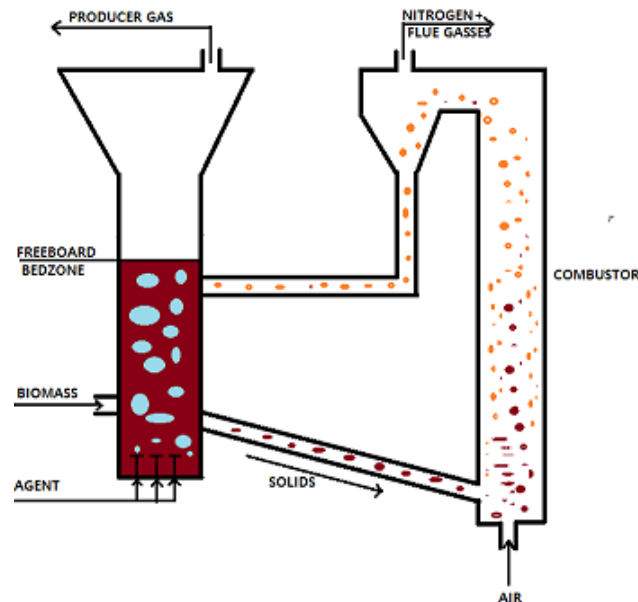
Figure 21: Visualization of FICFB Gasifier [16]

2.9.2 SilvaGas Gasifier (USA)

This gasifier was developed at the Battelle's Columbus Laboratories (BCL) in Columbus, Ohio, in partnership with FERCO, National Renewable Energy Laboratory (NREL), Burlington Electric Department and U.S. Department of Energy. The DFB technology had its first large-scale 40 MW$_{th}$ (200 odt/day) commercial plant built in 1997 at the Mc Neil power station, in Burlington, Vermont which was eventually increased to 350 odt/day at the same production efficiency. The demonstration plant was successfully operated for four years and was later decommissioned [33]. The overall energy efficiency of the process was estimated to be 80% [52]. The DFB technology uses two separate reactor chambers: gasification chamber and combustion chamber to produce medium calorific value product gas having heating value in the range of 15.5-17.3 MJ/Nm^3 [52]. Residual char is heated in the combustion chamber, which in turn heats the suspended bed material (sand) [33]. Heat transfer is accomplished between the two reactor chambers by circulation of bed material. The configuration is similar to the TU Wien gasifier except that in this configuration, the cyclone at the top of the gasification chamber separates the bed material from the syngas and recirculates it back to the combustor. The main tested feedstock for this gasifier included wood chips and pellets. Municipal Solid Waste (MSW), switchgrass, straw and papermill sludge are other potential feedstocks. The gasifier works at 800-850°C and at atmospheric pressure with steam as gasifying agent and air used for combustion [33]. The gasifier was successfully tested for gas co-firing in existing Mc Neil boiler. In 2009, Rentech acquired the gasification technology and planned on building a Biomass to Liquids (BtL) plant in Rialto, California which works on the

Fischer-Tropsch synthesis of urban waste wood. The expected output was 600 barrels of synthetic diesel fuel/day and 35 MWe of renewable electric power [33]. A schematic representation of the SilvaGas gasifier is shown in Figure 22.
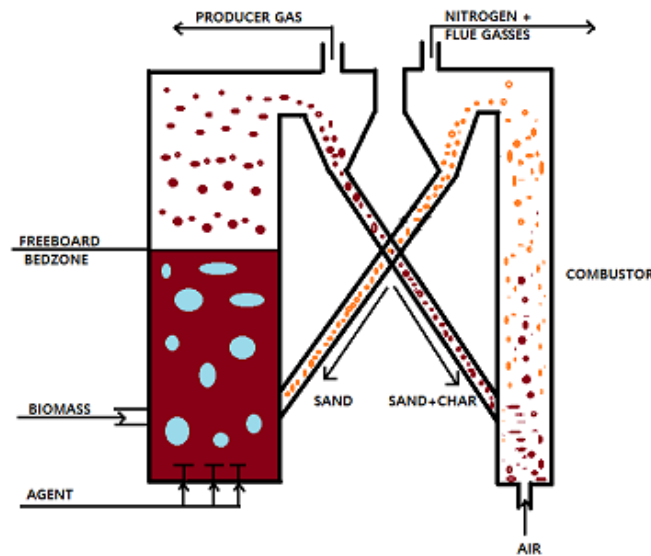
Figure 22: Visualization of Silva Gas Gasifier at Burlington, Vermont, USA [16]

2.9.3 Heat Pipe Reformer - HPR (Germany)

An alternative gasification technology was designed in Germany at Technical University of Munich in 1999 within the project BioHPR with two main 120 kW$_{th}$ input lab-scale prototypes built in 2001. The synthesis gas produced was used for operating a 30 kW microturbine and in generation for a solid oxide fuel cell (SOFC) [53]. Instead of circulating bed material, the heat transfer is achieved using heat pipes which are incorporated in the fluidized bed gasifier. The heat pipes are closed tubes that contain liquids undergoing evaporation and condensation based on the heat transfer to the liquid through the walls of the heat pipe. Use of heat pipes ensures three advantages: high heat transfer coefficient between the reaction chambers, significant reduction of heat transfer area and complete separation of the reaction chambers [54]. However, this gasifier design does suffer from certain challenges. Figure 23 representing the visualization of the working principle of the HPR is a simplified version. In reality, the HPR is an integrated system with reformer integrated in the combustion chamber. While this design reduces heat loss, it will possibly become a challenge for pressurised operation, which might prove as a hindrance during scale-up. The pressures for which the HPR is currently operated is between 2-10 bar [54]. Also, there is a tendency for hydrogen content in the product gas to be transferred to the heat pipes through diffusion [54]. Integration of heat pipes also poses the challenge of potential erosion at high velocities. Hence, it is required to maintain low velocities of the gas flow through the reformer. Wood pellets, hay pellets and sewage sludge pellets have been successfully tested as the feedstocks for the heat pipe reformer. The successful implementation of the 500 kW$_{th}$ CHP pilot plant in Pfaffenhofen, Germany by Agnion Energy Inc. in 2008 paved the way for development of the first 1.3 MW$_{th}$ commercial plant in Grassau, Germany in 2012 [54]. However, the company was later dissolved in 2013 due to insolvency. In 2015, a 100 kW plant for the production of SNG from brown coal and wood pellets was tested in the

CO$_2$SNGproject. A novel approach has been planned for in-situ removal of hydrogen via membranes in this concept. The HPR is currently being designed for a scale up to 50 MW [53].
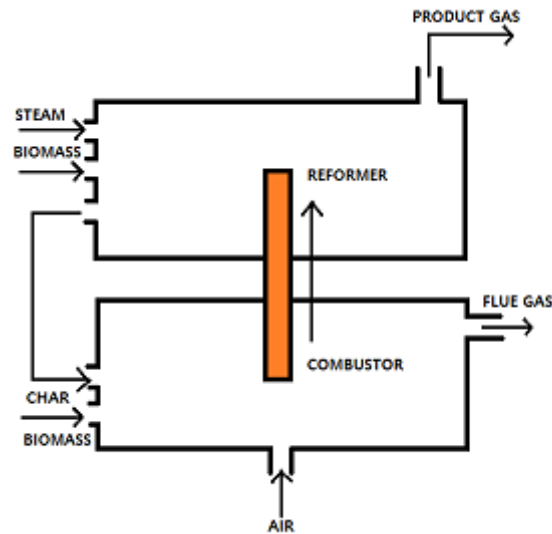
Figure 23: Visualization of Heat Pipe Reformer (HPR) in Germany [16]

2.9.4 ECN Milena gasifier (Netherlands)

The Milena gasifier was developed by the ECN, (now part of TNO) in Petten, Netherlands in partnership with a company in Alkmaar, HVC for construction and Royal Dahlman for oil-based gas washer (OLGA) technology incorporated for tar removal. This is a simpler concept compared to other DFB gasifiers. The combustor and gasifier operate at 925°C and 850°C, respectively [33]. The gasification takes place in a riser with steam used as gasification agent and the less reactive char generated being directed towards the combustor around the riser. The char is heated along with the circulating sand, and is recycled back to the riser. This configuration is more compact and suitable for pressurized operation [33]. It has been noted to have similar CGE and gas composition as the SilvaGas gasifier under similar process conditions [55]. However, the Milena gasifier uses a setting chamber to enable the separation of char and bed material from the synthesis gas, enabling high gas residence time and efficient tar reduction, instead of cyclone separator employed in the SilvaGas gasifier. The use of a riser for gasification as compared to BFB employed in FICFB significantly reduces steam required for gasification [55]. Wood, sunflower husks, straw and sewage sludge are some of the feedstocks successfully tested in this gasifier. The first design of Milena was made in the year 1999 [33]. Following the successful implementation of 25 kW lab scale operation in 2004, an 800 kW pilot plant was built in 2008 [56]. A 4 MW$_{th}$ bio-methane plant was built in Alkmaar (NL) and the technology is being applied to construct a 1 MW$_e$ gasifier in India using soya residue for generating electricity for local use [56]. The technology was also used for developing CHP plants from waste wood having capacities of 2-4 MWe. The 4 MW$_{th}$ bio-methane production was planned for a scale up between 50MW$_{th}$ - 500MW$_{th}$ production in 2012 [55] [57]. Figure 24 shows the visualization of the working principle of the ECN Milena gasifier.
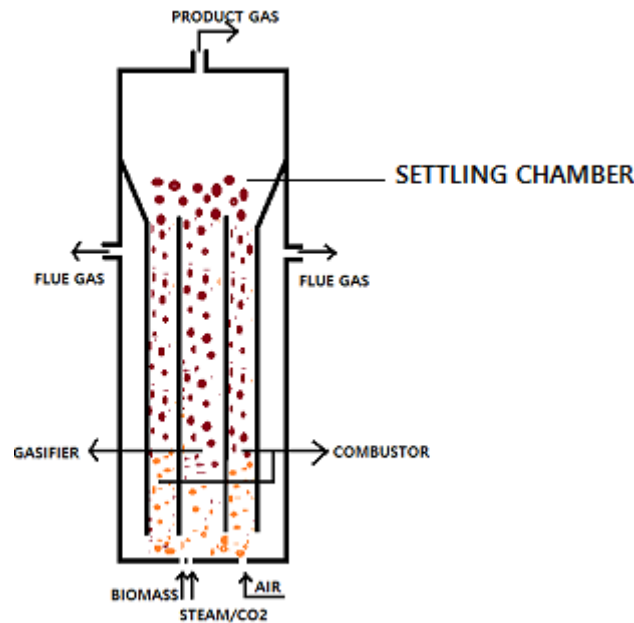
Figure 24: Visualization of ECN Milena Gasifier [16]

Appendix B presents the process conditions and efficiency in terms of carbon conversion, cold gas efficiency and/or total energy efficiency for the different gasifiers described above and also compares them with the data available for the IHBFBSR.

2.10 Biomass Gasification modelling in Aspen Plus® and Review of Gasifier Models developed in Aspen Plus®

This section focusses on the methodology adopted to simulate biomass gasification in Aspen Plus® and study of different gasifier models developed in Aspen Plus®. The advantage of using Aspen Plus® is its flexibility to simulate different reactor models and various chemical processes with the use of specialized tools available in the software and to determine the limitations of a process subjected to varying operating parameters. In addition, the software offers the advantage of carrying out a techno-economic feasibility analysis of a process [17].

Aspen Plus® modelling of biomass gasification can be based on an equilibrium or a kinetic approach. The equilibrium model predicts the composition of the final products based on the assumption that components are allowed to uniformly react for an infinite period of time. This is done in two ways. The first method is performed by considering the stoichiometric approach involving selection of equilibrium constants and appropriate chemical reactions [41]. This approach may not be suitable for complex reactions with inadequate information on stoichiometry or equilibrium constants [17]. The second method employs the non-stoichiometric approach that is based on Gibbs free energy minimization of the system. This approach is used where the stoichiometry of the reaction is not known. Even though the equilibrium model is easier to develop and can predict the influence of process parameters on product composition and the maximum achievable yield, however it does not represent practical gasifiers accurately as chemical equilibrium is not attained for most gasifiers at low temperatures and short residence times. Only very high temperatures (>1400°C) and use of

32

catalysts in the reactor can enable chemical equilibrium [42]. To take into consideration the various multistep physical and chemical interactions between the components in gasifiers, the kinetic approach has to be considered. This approach is based on the estimation of the yield and composition of the final product obtained from gasification after a finite period of time or at a specific location in the reactor [17]. Moreover, it takes into account various factors such as the reaction kinetics, hydrodynamics of the bedzone, residence time of the gas and the reactor geometry. This approach should be used to build models which can be more realistic when compared to gasifiers in use.

Aspen Plus® modelling involves specifying the components involved, followed by developing the process flowsheet and finally running the simulation. Biomass is usually defined as non-conventional component (compound whose chemical formula is not defined) described by its proximate and ultimate analysis, which does not participate in the simulation unless it gets broken down into its conventional constituents (C, H_2, O_2, S, N_2, Cl, H_2O). Different property methods can be chosen for simulating biomass gasification in Aspen Plus®. The most common property method used for accurate determination of thermodynamic properties in gasifier models in literature is the Peng-Robinson EOS (Equation of State) as used in [58] [59] [60] due to better determination and correlation of vapor pressures of pure components at high temperature. Moreover, it is possible to use different methods for different parts of the process such as selection of Peng-Robinson as base method and UNIQUAC activity coefficient method for better accuracy in Vapor-Liquid Equilibrium (VLE) as selected for gas cleaning in [58]. Another commonly used method is the RK-Aspen (Redlich-Kwong EOS) as in [42] which is also stated to be suitable for hydrocarbon processing applications [42].

The density and enthalpy of biomass is estimated with the help of built-in models in Aspen Plus®: DCOALIGT and HCOALGEN, respectively [17]. As discussed, in Section 2.6, the gasification process can be divided into four main sections: drying, pyrolysis/devolatilization, combustion and reforming followed by gas cleaning. The use of the various blocks available in Aspen Plus® for developing each section in the flowsheet depends on the complexity of the overall process.

Though many gasifier models are based on equilibrium approach, the focus here is on studying models developed in Aspen Plus® based on kinetic approach. A number of gasifier models based on kinetic approach have been considered for this purpose [61] [42] [44] [59] [62]. These are presented in Appendix C.

3. MATERIALS AND METHODS

This section describes the Indirectly Heated Bubbling Fluidized Bed Steam Reformer (IHBFBSR) setup at TU Delft and the materials used to carry out gasification tests in the IHBFBSR. The IHBFBSR is a BFB gasifier setup which operates at atmospheric pressure (P ~1 atm) and at temperatures between 700°C-850°C. This gasifier was established at TU Delft by collaboration with the Dutch company Petrogas Gas-Systems.

3.1 Gasification set up

The gasifier setup at TU Delft can be divided into five sections: -

- Feeding section
- Gasifying agent heating section
- Reaction section
- Burner section
- Gas and Tar Analysis Section
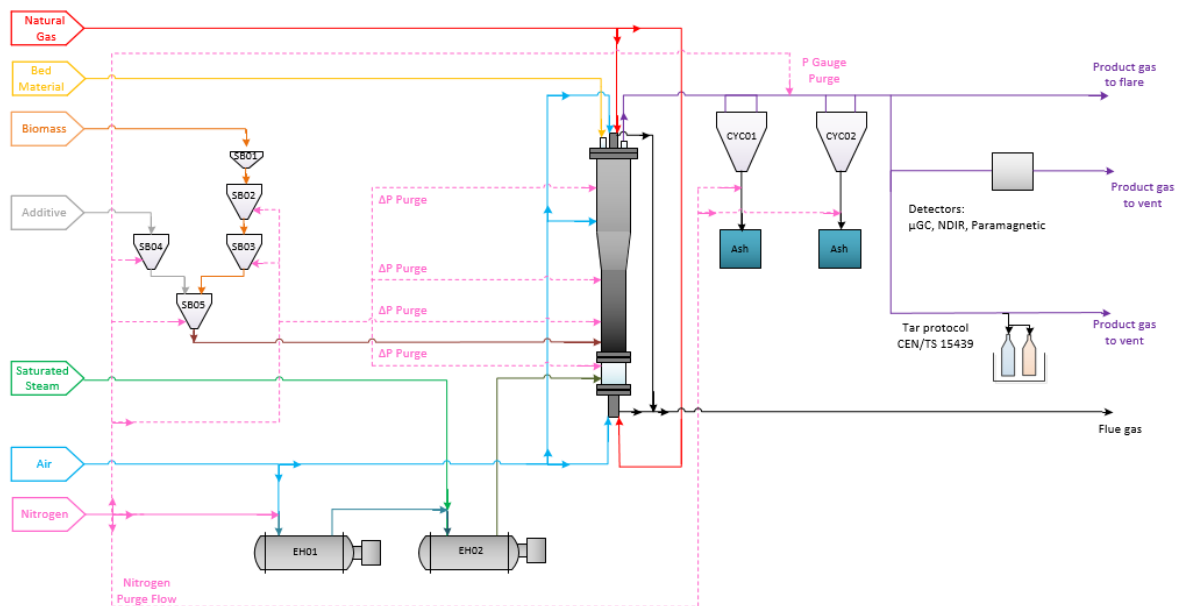
Figure 25: Schematic Representation of IHBFBSR setup at TU Delft

Figure 25 provides a schematic representation of the IHBFBSR setup at TU Delft. A description of the various sections in the gasifier setup are given below: -

➢ The feeding section consists of two bunkers; one for biomass feed and the other for additives. SB01, SB02, SB03, SB04 and SB05 represent the bunkers. SB01 is a funnel which is used to refill biomass during the experiment. SB02 and SB03 are the feeding bunkers for biomass. SB02 is pre-filled with biomass and the valve is opened for feeding the biomass during the experiment whenever there is an indication of most of the biomass been used. The biomass passes through intermediate bunker SB03 which is pressurized by nitrogen, to maintain inert feeding conditions. SB04 is the bunker

which is used for the additives. Additives are commonly used to avoid agglomeration when the biomass is not clean (biomass with high percentages of ash, nitrogen, sulphur or chlorine). In the IHBFBSR setup, generally clean biomass is used, hence there has been no requirement of using additives. The mixture of biomass, nitrogen and additives (optional) passes through SB05 and is fed through a screw feeder to the reactor. To avoid blockages in the feeding section, it is assured that the fan of the screw feeder is turning and there is sound as biomass falls into the bunkers where it is mixed with additives and nitrogen.

➢ The heating section is where the gasifying agents, which for the IHBFBSR setup, is a mixture of air and steam, are preheated before entering the reactor by means of two preheaters EH01 and EH02. Air from T=20°C is heated in the first pre-heater to 150°C. Steam from T=158°C is mixed with the heated air from the first pre-heater and fed to the second pre-heater, where it is heated to 607.5°C. The capacities of the two pre-heaters are 4.5kW and 6kW, respectively. N_2 also passes through the first preheater but it is used only for heating up the set up. This is the reason why N_2 is not heated in the first preheater for the model.

➢ The reaction section is where gasification takes place. The air-steam mixture passes through the wind box and is introduced below the reactor, with the biomass fed above the distributor plate. For the experiments 75 kg of bed material are used, which is also fed to the reactor from top prior to starting the experiments. The gasifier setup can be divided into the bed zone (dense phase) and the freeboard (bubble phase). The bedzone consists of the C-100 burner and the freeboard consists of the C-80 burner. The temperature in the bedzone and freeboard regions of the gasifier can be determined with the readings of seven thermocouples present in the respective regions as shown in Figure 8. The freeboard has variable diameter along its length, due to the geometry of the gasifier and the presence of C-80 burner. The diameter of the bedzone, gas-bed and freeboard regions with respect to height is shown in Table 14.

➢ The burner section is made of two radiant tube burners situated at the top and bottom of the gasifier. Natural gas is combusted with air for generation of heat in the burners. The air is preheated with flue gasses up to 60% of the combustion temperature in a counter current manner [16]. They are self-recuperative ceramic burners, made of silicon carbide (SiC) which operate at a temperature of 1250 °C. The bottom burner operates at a nominal capacity of 20 kW. The top burner operates at a nominal capacity of 12 kW.

➢ The fifth section of the gasifier setup is the gas and tar analysis section. A small sampling flow of the product gas is directed to the analysis section after separating the solids in the cyclone separator and the rest is combusted in a flare. The sample taken for analysis passes through a heated filter for removal of any solids left. After the filter the line is split into 2 parts:

- For tar sampling according to the tar protocol CEN/TS 15439. During the experiment, the samples with the tars are collected. They are analysed after the experiments using Gas-Chromatography with Flame Ionization Detector (GC-FID).

- For the gas analysis there is a water-cooled condenser and a secondary condenser composed by 4 bottles in an ice bath. 3 bottles are filled with isopropanol to ensure tar removal and 1 bottle is filled with silica gel to ensure moisture removal, followed by a paper filter and a pump. From there the product gas enters the Micro Gas Chromatography (µ-GC) for determination of CO, CO_2, H_2, CH_4 and N_2. After this the gas is split into 2 lines to the Non- Dispersive InfraRed (NDIR) spectroscopy - with specific interest in CO and CO_2 detection and the O_2 detector.

3.2 Materials Used

Experiments have been conducted with two different types of biomass, the Premium Green (GB) and Excellent Red (RB). These biomass types are supplied by the company Labee Group Moerdijk B.V and are shaped as pellets with a mean diameter of 6 mm and length in the range between 50 mm and 250 mm approximately. They are categorised as Class-A wood, with low level of contaminants and absence of screws, nails or other additional timber material. GB is sourced from secondary and tertiary forestry in the Netherlands, while RB is sourced from Scandinavian countries or Russia. The two types of biomass used for the experimental tests are characterised by their proximate and ultimate analysis. The proximate and ultimate analysis for GB and RB is given in Section 4.1.3. Also, particle size distribution (PSD) experiments have been conducted for these biomass types. The PSD obtained are presented in Section 4.1.3, while the procedure followed to perform the tests is presented in Section 3.3.

The bed material used for the tests is corundum, aluminium oxide Al_2O_3. Corundum typically forms unique shapes such as barrel-shaped prisms or hexagonal plates. Al_2O_3 corundum is categorised as 9 on the Mohs hardness scale [63], which makes it one of the most durable material. The bed material is provided by the company Unicorn ICS B.V and can be supplied in different grain size. For the project two different particle size are considered: 591 µm (Bed F046) and 492 µm (Bed F054). The PSD of the two-bed material types was performed by a former student by using a MicroTrac S3500. The tests have been carried out in triplicate. The results are presented in Section 4.1.3. The abovementioned values represent the weighted average of the values obtained experimentally. The data required for calculation for the weighted average is given in Table 11.

Table 6 shows the real density, bulk density and mean diameter of bed material used.

Table 6: Real Density, Bulk Density and Mean Particle Diameter of Bed Material Used

Bed Material	ρ_{real} (kg/m³)	ρ_{bulk} (kg/m³)	D_p (µm)
F046	3950	1636	591
F054	3950	1665	492

3.3 Particle size distribution (PSD) determination

The PSD determination was performed with a sieving vibration plate equipped with eight sieves (4.75 mm, 4 mm, 3.15 mm, 1.4 mm, 0.85 mm, 0.71 mm, 0.6 mm and 0.5 mm).

For performing PSD, four equipment were used: -

- Sieving Vibration Plate
- Weighing scale
- Sieves
- Selected material
- Cloth for cleaning

The material considered were: -

- the two biomasses: GB and RB (a bag of 15kg of each biomass);
- biochar obtained from tests (bed zone) with same input parameters and different biomass types: GB and RB (performed by sieving 75 kg of bed material + biochar obtained in the experiments)

The procedure adopted is presented following: -

First, the sieves were cleaned with paper and weighed on the weighing scale. The sieves are then arranged on the sieving vibration plate with the largest sieve (4.75 mm) on top and the sieve having the smallest gap (0.5 mm) at bottom. A clean container is taken and its weight is measured and noted. A sample of biomass/bed material whose PSD is to be determined is taken in the container. The sample is evenly distributed on the top most sieve placed on the sieving vibration plate. The sieves are placed on a large open plate at the end for support. The empty weight of this plate is also noted after cleaning. It is ensured that the sieves are sealed to be held tightly in position during vibration. If the setup is not sealed properly, it can result in lot of noise during vibration. Moreover, since the vibration plate does not have a closed bin at the end, there is a possibility of sample loss from the distance between the sieves, and from the gaps between the bottom of the last sieve and the open plate. This should be avoided to get an accurate PSD measurement. Therefore, it is required to seal the sieves to ensure minimum gaps between the sieves and the bottom plate. The amplitude of the sieving vibration plate is set to 0.65 mm/g. GB and RB were observed to have large particle sizes. Hence, to get accurate distribution of particles in all sieves, it was decided to vibrate this setup for four minutes. While performing PSD for finer particles, a lower time span can be selected for each run. The time span selected for each run while performing the PSD for bed material mixed with char was two minutes. This is also done to ensure that the char particles do not break because of longer duration of vibration. This process is repeated for the entire sample of biomass/bed material.

The PSD performed for both types of corundum shows that the particles have a range of size. However, due to modelling limitations, it was not possible to implement the PSD for bed material in Aspen Plus®. Hence, it is assumed that the particles of each bed material are spherical in nature, and are of the same diameter.

4. MODEL DEVELOPMENT

The main objective of this research is to optimize and validate the kinetic model developed for the IHBFBSR by a former student for his thesis work [16]. The kinetic model is built using the software Aspen Plus®. Appendix D gives the flowsheet diagram for the reference model and gives a description of determination method of the various pyrolysis products yield in the Fortran Code in the reference model which is used for our model. Section 4.1 describes the new model with the optimization procedure followed in the attempt to develop a robust model to predict the behaviour of the IHBFBSR under various operating conditions. Section 4.2 gives an overview to the methodology adopted for performing the sensitivity analyses and the chemical reactions considered in the burner for generating heat from the recycle stream.

4.1 Optimized Model Description

The reference kinetic model is optimized and the product composition obtained from the new model is validated with the latest experimental results from gasification tests conducted in the IHBFBSR. The Aspen Plus® flowsheet of the new model is given in Figure 26.
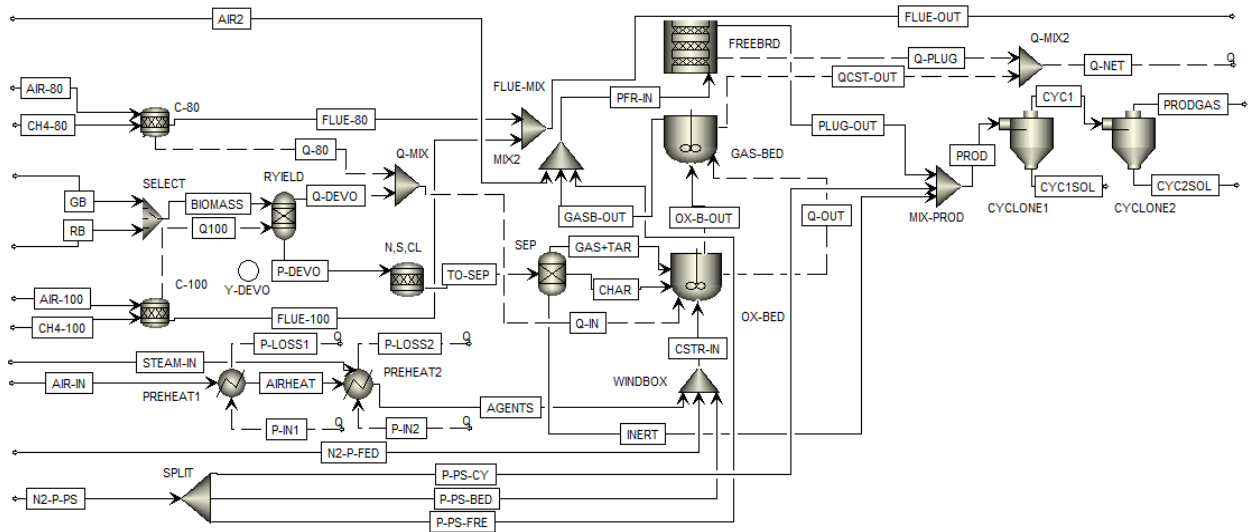
Figure 26: Aspen Plus® flowsheet of the New Kinetic Model of the IHBFBSR

4.1.1 Assumptions Considered for the Model

This section states all the assumptions which are taken into account in the new model.

➢ Biomass is considered as a non-conventional solid in Aspen Plus®.

➢ Ash produced during biomass pyrolysis is considered as a non-conventional inert solid.

➢ Char is assumed to be a conventional solid consisting of only carbon (graphite).

➢ The property method (EOS) chosen to model the gasification process is Peng-Robinson equation of state (Peng-Rob), due to its popularity in literature studies as seen in Section 2.10.

➢ Different degrees of complexity can be adopted for the modelling of the reactor hydrodynamics. Assuming a uniform distribution of gas and solid phases in the bedzone, it is chosen to adopt a zero-dimensional stirred tank reactor to represent the fluid dynamics in the bedzone. Since mainly gas phase is present in the freeboard region with limited axial mixing, it is chosen to model the freeboard as a one-dimensional PFR. Additionally, in the model, it is assumed that the oxidation reactions occur faster as compared to the reforming reactions because of higher reactivity of oxygen with the reactants as compared to steam, hence it is decided to add a third reactor (defined as gas-bed in the model) to simulate oxidation reactions occurring first in the bedzone, followed by reforming and phenol cracking reaction in the gas-bed. With secondary air supplied to the freeboard, both oxidation and reforming reactions are taken into account in the freeboard. It is chosen to simulate the gas-bed as a RCSTR block in Aspen Plus® having uniform mixing pattern similar to the bedzone.

➢ The kinetic parameters for the gasification reactions are taken from the literature. The reaction rates have been determined by experiments conducted on woody biomass at process conditions similar to the IHBFBSR.

➢ Due to limited time span, mass transfer limitations concerning the heterogenous char gasification reactions have not been investigated; it has not been taken into consideration in the model. A Shrinking Density Model for char conversion without mass transfer limitations has been considered.

➢ The model is operated at steady state, isothermal conditions with a constant specified temperature in each reactor block. The steady state conditions are for one hour.

➢ It is assumed that biomass reacts completely in the pyrolysis step forming gases, tar and char leaving no unreacted biomass.

➢ Only CO, CO_2, H_2 and CH_4 are the gaseous products formed during pyrolysis. The formation of higher hydrocarbons like C_2H_4 is not considered for the model.

➢ N_2, Cl and S in biomass are assumed to react completely to NH_3, HCl and H_2S and do not take part in the gasification reaction. Hence, they are assumed as inert.

➢ The PSD for the two biomass types and the corresponding char and ash generated have been taken into account in this model, hence the stream class in Aspen Plus® is specified as MCINCPSD[1] (Considering mixed, conventional and non-conventional streams with PSD).

➢ The tars generated during biomass pyrolysis is assumed to be phenol. It is also considered that phenol undergoes cracking in the gasifier to generate more tars: benzene and naphthalene.

---

[1]MCINCPSD - This is the stream class used in Aspen Plus® when conventional solids (homogenous solids with a definite molecular weight and chemical formula) and non-conventional solids (heterogenous solids without a definite molecular weight and chemical formula) are present in the model with PSD available for both type of solids.

> ➢ The cyclone separators are assumed to remove all solids from the product gas obtained from the gasifier.

4.1.2 Description of the Flowsheet of New Model

The Aspen Plus® flowsheet of the new kinetic model of the IHBFBSR is given in Figure 26. The model is developed to predict the performance of the IHBFBSR setup which receives heat required for gasification from two radiant tube burners located at the top and bottom of the gasifier. These are depicted in Aspen Plus® by two stoichiometric reactors labelled as C-80 and C-100. Due to modelling limitations, it has not been possible to model these burners as a part of the gasifier as is present in the actual gasifier setup. The feed selection is done with the use of a selector block in Aspen Plus® which chooses to run the simulation with GB or RB as the biomass type. The heat from the bottom burner C-100 is fed to the pyrolysis reactor represented by RYield block. The heat generated from the RYield block and the top burner C-80 together supply heat required for the gasification reactions. The pyrolysis yield reactor simulates the devolatilization process taking place in the IHBFBSR based on input from an external calculator block labelled as Y-Devo. The calculator block takes two inputs: pyrolysis temperature from the RYield block, and biomass type from the selector block and calculates the mass yields of H_2, CO, CH_4, CO_2, H_2O, tar and char fraction. The calculation of the mass yield of different fractions is implemented in a Fortran Code written in the calculator block. The heating section of the IHBFBSR setup explained in Section 3.1 is modelled by using two preheaters named as Preheat 1 and Preheat 2 in the model. A mixture of air and steam is used as the gasification agent. Air is heated to a temperature of 150°C in the first preheater, and the heated air along with incoming steam is heated to a temperature of 607.5°C in the second preheater. The heated agent is then sent to the gasification section. The N_2 purge stream has been divided into two main streams. The first stream is mixed with the gasification agent and introduced into the bedzone. The second stream is further split into three main streams, with one stream going to the bedzone region of the gasifier, the second stream going to the freeboard region and the third stream being sent to the cyclones. The N_2 purge streams have been modelled in this manner to reflect the nitrogen flows in the actual gasifier setup. The output stream from the pyrolysis section passes through a stoichiometric reactor block where N_2, Cl and S present in the stream from biomass reacts completely to form NH_3, HCl and H_2S, respectively. These have been assumed to be inert and do not participate in the gasification reactions. The output stream from the stoichiometric reactor block for N_2, Cl and S conversion passes through an ideal separator block which separates the incoming stream into gas+tar, char and inerts. The gasification section is modelled as a combination of three reactor blocks in Aspen Plus®. The visualisation of the IHBFBSR with its corresponding division into three sections in Aspen Plus® is given in Figure 28. The three sections considered for modelling purpose are the bedzone, the gasbed and the freeboard. The bedzone is modelled by an RCSTR block hosting the oxidation reactions. As discussed in Section 3.2, for the experiments conducted in the IHBFBSR whose results have been used to validate the model, there are two different types of bed material that have been used: F046 and F054. The calculation of the volume of the RCSTR representing the bedzone, based on the selection of the bed material type is described in Section 4.1.6. The gasbed is modelled by another RCSTR block which hosts the cracking and reforming reactions. For certain experiments used to validate the model, secondary air has been fed to the freeboard region to facilitate cracking of tar. Hence, a secondary air stream is mixed with the outlet of the gas-bed and the N_2 purge stream and fed to the freeboard which is modelled by an RPlug reactor block. It is usually expected that the

freeboard region mainly hosts the reforming reactions because the reactants present in the gasifier would have already undergone oxidation, thus consuming all oxygen, however due to the addition of secondary air, it has been considered to include both oxidation and reforming reactions in the freeboard reactor block. The temperature specification of the different gasifier sections is taken from thermocouple measurements present at different heights in the gasifier setup. The product gas obtained from the RPlug reactor block is mixed with N_2 purge and inerts stream and fed to the two cyclone separators which separate unreacted char and ash from the product stream and provide a solids-free synthesis gas. The joint efficiency of the two cyclone separators is assumed to be 100%. The flue gas generated from the combustion of natural gas in the burners is released to the atmosphere after taking into account its suitability in terms of the acceptable limits for emission.

4.1.3 Proximate Analysis, Ultimate Analysis and Particle Size Distribution (PSD)

The proximate and ultimate analysis for GB and RB along with its HHV and bulk density is given in Table 7.

Table 7: Proximate and Ultimate Analysis for RB and GB with bulk density and experimental determination of HHV [16]

Component	RB	GB	Unit
Ultimate Analysis			
C	47.88 ± 0.08	48.41 ± 0.02	wt % (daf)
H	6.44 ± 0.07	6.02 ± 0.02	wt % (daf)
O	45.62 ± 0.02	45.26 ± 0.02	wt % (daf)
N	0.06 ± 0.01	0.30 ± 0.03	wt % (daf)
S	0.010 ± 0.001	0.010 ± 0.001	wt % (daf)
Proximate Analysis			
Moisture	5.57 ± 0.11	5.08 ± 0.05	wt % (ar)
VM	79.90 ± 0.81	75.22 ± 0.47	wt % (ar)
FC	14.07	19.00	wt % (ar)
Ash	0.46 ± 0.12	0.69 ± 0.03	wt % (ar)
HHV experimental	19.5 ± 0.02	18.89 ± 0.1	MJ/kg
Bulk Density	616 ± 7	625 ± 5	kg/m^3

PSD determination has been performed for biomass and biochar. The PSD for ash and bed material which have been performed earlier by former students are also available to be implemented in the model. The procedure for performing the PSD experiments is given in Section 3.3. The PSD for GB, RB, char and ash generated for each biomass in given in Table 8, 9 and 10 respectively.

The PSD along with their proximate and ultimate analysis for biomass is fed into the stream lines for GB and RB before the selector. The PSD for the specific char and ash is fed into RYield pyrolysis reactor block in Aspen Plus®. The PSD for ash is defined under NCPSD

(Non-Conventional Solid with PSD). The PSD for char is defined under CIPSD (Conventional Inert Solid with PSD).

Table 8: PSD for Green Biomass (GB) and Red Biomass (RB)

RANGE [μm]	%wt	
	GB	RB
<500.0	$5.98 \cdot 10^{-01}$	$7.65 \cdot 10^{-01}$
500.0-600.0	$4.60 \cdot 10^{-02}$	$7.85 \cdot 10^{-02}$
600.0-710.0	$1.07 \cdot 10^{-01}$	$2.94 \cdot 10^{-01}$
710.0-850.0	$7.66 \cdot 10^{-02}$	$9.81 \cdot 10^{-02}$
850.0-1400	$1.03 \cdot 10^{+00}$	$1.31 \cdot 10^{+00}$
1400.0-3500.0	$2.10 \cdot 10^{+00}$	$2.33 \cdot 10^{+00}$
3500.0-4000.0	$1.35 \cdot 10^{+00}$	$1.12 \cdot 10^{+00}$
4000.0-4750.0	$1.29 \cdot 10^{+00}$	$5.88 \cdot 10^{-01}$
4750.0-6000.0	$9.34 \cdot 10^{+01}$	$9.34 \cdot 10^{+01}$

Table 9: PSD for Char (GB) and Char (RB)

RANGE [μm]	%wt	
	Char(GB)	Char(RB)
124.5-500.0	$2.51 \cdot 10^{+01}$	$5.35 \cdot 10^{+01}$
500.0-600.0	$4.61 \cdot 10^{+00}$	$4.75 \cdot 10^{-01}$
600.0-710.0	$5.49 \cdot 10^{+00}$	$5.93 \cdot 10^{-01}$
710.0-850.0	$3.79 \cdot 10^{+00}$	$0.00 \cdot 10^{+00}$
850.0-1400	$4.20 \cdot 10^{+00}$	$8.66 \cdot 10^{+00}$
1400.0-3500.0	$9.10 \cdot 10^{+00}$	$1.92 \cdot 10^{+01}$
3500.0-4000.0	$9.22 \cdot 10^{+00}$	$1.10 \cdot 10^{+01}$
4000.0-4750.0	$1.18 \cdot 10^{+01}$	$1.78 \cdot 10^{+00}$
4750.0-6000.0	$2.67 \cdot 10^{+01}$	$4.75 \cdot 10^{+00}$

Table 10: PSD for Ash (GB) and Ash (RB)

RANGE [μm]	%wt	
	Ash(GB)	Ash (RB)
4.62-5.50	-	$2.07 \cdot 10^{-01}$
5.50-6.54	$2.40 \cdot 10^{-01}$	$4.97 \cdot 10^{-01}$
6.54-7.78	$5.33 \cdot 10^{-01}$	$8.13 \cdot 10^{-01}$
7.78-9.25	$8.70 \cdot 10^{-01}$	$1.27 \cdot 10^{+00}$
9.25-11.00	$1.31 \cdot 10^{+00}$	$1.76 \cdot 10^{+00}$
11.00-13.08	$1.98 \cdot 10^{+00}$	$2.43 \cdot 10^{+00}$
13.08-15.56	$2.76 \cdot 10^{+00}$	$3.27 \cdot 10^{+00}$
15.56-18.50	$3.72 \cdot 10^{+00}$	$4.67 \cdot 10^{+00}$
18.50-22.00	$5.52 \cdot 10^{+00}$	$7.32 \cdot 10^{+00}$
22.00-26.16	$7.96 \cdot 10^{+00}$	$1.01 \cdot 10^{+01}$
26.16-31.11	$1.06 \cdot 10^{+01}$	$1.13 \cdot 10^{+01}$
31.11-37.00	$1.23 \cdot 10^{+01}$	$1.13 \cdot 10^{+01}$
37.00-44.00	$1.17 \cdot 10^{+01}$	$1.03 \cdot 10^{+01}$
44.00-52.33	$9.92 \cdot 10^{+00}$	$9.11 \cdot 10^{+00}$

52.33-62.23	$7.54 \cdot 10^{+00}$	$7.26 \cdot 10^{+00}$
62.23-74.00	$5.78 \cdot 10^{+00}$	$5.10 \cdot 10^{+00}$
74.00-88.00	$5.10 \cdot 10^{+00}$	$3.79 \cdot 10^{+00}$
88.00-104.70	$4.85 \cdot 10^{+00}$	$3.23 \cdot 10^{+00}$
104.70-124.50	$4.13 \cdot 10^{+00}$	$3.00 \cdot 10^{+00}$
124.50-148.00	$2.39 \cdot 10^{+00}$	$2.19 \cdot 10^{+00}$
148.00-176.00	$8.03 \cdot 10^{-01}$	$9.77 \cdot 10^{-01}$
176.00-209.30	-	$1.13 \cdot 10^{-01}$

Unfortunately, the PSD determinations for bed material F046 and F054 could not be implemented in Aspen Plus® due to modelling difficulties. It is still taken into account for determining the average mean diameter of the bed material particle size used in the first CSTR in Aspen Plus® depending on the type of bed material chosen. The formula for calculating the same is given by Eq 4.7 in Section 4.1.6.

The PSD for the bed material is given in Table 11.

Table 11: PSD for bed material F046 and F054

Range [μm]	Average [μm]	wt%	
		F046	F054
124.5-148.0	136.25	$0.00 \cdot 10^{+00}$	$1.20 \cdot 10^{-01}$
148.0-176.0	162.00	$0.00 \cdot 10^{+00}$	$3.67 \cdot 10^{-01}$
176.0-209.3	192.65	$2.57 \cdot 10^{-01}$	$8.13 \cdot 10^{-01}$
209.3-248.9	229.10	$7.47 \cdot 10^{-01}$	$1.55 \cdot 10^{+00}$
248.9-296.0	272.45	$1.77 \cdot 10^{+00}$	$3.37 \cdot 10^{+00}$
296.0-352.0	324.00	$3.91 \cdot 10^{+00}$	$8.20 \cdot 10^{+00}$
352.0-418.6	385.30	$7.62 \cdot 10^{+00}$	$1.76 \cdot 10^{+01}$
418.6-497.8	458.20	$1.37 \cdot 10^{+01}$	$2.60 \cdot 10^{+01}$
497.8-592.0	544.90	$2.22 \cdot 10^{+01}$	$2.28 \cdot 10^{+01}$
592.0-704.0	648.00	$2.52 \cdot 10^{+01}$	$1.23 \cdot 10^{+01}$
704.0-837.2	770.60	$2.08 \cdot 10^{+01}$	$4.31 \cdot 10^{+00}$
837.2-995.6	916.40	$3.76 \cdot 10^{+00}$	$1.59 \cdot 10^{+00}$
995.6-1184.0	1089.80	$0.00 \cdot 10^{+00}$	$6.47 \cdot 10^{-01}$
1184.0-1408.0	1296.00	$0.00 \cdot 10^{+00}$	$1.60 \cdot 10^{-01}$
1408.0-1500.0	1454.00	$0.00 \cdot 10^{+00}$	$1.57 \cdot 10^{-01}$

4.1.4 Mass Balance in Fortran File

The Fortran code calculates the mass yields of the devolatilization products based on experimental results derived at different pyrolysis temperature for each type of biomass. As discussed in the assumptions, biomass is considered to devolatilize completely to form gases, tar and char. The conversion of biomass feed into solid, liquid and gaseous fraction with their method of determination in the model is illustrated in Figure 27.
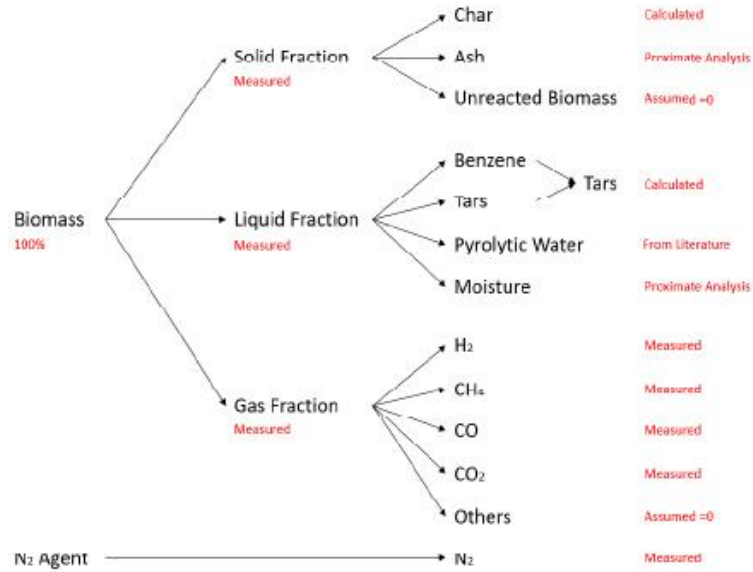
Figure 27: Biomass Pyrolysis Products assumed in Model and their method of determination [16]

The mass yields of solid fraction, liquid fraction and gas fraction, along with the yields of specific components of the gas fraction (CO, H_2, CH_4, CO_2) have been taken from experimental results from tests conducted in the CDS Analytical Pyroprobe 5000 Pyroprobe apparatus at a heating rate of 600°/s and at temperatures of 600°C, 700°C, 800°C, 900°C and 1000°C. These experiments are categorized to be performed under fast pyrolysis conditions, with a residence time (hold time) of 12 seconds. The pyrolysis step is modelled based on the results obtained from these experiments as they are in resemblance to the conditions expected to exist in the IHBFBSR. The experimentally determined mass % of the solid, liquid and gaseous fraction can be found in Appendix E.

As it can be seen from the Pyroprobe results for the experiments, the mass balance does not close. Around 20-30% of the mass balance is not accounted for in each experiment. The Fortran code implemented in the Y-Devo calculator block in Aspen block® takes into account this mass deviation. According to the study on fast pyrolysis of woody biomass in the Pyroprobe reactor by Christos Tsekos [64], the mass deviation can be contributed by all three fractions; the gaseous, liquid and solid fraction. The most plausible reason can be attributed to the measurement of liquid fraction; mostly from the ineffective condensation of vapours to liquids and the ineffective dissolution of liquids in iso-propanol for analysis of the liquid fraction. Only CO, CO_2, H_2 and CH_4, contributing to the gaseous yield is measured experimentally and used for modelling purpose. The inability of the μ-GC to determine higher volatile hydrocarbons such as ethylene (C_2H_4) and propylene (C_3H_6) contributing to the gaseous yield, especially at higher temperatures can also contribute to this mass deviation. According to [64], the percentage of higher hydrocarbons can account for almost 5% weight of the biomass feed on a dry basis. The pyrolytic water is not accounted for on an experimental basis due to the non-availability of the required apparatus, which could make up for 10-12% of the biomass feed on dry basis [64], and is assumed from literature by an empirical relation. Finally, human error can always be a possibility in experimental measurements of the solid, liquid and gases obtained during pyrolysis.

For this reason, the mass yields (in %) of the solid, liquid and gaseous fraction obtained from the experiments in Pyroprobe apparatus are normalized to 100%, and the corresponding normalized mass yields of H_2, CO, CO_2 and CH_4 along with solid and liquid fraction is calculated and implemented in MATLAB®. Based on the experimental percentage of the gas, solid, liquid fraction and of specific gaseous components from pyrolysis, the yield curves have been generated as a function of pyrolysis temperature for each biomass. The coefficients of the mass yield of pyrolysis products as a function of temperature are derived from the best fit curves described by a 4th degree polynomial in MATLAB®. Appendix F describes the coefficients obtained for the optimized model from MATLAB® using polyfit function. The mass yields of H_2, CO_2, CH_4, CO, liquid fraction and solid fraction as a function of temperature are described by the polynomial function in Eq 4.1 [16]. Here Y_i denotes the mass yields of particular component i; a, b, c, d, e are the coefficients obtained from MATLAB®.

$$Y_i = aT^4 + bT^3 + cT^2 + dT + e \qquad \text{(Eq 4.1)}$$

The consideration of ash, pyrolytic water, char and water vapour in the Fortran Code is based from the reference model. This is given in Appendix D.

4.1.5 Phenol as Model Tar in Fortran Code

The new model considers phenol as the model tar compound instead of four lumped tar groups (with benzene, toluene, naphthalene and phenol representing the four groups of tars) used in the reference model for the pyrolysis block RYield. The reason for choosing phenol over four lumped tar groups (even though lumped tars is expected to have a greater accuracy in terms of representing the tar formation during biomass gasification) is explained in this section. Initially, the consideration of four lumped tar groups was made for the new model. However, it was observed during validation that the tar fraction produced in the synthesis gas from the model was much higher than the tar fraction analysed from the experiments. The most possible cause for this overestimation was assumed to be the reason, that at that stage normalization of the mass yields was not implemented in the Fortran Code, and the entire mass loss observed in Pyroprobe results was attributed to the liquid fraction, of which tar constituted a major part. This issue was resolved by normalizing the solid, liquid and gaseous yields from pyrolysis as described in Section 4.1.4. The tar samples from the Pyroprobe experiments have not been analysed experimentally, due to limited time span. For analysing the tar obtained from gasification tests used for validation, the GC-FID technique was used. According to [64], phenol is the most predominant tar species among others from biomass pyrolysis which is measured experimentally in the temperature range of 700-900°C. This is similar to the temperature range for which the model is validated. A clear conclusion regarding the behaviour of phenol at high temperatures in terms of decomposition to polyaromatics like naphthalene or acceleration in secondary reactions and increased lignin formation leading to increase in the production of phenol has not been made in [64]. However, the trends derived from experimental results for pyrolysis show that phenol possibly cracks into polyaromatic species like naphthalene at higher temperatures in the range specified before [64]. These reasons have led to the assumption of phenol as a model tar compound in the Fortran File. The phenol cracking reaction is implemented in the gasifier model. According to the chemical reaction, phenol cracks into benzene, naphtha, hydrogen and methane during gasification process. The cracking reaction is specified in Table 15 describing the list of reactions used in the model.

The Fortran Code implemented for the optimized model is given in Appendix G.

4.1.6 Bedzone, Gas-Bed and Freeboard
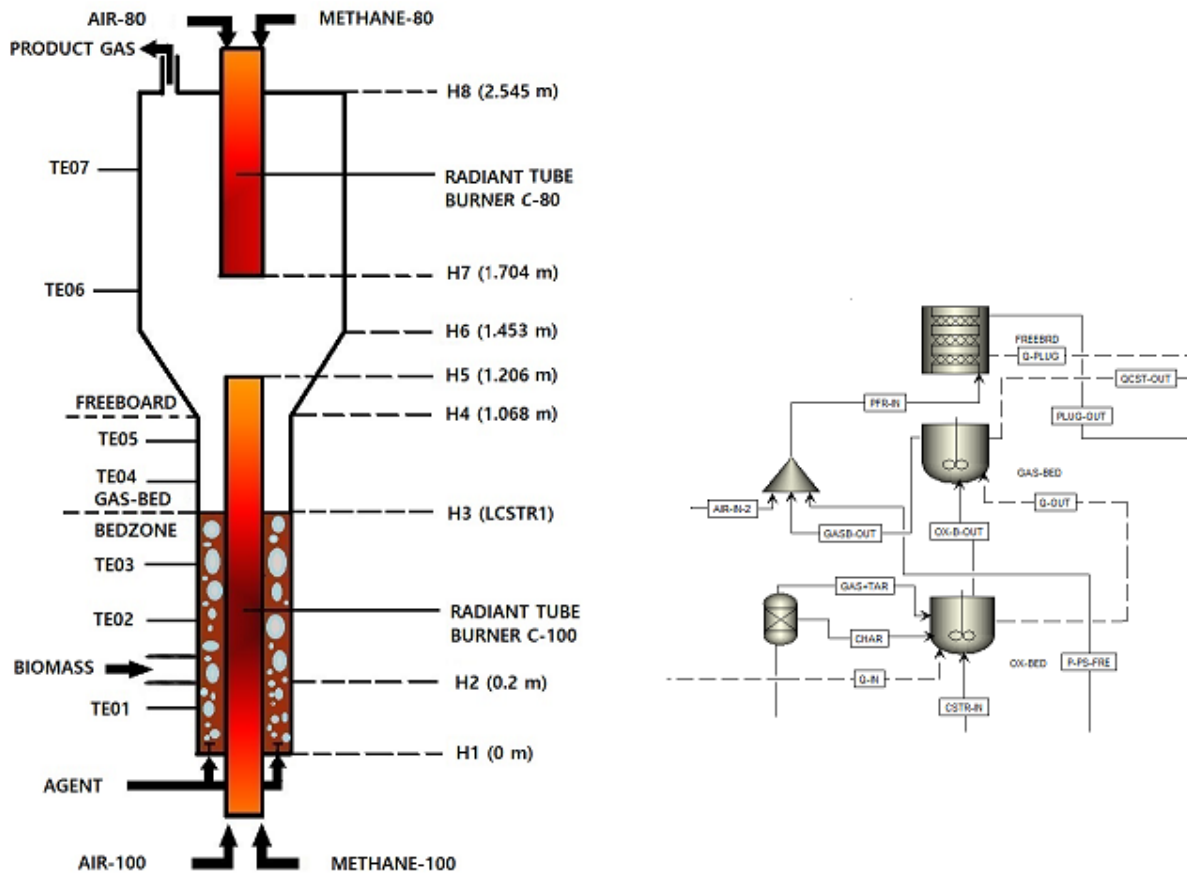
Figure 28: Visualization of the IHBFBSR setup and its division into bedzone (ox-bed), gas-bed and freeboard in Aspen Plus®-modelling the setup in Aspen Plus®

Figure 28 represents the visualization of the IHBFBSR and the subsequent manner in which it is modelled in Aspen Plus®. The bedzone is modelled as a CSTR. The region above the bedzone upto height H4 in the gasifier setup is modelled as a second CSTR assuming uniform mixing pattern. The total volume of two CSTR's (gasifier height upto H4) is measured to be 65.7 l. The volume of first CSTR and the bedzone height denoted by L_{CSTR1} in Figure 28, is based on the type of bed material selected for gasification. The volume of the second CSTR is calculated by subtracting the volume of the first CSTR from the total volume. The two bed material types used for the experiments are F054 and F046. The bedzone operates at atmospheric pressure. The pressure used in the gas-bed and freeboard region is specified based on the outlet pressure of the product gas obtained from each experiment used for validation. The temperatures determined by the thermocouples for the bedzone, gas-bed and freeboard are provided in Table 18.

The reactor volume of the first CSTR is considered to be equal to the volume of the vapor phase in the bedzone. This equals the volume of the bedzone at fluidization minus the volume occupied by the solid bed material. At minimum fluidization, it is assumed that the bed material expands with a factor of 1.2 with respect to fixed bed configuration, irrespective of the type of

bed material [16]. It is also assumed that the cross-sectional area of the bedzone remains constant hence the increase in volume due to fluidization is seen as increase in the bedzone height. This is represented by Eq 4.2 and 4.3.

$$V_{fluid} = L_{fluid} A_{Reactor} \qquad \text{(Eq 4.2)}$$

$$L_{fluid} = 1.2 L_{fixed} \qquad \text{(Eq 4.3)}$$

The cross-sectional area of the reactor is calculated from the mean hydraulic diameter given by Eq 4.4.

$$A_{Reactor} = 0.25\pi D_{Reactor}{}^2 \qquad \text{(Eq 4.4)}$$

As it can be seen in Figure 28, the radiant tube burner C-100 is present along the entire length of the bedzone, resulting in a constant diameter across the height of the bedzone. The constant mean hydraulic diameter of the reactor for the bedzone is calculated by Eq 4.5.

$$D_{Reactor} = \sqrt{D_{in}{}^2 - D_{burn}{}^2} \qquad \text{(Eq 4.5)}$$

D_{in} represents the inner diameter of the bedzone and is measured to be equal to 346 mm. D_{burn} represents the diameter of the burner in the bedzone which is equal to 150 mm. Hence, from Eq 4.5, the mean hydraulic diameter of the bedzone equals to 311.8 mm. A total of 75 kg of bed material is used for the experiments. Table 6 shows the real and bulk densities of the bed material F046 and F054. This can be used to calculate the voidage factor of each bed material type in fixed regime. This is denoted by Eq 4.6.

$$\epsilon_{Fixed} = 1 - \frac{\rho_{bulk}}{\rho_{real}} \qquad \text{(Eq 4.6)}$$

The diameter of each bed material is calculated from the PSD performed for the bed material, which has been given in Table 11. The mean diameter of the bed material particle size is calculated with the help of Eq 4.7.

$$Dp = \frac{\sum Average * wt\%}{100} \qquad \text{(Eq 4.7)}$$

Without the introduction of an agent, the bedzone is in fixed regime, denoted by the first diagram in Figure 18. The height of the bedzone in fixed regime is calculated by Eq 4.8. The height of the bed under fluidized condition can then be calculated by Eq 4.3.

$$L_{fixed} = \frac{M_{bed}}{A_{Reactor} \rho_{bulk}} \qquad \text{(Eq 4.8)}$$

As stated before, the volume of the CSTR is assumed to be equal to the volume of the bedzone at fluidization minus the volume of bed material. This calculation is given by Eq 4.9.

$$V_{CSTR} = V_{fluid} - V_{bed} \qquad \text{(Eq 4.9)}$$

The volume of bed can be calculated by dividing the mass of bed material upon the real density occupied by the bed particles (without consideration of volume occupied by pores). This is given in Eq 4.10.

$$V_{bed} = \frac{M_{bed}}{\rho_{real}} \qquad \text{(Eq 4.10)}$$

The properties of the bed material used and the calculation of the various parameters taken into account for the determination of the volume of the first CSTR are specified in Table 12 and 13.

Table 12: Properties of Bed Material Used and Calculation of the volume of first CSTR in Aspen Plus®

Bed Material	ρ_{real} (kg/m³)	ρ_{bulk} (kg/m³)	D_p (µm)	L_{fixed} (m)	ϵ_{Fixed}	V_{fluid} (l)	V_{CSTR} (l)	L_{CSTR1} (m)	L_{fluid} (m)
F046	3950	1636	591	0.60	0.586	55.012	36.0	0.721	0.721
F054	3950	1665	492	0.59	0.578	54.054	35.1	0.708	0.708

Table 13: Bedzone Diameter, Mass of Bed Material, Area of reactor and Volume of Bed Calculation

D_{in} (mm)	D_{burn}(mm)	$D_{Reactor}$(mm)	M_{bed} (kg)	$A_{Reactor}$(m²)	V_{bed} (l)
346	150	311.8	75	0.076	18.99

The volume of the second CSTR is calculated as the difference between the total measured volume and the volume of the first CSTR.

The freeboard is modelled as a PFR. The freeboard operates at the temperature as determined by the thermocouples shown in Figure 28. The total height of the bedzone and freeboard combined equals 2.454 m. The length of PFR is calculated by Eq 4.11.

$$L_{PFR} = 2.454 - (L_{CSTR1} + L_{CSTR2}) \qquad \text{(Eq 4.11)}$$

The selection of bed material type has an influence on the volume of the first CSTR as seen in Table 12. The total calculated volume of the two CSTR's is 65.7 l, as mentioned before, irrespective of the bed material selection. Hence, the volume of the gas-bed also varies according to the type of bed material chosen. The height of the two CSTR's (L_{CSTR1} + L_{CSTR2}) remains constant at H4 = 1.068 m. Hence, from Eq 4.11, the height of the PFR is equal to 1.386 m.

From Figure 28, it can be observed that the diameter of the freeboard and gas-bed is not constant because of the geometry of the reactor and due to the presence of the top burner in the freeboard.

The variation of the diameter in the PFR as a function of height, as calculated with the help of Eq 4.5, is shown in Table 14.

Table 14: Diameter of PFR at different heights of the gasifier setup as per Figure 28

Reactor Section	Height (Hi)	Height (m)	D_{in} (mm)	D_{burn} (mm)	$D_{reactor}$ (mm)
CSTR1	H1	0	346	150	311.8
	H2	0.2	346	150	311.8
	H3	L_{CSTR1}	346	150	311.8
CSTR2	H3	L_{CSTR1}	346	150	311.8
	H4	1.068	346	150	311.8
PFR	H4	1.068	346	150	311.8
	H5	1.206	382.2	150	351.5
	H6	1.453	447	0	447
	H7	1.704	447	100	435.7
	H8	2.454	447	100	435.7

4.1.7 Gasification Reactions

The optimized model is validated with the first steam-air gasification tests. The gasifier setup is divided into two CSTRs and a PFR. The first CSTR considers the oxidation reactions of CO, H_2, CH_4 and char. The second CSTR considers the reforming reactions of CH_4 (methane-steam reforming or MSR), char-reforming, phenol reforming, phenol cracking along with Boudouard and WGS reactions. Benzene and naphthalene obtained from phenol cracking are also assumed to undergo oxidation with remaining air in the freeboard. Secondary air is supplied to the freeboard region to facilitate tar cracking. With the presence of air in the freeboard regions, it is assumed that all the oxidation reactions occur along with the reforming reactions. The reactions considered in the model along with the gasifier section where it is specified in Aspen Plus® are represented in Table 15. The kinetic reaction rate for these gasification reactions is based on Power Law or Langmuir Hinshelwood (LHHW) kinetics. The type of kinetics considered for each reaction along with their kinetic parameters are described in Appendix H from [65] [66] [67].

Table 15: Reactions considered in the gasification model and the gasifier section in which it is specified in Aspen Plus®
[65] [67] [66]

Reaction no.	Reaction name	Gasifier section	Reaction Equation
1	Boudouard	Gas-Bed + Freeboard	$C + CO_2 \rightarrow 2CO$
2	Water Gas Shift	Gas-Bed + Freeboard	$CO + H_2O \rightarrow CO_2 + H_2$
OXIDATION			
3	Char Oxidation	Bedzone + Freeboard	$\alpha C + O_2 \rightarrow 2(\alpha\text{-}1)\,CO + (2\text{-}\alpha)\,CO_2$
4	Hydrogen Oxidation	Bedzone + Freeboard	$H_2 + 0.5O_2 \rightarrow H_2O$
5	Carbon Monoxide Oxidation	Bedzone + Freeboard	$CO + 0.5O_2 \rightarrow CO_2$
6	Methane Oxidation	Bedzone + Freeboard	$CH_4 + 0.5O_2 \rightarrow CO + 2H_2$
7	Benzene Oxidation	Freeboard	$C_6H_6 + 3O_2 \rightarrow 6CO + 3H_2$
8	Naphthalene Oxidation	Freeboard	$C_{10}H_8 + 7O_2 \rightarrow 10CO + 4H_2O$
REFORMING			
9	Water Gas	Gas-Bed + Freeboard	$C + 1.2\,H_2O \rightarrow 0.8CO + 0.2CO_2 + 1.2H_2$
10	Methane Reforming	Gas-Bed + Freeboard	$CH_4 + H_2O \rightarrow CO + 3\,H_2$
11	Phenol Reforming	Gas-Bed + Freeboard	$C_6H_5OH + 3H_2O \rightarrow 2CO + CO_2 + 2.95CH_4 + 0.05C + 0.1H_2$
12	Benzene Reforming	Freeboard	$C_6H_6 + 2H_2O \rightarrow 1.5C + 2.5CH_4 + 2CO$
CRACKING			
13	Phenol Cracking	Gas-Bed	$C_6H_5OH \rightarrow CO + 0.4\,C_{10}H_8 + 0.15C_6H_6 + 0.1\,CH_4 + 0.75H_2$

4.1.8 Cyclone Separator

This section describes the implementation of two cyclone separators in series to remove all solids from the product gas. The datasheet for the cyclones, provided by Petrogas Gas-Systems is used to specify the required dimensions in Aspen Plus®. The information required for the model is taken from there and given in Appendix I. The summary of the data from the datasheet which is used in Aspen Plus® is given in Table 16.
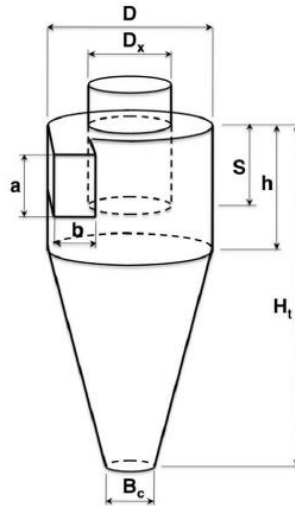
Figure 29: Schematic Representation of Stairmand Cyclone [68]

Figure 29 provides the schematic representation of a high efficiency Stairmand cyclone separator [68]. The important parameters used for specifying the dimensions of a cyclone separator for our study can be understood from this figure. The main geometrical parameters of a cyclone separator are:

- Diameter of cyclone D

- Cyclone Total Height H_t

- Cyclone Height h

- Length of cone section H_t - h

- Vortex finder length S

- Diameter of overflow D_x

- Diameter of underflow B_c

- Height a and width b of inlet

Table 16:Input Parameters for Cyclone Separator taken from datasheet provided by Petrogas Gas-Systems

Simulation Parameters of Cyclone 1 and 2	
Diameter - D (mm)	141.3
Length/Height of cyclone - h (mm)	256
Length of cone section - H_t - h (mm)	201
Length of vortex finder - S (mm)	79
Diameter of overflow - D_x (mm)	60.32
Diameter of underflow - B_c(mm)	60.2
Inlet configuration	Rectangular
Height of inlet - a (mm)	72
Width of inlet - b (mm)	70.65

The aim of introducing the cyclone separator is to remove all unconverted char and ash from the product gas. As stated before, in Aspen Plus®, char has been defined as a conventional solid: solid carbon. It has been discussed in Section 2.6 that small amounts of oxygen, hydrogen

51

and ash are also found in char [36]. According to [69], also small amounts of nitrogen are found in biochar. Ash has been defined as a non-conventional solid whose definite formula is not known. Looking at the PSD for char and ash, as reported in Table 9 and Table 10 respectively, it can be observed that the size of char particles ranges from 124.5 µm to 6000 µm, while the size of ash particles ranges from 4.62 µm to 209.3 µm. It can be observed that most of the ash particles are smaller than the char particles. For designing the cyclone, two scenarios are considered for the efficiency selection of the cyclones to study the PSD variations of char and ash at the inlet and outlet streams of both cyclones. These scenarios are presented below: -

SCENARIO 1

The efficiency of the cyclones is selected in such a way that 50% of all the char and ash particles are removed by the first cyclone and the outlet product from the first cyclone contains 50% of the solids to be transferred to the second cyclone. The second cyclone removes the remaining solids and releases a solid-free product gas.

SCENARIO 2

The global mesh for PSD in Aspen Plus® is defined in such a way that it contains the particle size ranges for biomass, char and ash. Since the global mesh considers the PSD for all the three components, the maximum size defined in the global mesh PSD is 6000 µm which is the highest particle size among all the particle size of all the three components. For this scenario, the midpoint of the particle size range is chosen, i.e., 3000 µm. The cyclone efficiency specification is done such that the cyclone works based on the assumption of larger particles getting removed at a greater efficiency than the smaller particles. Hence, for the first cyclone, a 100% efficiency is selected for particles larger than 3125 µm (closest value to 3000 µm, according to the particle size ranges in the global PSD mesh) and for the rest of the particles (0-3125 µm), a 50% efficiency is used. It is assumed that the second cyclone removes the rest of the particles. By looking at the PSD for char and ash from Table 9 and Table 10 respectively, it can be seen that in this scenario approximately 50% weight fraction of the char particles (greater than 3125 µm) are removed completely from the first cyclone leaving a gas stream containing all the ash and 50% weight fraction of char. The second cyclone then works to remove all the remaining ash and char from the gas releasing a solid-free product gas.

The impact of simulating the cyclones based on the two scenarios on the PSD of the solids in the stream before and after the cyclones is reported in Appendix J.

4.1.9 Comparison between the Reference Model and Optimized Model

Based on a number of different parameters, the comparison between the reference model and the optimized model can be summarised in Table 17.

Table 17: Comparison between the Reference Model by Kwakkenbos [16] and own Optimized Model

Parameters	Reference Model	Optimized Model
Feed Characterization	Proximate and Ultimate Analysis	Proximate Analysis, Ultimate Analysis, PSD
Heating Section	One preheater heating air, steam and nitrogen from 20°C to 650°C	Two preheaters, with air heated in the first one and steam heated in second preheater. The air is heated

		to 150°C and steam/air mixture is heated to 607.5°C in the second preheater. The set temperature in the second preheater is 650°C but this temperature is not usually reached during the tests. The temperature reached is generally 607.5°C.
Pyrolysis section	Modelled by RYield reactor block which gives the mass yield as a function of temperature specified. The mass yields are calculated in Fortran code.	The procedure is similar to the reference model, with normalization of mass yields for solid, liquid and gaseous fraction and modelling of Phenol as tar in the Fortran code.
Gasification Section	Gasifier divided into bedzone and freeboard region represented by RCSTR and RPlug block in Aspen Plus® respectively.	Gasifier divided into bedzone, gas-bed and freeboard region. Bedzone and gas-bed represented by RCSTR and freeboard represented by RPlug block in Aspen Plus®.
N$_2$ Purge Streams	A single stream of N$_2$ is heated in the preheater and sent to the gasification section.	To resemble the actual gasifier setup, the N$_2$ stream is divided into two main streams. The first stream is mixed with the gasification agent and sent to the bedzone. The second stream is further split into three main streams, with one stream going to the bedzone region of the gasifier, the second stream going to the freeboard region and the third stream being sent to the cyclones.
Fortran Code	Mass yields calculated as a function of pyrolysis temperature based on experimental results obtained in Pyroprobe apparatus and yield curves generated in MATLAB®. The mass deviation is taken into account by assuming mass loss in liquid fraction.	Mass yields calculated in the same manner, mass deviation taken into account by normalization of solid, liquid and gaseous fraction obtained from Pyroprobe apparatus.
Tar specification	Four lumped groups – Benzene, Toluene, Phenol and Naphthalene	Phenol as model tar cracking to benzene and naphthalene in gasifier
Gasification Kinetics	From literature; kinetics based on Power Law and LHHW kinetics	Included kinetics for phenol cracking reaction as per Power Law kinetics; other reaction kinetics

		similar to the reference model
Kinetic reactions	Homogenous phase oxidation and reforming reactions of CO, CH_4, CO_2, H_2 and tar and heterogenous char oxidation and reforming, WGS and Boudouard	Same reactions in addition to phenol cracking introduced in gas-bed
Solid separation	Ideal Separator	2 Cyclone Separators in resemblance with the actual gasifier setup

4.2 Sensitivity Analysis, Recycle Stream, Heat and Mass Balance

After validating the model with the latest experimental results, a specific experiment is chosen:

- To perform a sensitivity analysis with respect to varying SB*, primary and secondary air intake and to observe its effect on the product gas composition in terms of yield of permanent gases, N_2, H_2O, tar percentage in product gas, CC and OE. In addition, it is decided to study the impact of the varying parameters on H_2/CO ratio, to analyse the optimum conditions under which the product gas obtained from the gasifier model can be used to produce methanol after subsequent cleaning. Effect of the varying parameters on other gas ratios CO/CO_2 and CH_4/H_2 and on the product gas temperature is also studied.
- To study the possibility of recycling the product gas back to the burners to eliminate the consumption of methane for generating heat supplied to the pyrolysis reactor block and the gasification section, in order to make the model sustainable
- To perform a mass and heat balance for the chosen test

As discussed in Section 2.6, biomass gasification can be used for the production of various liquid and gaseous fuels, one of which is methanol. There has been a growing interest in the production of methanol from biomass gasification, which has proved its use as a fuel in IC engines and as a starting material for the manufacture of various chemicals such as formaldehyde, acetic acid and ether [58].

A number of parameters such as temperature, pressure and selection of CO or CO_2 hydrogenation for methanol synthesis play an important role in the optimal production of methanol. One of the most important parameters used by different methanol synthesis technologies is the stoichiometric ratio of H_2/CO or $(H_2-CO_2)/(CO_2+CO)$ [58]. Though the latter is a preferred ratio to be evaluated for methanol production, the H_2/CO ratio is more commonly used as a parameter to be optimized in various methanol production technologies, which has to be close to 2:1 for an optimal methanol yield [58]. In case of choosing the $(H_2-CO_2)/(CO_2+CO)$ ratio, the value has to be close to 2.05 [58]. The H_2/CO ratio and $(H_2-CO_2)/(CO_2+CO)$ is calculated from the model for the eight tests used for validation is given in Table 23.

The chemical reactions considered in the model for the recycle stream are given by Eq 4.12, Eq 4.13, Eq 4.14, Eq 4.15, Eq 4.16. In case of using natural gas for combustion, only Eq 4.12 is considered. It should be noted that phenol has been observed to crack completely to benzene and naphthalene (along with hydrogen and methane), hence no reaction for phenol combustion has been considered.

$$CH_4 + 2O_2 \rightarrow CO_2 + 2H_2O \qquad \text{(Eq 4.12)}$$

$$2CO + O_2 \rightarrow 2CO_2 \qquad \text{(Eq 4.13)}$$

$$2H_2 + O_2 \rightarrow 2H_2O \qquad \text{(Eq 4.14)}$$

$$C_6H_6 + 7.5O_2 \rightarrow 6CO_2 + 3H_2O \qquad \text{(Eq 4.15)}$$

$$C_{10}H_8 + 12O_2 \rightarrow 10CO_2 + 4H_2O \qquad \text{(Eq 4.16)}$$
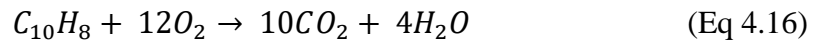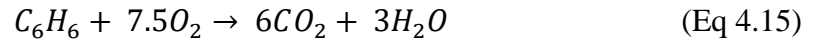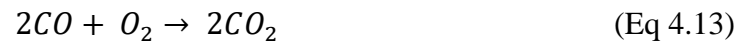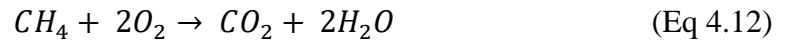
Appendix K presents the flowsheet diagram in Aspen Plus® with the recycle stream.

5. RESULTS AND DISCUSSION

The results of experiments conducted with GB and RB under varying operating parameters are used for validation. About 75 kg of two different bed materials F046 and F054 have been used for the gasification tests. The temperatures used in the model for the oxidation bed, gas-bed and freeboard region is taken as the average of the temperatures calculated by the thermocouples present in different regions of the gasifier, as seen in Figure 28. These temperatures have been measured and are specified in the model. It has been assumed that the pressure of the freeboard and gas-bed region is equal to the outlet pressure of the product gas. Table 18 shows the average of the temperatures noted for the bedzone, gasbed and the freeboard by the different thermocouples in each gasification test.

Table 18: Average of the temperatures measured by thermocouples for bedzone, gas-bed and freeboard regions

Date	Test no.	Average Bed Temperature from TE01, TE02, TE03 (°C)	Gas-Bed Average Temp from TE04 and TE05 (°C)	Freeboard Average Temp from TE06 and TE07 (°C)
07-10-20	1	839	863	857
12-10-20	2	839	862	857
14-10-20	3	836	860	854
19-10-20	4	833	871	857
25-11-20	5	839	872	859
27-11-20	6	833	790	818
04-12-20	7	704	813	825
15-12-20	8	722	754	856

The input parameters used for the gasification tests are given in Table 19.

Table 19: Input Parameters of the Experiments Used for Validation of Model

Test No.	Bed Material	Bed material (kg)	Biomass Type	Average Bedzone temperature (°C)	Gas-Bed temperature (°C)	Freeboard temperature (°C)	Steam Flowrate (kg/hr)	Biomass Flowrate (kg/hr)	Primary Air Flowrate (kg/hr)	Secondary Air Flowrate (kg/hr)	N_2 purge (kg/hr)	λ	SB*	Outlet Pressure (mbar)
1	F054		GB	839	863	857	9.0	10	11.3	0	6.6	0.20	0.95	69
2	F054		GB	839	862	857	10.8	10	11.3	0	6.6	0.20	1.13	80
3	F054		GB	836	860	854	7.3	10	11.2	0	6.5	0.19	0.78	82
4	F046	75	GB	833	871	857	10.4	10	11.3	0	6.6	0.20	1.09	112
5	F054		RB	839	872	859	10.7	10	11.3	0	6.6	0.20	1.12	89
6	F046		RB	833	790	818	10.5	10	11.3	0	6.6	0.20	1.10	107
7	F046		RB	704	813	825	8.7	8	1.9	8.0	6.6	0.04	1.14	67
8	F054		RB	722	754	856	8.8	8	1.9	8.0	6.6	0.04	1.15	70

The gasification tests can be classified as high-temperature/ low temperature tests based on the temperature of the bedzone. Tests 1, 2, 3 and 4 performed with GB and Tests 5 and 6 performed with RB as feedstock are classified as high-temperature tests. Tests 7 and 8 performed with RB as feedstock are classified as low-temperature tests.

Based on the agent flowrate, different conversion factors for density of char are assumed for the Boudouard, water gas/char gasification and methane steam reforming (MSR) reaction in the freeboard (PFR). The density factors are assumed in each test and the calculated kinetic reaction rates for the above-mentioned reactions are given in Appendix L.

5.1 Validation of Model – Measuring Absolute and Relative Error

The model is validated with respect to product gas composition and different key performance parameters. The results are presented in the following sections. The absolute and relative errors between the model and the experiments for the permanent gases is presented in Appendix M and for CC, CGE and OE, is given in Appendix O.

5.1.1. Permanent Gases Yield (dry N_2 free tar free basis), N_2 (dry tar free basis), and H_2O

The yield of permanent gases is characterized via the volume % of H_2, CO, CO_2, CH_4 on a dry N_2 free tar free basis. For calculating the volume % of permanent gases from the model, H_2, CO, CO_2, and CH_4 molar flowrate values are taken and are normalized to 100% such that the product gas contains only these permanent gases.

The volume % of N_2 on dry tar free basis is calculated as the molar flowrate of N_2 divided by the total molar flowrate of the product gas such that the product gas contains N_2 and all the permanent gases: H_2, CO, CO_2, and CH_4 for this calculation.

The volume % of H_2O is calculated as the molar flowrate of H_2O divided by the total molar flowrate of the product gas containing all components (wet gas basis).

5.1.1.1. Green Biomass (GB)- High Temperature Tests

The results from the model simulation with the input parameters pertaining to Test 1, 2, 3 and 4 are compared with the experimental results for these tests and presented in Figure 30.

Figure 30: Validation of Permanent gases (dry N_2 free tar free basis), N_2 (dry tar free basis) and H_2O (wet gas basis) for Test 1, 2, 3, 4 with GB

The following observations can be made from the graphs:

➢ Overall, the model follows the experimental trends well for the first three tests, with a slight exception in case of CO_2 volume% observed for Test 3. For the experiments, the CO_2 values for the first three tests increases in the following order: SB* 0.95, 1.13 and 0.78 respectively, whereas from the model, the CO_2 value increases in the following order: SB* 0.95, 0.78 and 1.13. However, the experimental and model values are very close.

➢ Taking only SB* into account, the volume % of H_2 increases with increasing SB* and the volume% of CO and CH_4 decrease with increasing SB* in the model. This follows the same trend as observed in the experiments. The decrease in CO and increase in H_2 with increasing SB* matches similar observations made in [44], and the decrease in CH_4 with increase in SB* matches with the observations made in [60].

➢ Among the permanent gases yield measured from first three tests, the maximum absolute error is calculated to be 2.5 for H_2 obtained from Test 3. The corresponding relative error of 8% is within the range as specified for the gas composition obtained from the gasifier model in [59]. The maximum absolute error among the other gases for the first three tests lie within 1.7 for CO, 0.8 for CO_2 and 0.1 for CH_4.

➢ It can be observed that simulation for Test 4 shows more deviation as compared to the other cases. An overestimation of H_2 can be seen in the model with a maximum absolute error of 9.6 measured for the same.

➢ The other gases are slightly underestimated in Test 4 with the maximum absolute error within 2.5 for CO, 4.8 for CO_2 and 2.3 for CH_4. This test does not follow the experimental trend as other tests for GB.

- ➤ N_2 estimation from the model is always below the experimental values. The maximum absolute error measured from the first three tests is within 3. Test 4 does not follow the experimental trend as other gases, and shows a higher deviation with a maximum absolute error of 9.
- ➤ The volume % of H_2O calculated from the model follows the experimental trend well for the Test 1, 2 and 3, with a maximum absolute error of 1 obtained for these tests. The values from the model are above those measured from the experiment for the first three tests whereas for Test 4, they are slightly underestimated from the experimental value with an absolute error of 2.8.

Generally, the effect of varying SB* on CO_2 production cannot be accurately determined from the tests because of different temperatures and pressures used in the first three tests. It is stated in the kinetic model built in [62] that increasing the SB* increased the CO_2 concentration in the product gas. In [44] also, the effect of increasing SB* from 0.5 to 1 at 700°C and 820°C on the product gas composition is shown. From the simulation results, it is observed that CO_2 concentration is not much affected by increasing the SB* whereas the experimental trend shows a slight increase in CO_2 concentration at 820°C with the increase in SB* within the same range, as reported in [44]. However, in [60], it is reported that CO_2 decreases with increase in SB* from 0.3-0.75 for palm kernel gasification in inter-connected fluidized bed at a gasifier temperature of 650°C. [70] states a slight increase in CO_2 reported for increasing SB* at a gasifier temperature of 870°C.

Overall, the permanent gases yield obtained from the model are in good agreement in the experimental values, with the exception of a higher deviation for H_2 obtained from Test 4. It should be noted from Table 19 that there are differences in temperatures and steam flow rates used for Test 1, 2, 3 and 4. Hence a clear understanding of the exact reason as to why the model shows a larger deviation in case of Test 4 lacks. It can be seen that Test 4 uses a different bed material type than the other three tests. Although a notable difference cannot be made between the two values obtained from the bedzone volume calculations in Table 12 for F046 and F054 to be implemented in the model, it should be taken into account that the PSD for each bed material is not considered in the model, which might play some role in influencing the product gas composition. From the PSD, the mean bed material diameter calculated is 591 µm for F046 and 492 µm for F054. It is possible that bed material particle size might impact (possible) catalytic reactions due to accumulation of unreacted char, though the bed is considered to be reasonably inert despite corundum not being totally pure Al_2O_3. Both the bed material types are classified as Geldart B solids undergoing fast bubbling regime as per literature study done in Section 2.8.1; however, a more detailed calculation of bed hydrodynamics can be of help in understanding the differences among the behaviour of various bed material types under fluidization.

The input parameters used for all the four tests shows certain differences. However, it can be observed that the temperatures used in each test are close to each other with Test 4 having a higher temperature in the gas-bed and a slightly lower temperature in the bedzone as compared to the other three tests. With respect to steam flowrate, Test 4 has the closest value to Test 2. The pressure of the outlet gas obtained from Test 4 is little higher as compared to Test 2 and other tests. In general, H_2 production is favoured at higher temperatures due to endothermic char gasification, steam reforming and tar cracking reactions. As per observations made in [44] and [60], CO and H_2 increased while CO_2 and CH_4 decreased at higher temperature due to the

promotion of the endothermic methane steam reforming (MSR), water gas and Boudouard reaction. According to the literature survey done in [62], two studies stated having a positive influence on the yields of H_2, CH_4 and CO_2 concentration due to increase in the operating pressure because of increased reaction rate occurring in hydrocarbon reactions and WGS. However, the pressures involved varied from 2 to 10 bar and from 1 to 3 atm in the two cases. Another research work showed an opposite influence with a pressure increase from 0.5 bar to 2 bar causing a decline in H_2 and CO concentrations during steam-CO_2 gasification of bituminous coal at 850°C. This was due to the pressure shift in reforming reactions to the side with fewer molecules according to the Le Chatelier's Principle [62]. However, it should be noted that the IHBFBSR operates at atmospheric pressure, with the product gas having a lower pressure in all the experiments, due to pressure changes in the reactor. Moreover, the difference in the outlet pressure for Test 4 with respect to the values obtained for the other three tests cannot be considered very significant to produce a large deviation as observed. Overall, the reason for deviation in Test 4 has to be explored.

Overall, the average relative errors among the four tests for GB for each component is as follows: 4% for CO, 4.8% for CO, 11.2% for H_2, 6.8% for CH_4. The slightly higher error for H_2 is due to the higher deviation observed for Test 3. These errors are still within the range as reported in [59] and [61]. The average relative errors for N_2 and H_2O are 7.1% and 3.7%, respectively.

5.1.1.2. Red Biomass (RB)- High Temperature Tests

The results from the model simulation with the input parameters pertaining to Test 5 and 6 are compared with the experimental results for these tests and presented in Figure 31.
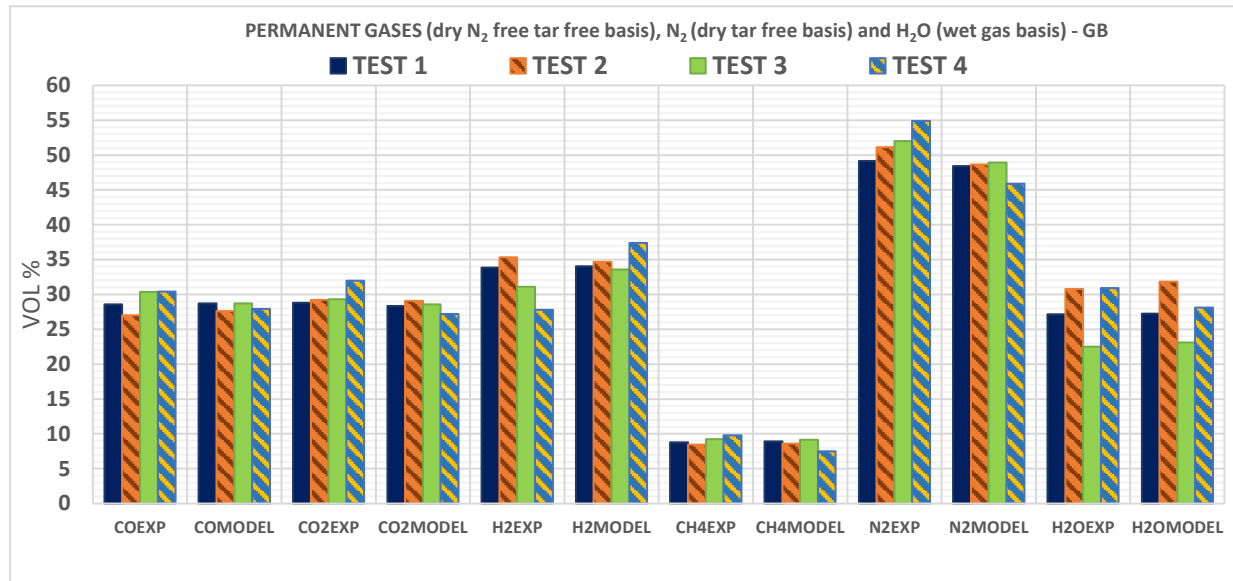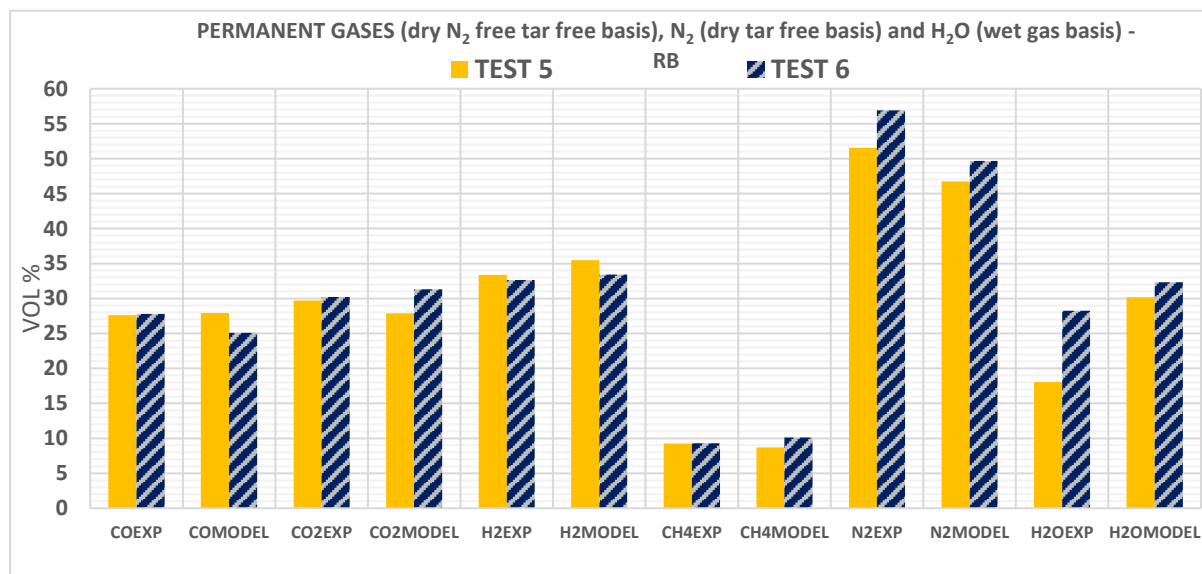

Figure 31: Validation of Permanent gases (dry N₂ free tar free basis), N₂ (dry tar free basis) and H₂O (wet gas basis) for Test 5 and 6 with RB

The following observations can be made from Figure 31.

➢ CO_2, H_2, CH_4, N_2 and H_2O volume percentages in the product gas follow the experimental trend for the high temperature tests with RB.

➢ The CO obtained from the model for Test 6 is lower than that obtained from the model for Test 5 whereas CO obtained from the experiments in Test 6 is slightly higher than that obtained from Test 5 with a very low difference.

➢ The maximum absolute error among the permanent gases is calculated to be 2.6 (relative error of 9%) for CO obtained for Test 6 performed with F046. This is within the average error range in [61]. The maximum absolute error among the other gases is calculated to be 2.1 for H_2, 1.8 for CO_2 and 0.8 for CH_4.

➢ The N_2 from the model is lower than N_2 from the experiments as in case of tests with GB. The difference for these tests is larger with a maximum absolute error of 13.1 calculated for Test 5.

➢ H_2O values obtained from the model are higher than the experimental values for both tests. A relatively large deviation is observed for H_2O in Test 5 showing an overestimation with a maximum absolute error of 12.2. The exact reason for this deviation could not be investigated yet. It should be noted that deviations for H_2O can be partly attributed to the fact that it is more difficult to be quantified experimentally compared to other gases. It should be noted that the experimental value in this case is particularly low compared to other tests, while an exact reason for this has to be found. From the kinetic gasifier model developed in [62], a similar deviation could be observed for H_2O concentration during gasification at 750°C at a SB* value of 1.08. However, this difference was more fuel-specific rather than being based on the operating parameters. The exact reason for the deviation was not specified; however, it was concluded that WGS and MSR reactions play a dominant role in influencing the product composition, and hence the kinetics chosen for these reactions can affect the gas composition in the model [62].

From the literature review done regarding the various gasifier models in Aspen Plus® in Appendix C, most models are found not to consider N_2 and S reactions during gasification. According to [71], apart from the formation of NH_3 which has been considered in our model; HCN, char-bound nitrogen, tar-bound nitrogen and gaseous diatomic nitrogen N_2 can also be produced from the fuel-bound nitrogen present in biomass feedstocks during gasification. However, nitrogen amounts are quite low for GB and RB, hence, the above-mentioned reason cannot contribute to a large deviation between experimental and model values. A more plausible cause can be attributed to the inlet inaccuracies in N_2 flow and possible leakage from bunkers and sampling line during experiments.

The model considers the assumption of oxidation reactions occurring in the bedzone followed by reforming and cracking reactions in the gas-bed because of the faster reaction of gaseous components with oxygen as compared to the reactions with steam. Test 5 uses a higher temperature in the bedzone, gas-bed and freeboard regions compared to Test 6 and other tests with RB. It is possible that endothermic char gasification and MSR reactions probably are becoming more enhanced in the bedzone region of the gasifier along with oxidation reactions, which can lead to the consumption of H_2O in the gasifier, thus giving a higher value of H_2O from the model.

5.1.1.3. Red Biomass (RB)- Low Temperature Tests

The results from the model simulation with the input parameters pertaining to Test 7 and 8 are compared with the experimental results for these tests and presented in Figure 32.
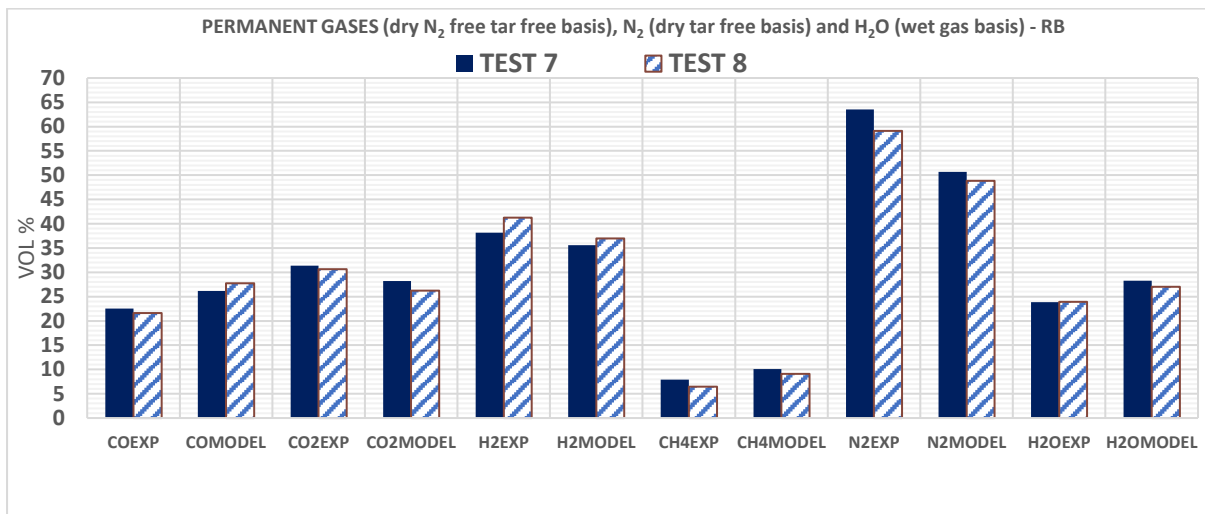
Figure 32: Validation of Permanent gases (dry N_2 free tar free basis), N_2 (dry tar free basis) and H_2O (wet gas basis) for Test 5 and 6 with RB

The following observations can be made from Figure 32.

➤ Tests 7 and 8 follow the experimental trend except for CO and H_2O.
➤ The maximum absolute error calculated among the permanent gases is 6.1 (relative error of 28%) for CO obtained for Test 8 performed with F054. This is within the average error in [61]. The errors for other gases lie within 4.4 for CO_2, 4.3 for H_2, and 2.5 for CH_4.
➤ The maximum absolute error calculated for N_2 and H_2O is for Test 7 performed with F046: 12.8 and 4.4 respectively. N_2 values from model are lower than the experimental results as previous cases. Similarly, the H_2O values from the model is higher than the experiments.
➤ The maximum value of H_2 among all tests for RB is obtained from Test 8 for both the experimental and model value, which matches with the observation made in [62] that a higher SB*at lower temperatures ($< 800°C$) has a more positive impact on the yield of H_2 than at higher temperatures.
➤ The values obtained from the model for Test 7 and 8 gives a higher value of CO, a lower value of CO_2, a lower value of H_2 and a higher value of CH_4 as compared to the experimental results.

A possible cause for discrepancies in terms of higher deviation observed for low temperature tests with RB as compared to the high temperature tests with both GB and RB could be due to the fact that secondary air supplied to the freeboard region enhances the thermal cracking of tars which can subsequently impact the yield of other components like CH_4, H_2 and CO in the product gas. The model considers the assumption of phenol as a model tar in the pyrolysis reactor cracking into benzene and naphthalene in the gas-bed. In reality a variety of tars are formed during pyrolysis which take part in biomass gasification. Also, another possible cause of deviation can be attributed to the probability that a fraction of secondary air can diffuse from the freeboard into other regions of the gasifier during the experiments, particularly facilitating

char combustion and other oxidation reactions in the dense zone of the gasifier/gas-bed, whereas in the model the secondary air is fed only to the freeboard region. This may partly explain the slightly higher concentration of CO_2 obtained from the experiments due to enhanced oxidation. CO and H_2O are also produced during the oxidation reactions; however, lower values might be because of consumption in the exothermic WGS reaction getting enhanced at lower temperatures, which could subsequently also increase CO_2.

The average relative errors among the gases for the tests with RB are as follows: 13.5% for CO, 8.5% for CO_2, 6.4% H_2 and 15% CH_4. These are higher as compared to the tests with GB, due to higher deviation observed for the tests with secondary air. The possible reasons for deviations are discussed above. These values lie within the values for the average error percentages reported in [61]. The average relative errors for N_2 and H_2O are 17.5% and 28%, respectively.

5.1.2 Carbon Conversion (CC), Cold Gas Efficiency (CGE), and Overall Efficiency (OE)

The residual char from the model is measured as char obtained in the product gas before entering the cyclone separators. This is used to calculate the carbon conversion of the model according to Eq 1.1. The formula for CC requires the residual char obtained from the model and the carbon present in the biomass feed. The carbon present in biomass feed can be obtained from the proximate analysis of the respective biomass type from Table 7.

For calculating the CGE, the total gas flow rate from the model is noted. This is converted to a dry basis by subtracting the flowrate of H_2O from the total gas flowrate in suitable units. This value is then multiplied by the LHV of the product gas on a dry basis, which is calculated based on the LHV of the CO, H_2 and CH_4 yield in the product gas. The values considered for LHV of CO, H_2 and CH_4 are 12.63, 10.79 and 35.82 in MJ/ Nm^3 respectively, taken from [72]. The formula for calculating the CGE is given in Eq 1.2.

The OE takes into account the power generated by burners and the preheaters. It is based on the same formula for CGE except with the addition of power generated by the burners and preheaters in the denominator. Eq 1.3 provides the formula for calculating the OE of the process. P_{in} denotes the power supplied by the burners and the preheaters. The final formula is given in Eq 5.1. It should be noted that the burners are not always on and this is considered for both the experiment and model during the calculation of burner efficiencies. The data required for calculation of burner efficiencies in each test is given in Appendix N.

$$OE = \sum_{i=1}^{n} \left(\frac{m_i LHV_i}{m_{fuel} LHV_{fuel} + \sum_{i=1}^{2}(P_{burner,i}\, \eta_{burner,i}) + P_{preheaters}} \right) \quad \text{(Eq 5.1)}$$

It has been observed during the experiments that there is mass loss ranging from 4-8.5% for tests with GB and from 14-27% for tests with RB. This loss has been defined as the global error (GE). The GE has been taken into account in the total gas flowrate in m^3/hr obtained from the model during the calculation of CGE and OE.

5.1.2.1. Green Biomass (GB)- High Temperature Tests

The results for CC, CGE and OE from the model and experiment for Test 1, 2, 3 and 4 with GB are compared and presented in Figure 33.
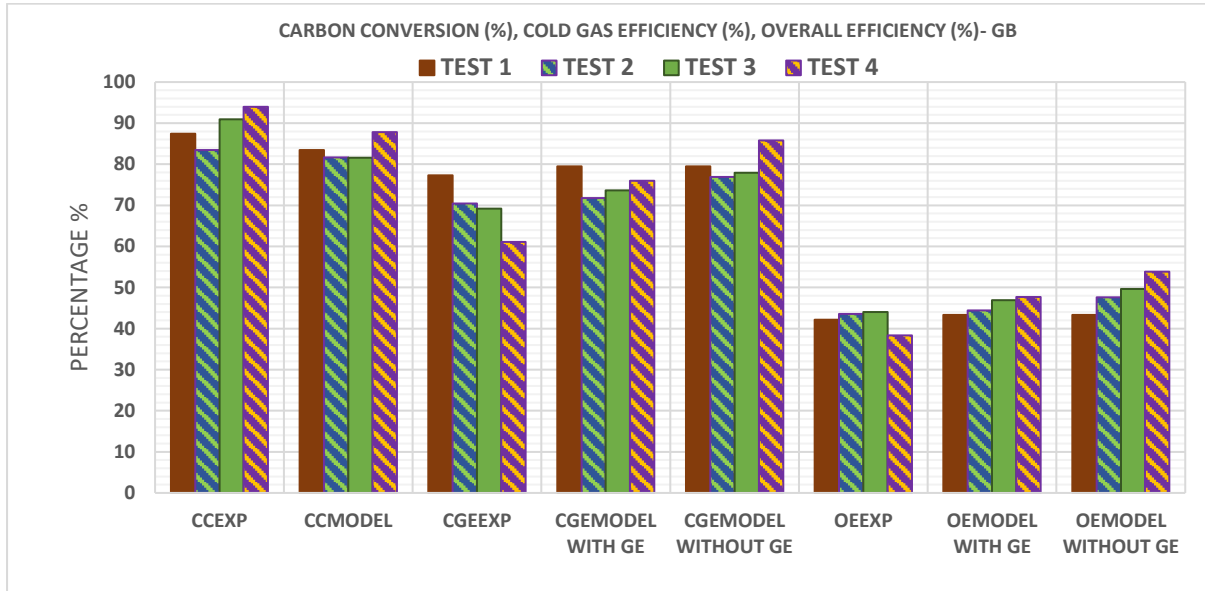
Figure 33: Validation CC, CGE and OE for Test 1, 2, 3 and 4 with GB

The following observations can be made from Figure 33.

- ➢ The model follows the experimental trend fairly for Test 1 and 2 for CC and CGE. It should be taken into account that different conversion factors are assumed for char density reduction in the Boudouard reaction, MSR and water gas reaction in the freeboard, which affect the CC and CGE.
- ➢ There is an increasing trend observed for the experimental and model results obtained for the overall efficiency for Test 1, 2, and 3.
- ➢ Test 4 does not follow the experimental trend for CGE and OE.
- ➢ The maximum absolute error observed for CC is 9.4 for Test 3, 14.9 for CGE in Test 4 and 9.4 for OE, also in Test 4. The errors for CGE and OE are reported by considering the values obtained after taking the GE into account. These errors are within the range observed in the CGE and CC calculations from the kinetic model given in [62]. A comparison of these errors with values obtained without considering GE can be seen in Appendix O.
- ➢ The CGE and OE values calculated from the model are always higher as compared to the experiments.

The model fairly resembles the experiment in terms of CC, CGE and OE comparison for Test 1, 2 and 3 and shows certain deviation for Test 4. However, as discussed, the deviations till lie within the range as reported in the kinetic model given in [62]. By accounting for the GE in the CGE and OE calculations, the deviation between the model and experimental value of CGE and OE is reduced. However, the GE for gasification tests with GB is not very high, hence not much difference is observed between the values with without GE.

The average relative errors among these tests for CC, CGE (with GE), and OE is within 5.5%, 8.25% and 8.5%, respectively.

5.1.2.2. Red Biomass (RB)- High Temperature Tests

The results for CC, CGE and OE for Test 5 and 6 from the model and experiment for RB is presented in Figure 34.
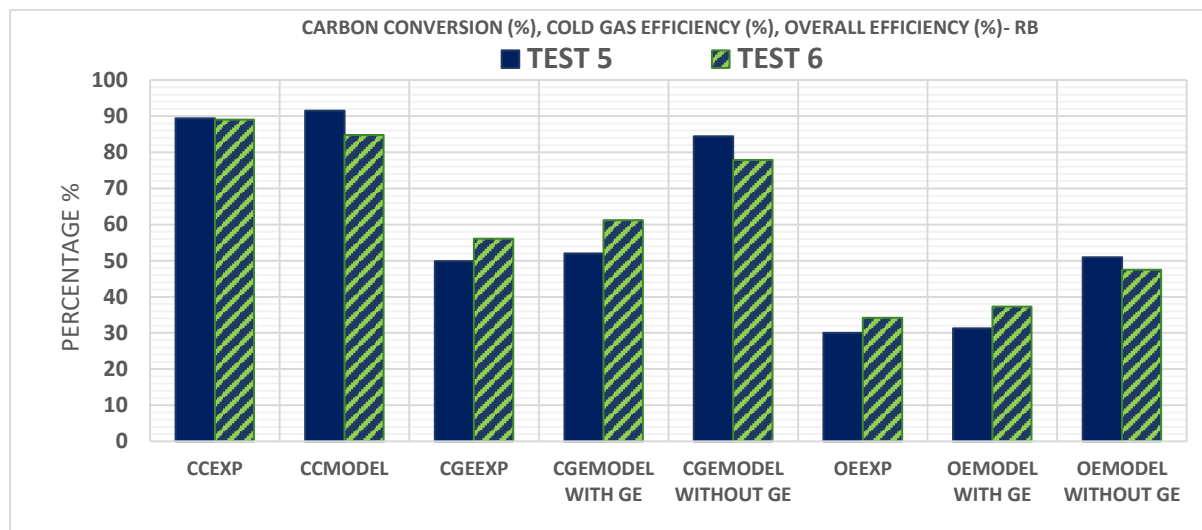
Figure 34: Validation CC, CGE and OE for Test 5 and 6 with RB

The following observations can be made from Figure 34.

➢ The model follows the experimental trend fairly except for CC. The CGE and OE calculations without accounting for GE show an opposite trend. However, the values with GE should be considered a more accurate depiction of the CGE and OE obtained from the model as it takes into account the mass loss during the experiments.

➢ The maximum absolute error observed for CC, CGE and OE lie within 7, 2.5 and 1.5, respectively. These errors for CGE and OE are reported by considering the values obtained after taking the GE into account.

➢ The CGE and OE values calculated from the model are higher as compared to the experimental results.

The model fairly resembles the experiment in terms of CC, CGE and OE comparison for Test 5 and 6. By accounting for GE in the CGE and OE calculations, the difference between the model and experimental value for CGE and OE is reduced. Since the GE for gasification tests with RB is high, a notable difference is observed between the values for CGE and OE with and without GE.

The average relative errors among these tests for CC is within 5% and within 4% for both CGE (with GE) and OE.

5.1.2.3. Red Biomass (RB)- Low Temperature Tests

The results for CC, CGE and OE for Test 7 and 8 from the model and experiment for RB is presented in Figure 35.
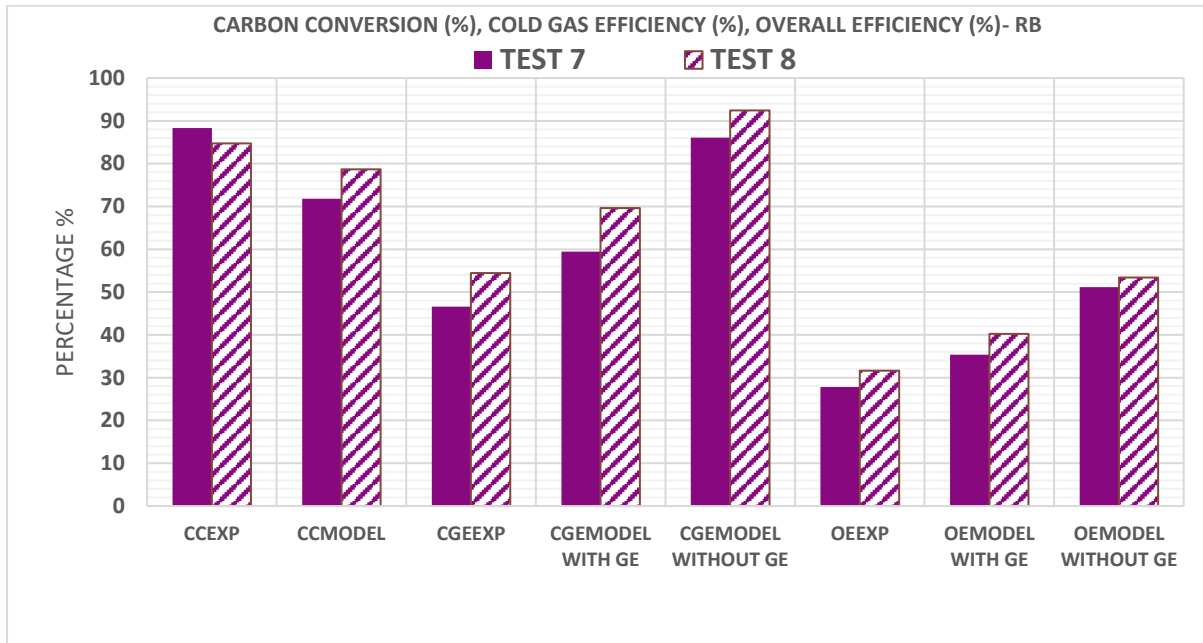
Figure 35: Validation CC, CGE and OE for Test 7 and 8 with RB

Similar observations can be made for Figure 35 as the observations made for Figure 34 with the exception of:

➢ The carbon conversion obtained for Test 7 and 8 for the model has more deviation as compared to Test 5 and 6 for RB. This can be attributed to the possibility of the secondary air diffusing into other regions of the gasifier during the experiments and enhancing char combustion in the dense zone of the gasifier as stated in previous section, thus giving a higher CC from experiments.

➢ Here CGE and OE values from the model are in trend with the experimental observations for both results: with GE and without GE.

➢ The maximum absolute error observed is 16.5 for CC, 15.2 for CGE and 8.6 for OE. These errors for CGE and OE are reported by considering the values obtained after taking the GE into account. The deviation for CC is slightly higher in this case; but the deviation observed for CGE is within the range obtained from the kinetic model in [62].

The average relative errors among these tests for CC is within 12.5% and within 27% for both CGE (with GE) and OE.

The differences observed in the CC, CGE and OE calculations for low temperature tests with RB are higher as compared to other tests. Apart from the reasons stated before for the possible cause of deviations in case of low-temperature tests with secondary air, the overestimation of CO and CH_4 components from the model for these tests can also contribute to a higher CGE and consequently a higher OE from the model.

5.1.3 Total Tars (Volume % in Total Gas on Dry Basis) for GB and RB

The volume % of tars are calculated by dividing the total flowrate of tars obtained from the model by the total flowrate of the dry gas (containing all components except H_2O). Benzene, naphthalene and phenol are considered as tar species for the model. As discussed before, only phenol is considered as the tar species in the pyrolysis reactor block in Aspen Plus®. Naphthalene and benzene are derived from phenol cracking in the gas-bed. It has been observed that for all the tests, phenol cracks completely leaving no residual phenol in the product gas. Hence, the tars calculated in this section are the total tars comprising only of naphthalene and benzene in the product gas. It must be noted that although according to the definition of tars given in Section 2.6; benzene does not actually classify as tar, it has been considered as a tar component in the model as done for some of the other gasifier models given in Appendix C. The results with the experimental and model values are presented in Table 20 for GB and RB, respectively.

Table 20: Validation of Total Tars Vol% on dry basis from experiment and model for all tests

TEST NO.	EXP VOL %	MODEL VOL %	ABSOLUTE ERROR [exp-model]	RELATIVE ERROR [abs(exp-model)/exp]
GB				
1	0.368	0.083	0.285	0.775
2	0.141	0.083	0.058	0.414
3	0.470	0.086	0.384	0.817
4	0.205	0.082	0.123	0.599
RB				
5	0.326	0.086	0.241	0.738
6	0.422	0.093	0.330	0.780
7	0.092	0.032	0.061	0.657
8	0.048	0.031	0.018	0.369

It is observed that the tar content of the product gas predicted by the model is always lower than the tars measured during the experiments; largely due to the of the assumption of phenol as model tar in the pyrolysis reactor block in the model. In reality, many tar species are formed during pyrolysis stage, which take part in biomass gasification. A consideration of these components in the pyrolysis block and subsequently in the gasification section of the model is expected to improve the results in terms of achieving values closer to the experiments, especially for permanent gases such as CH_4, H_2 and CO which are formed during the oxidation, reforming and cracking of these tar species. However, within the limited time frame, this was the best possible result achieved with respect to tar analysis from the model.

It is suggested to analyse tars along with gases, liquid and solid fraction obtained during pyrolysis experiments performed in Pyroprobe apparatus with HPLC or GC-FID, as is done for tar analysis from the product gas from the gasifier. In this way, devolatilization curves can be generated for the different tars analysed and the yield of the various tar species can be determined as a function of temperature and implemented in the Fortran code similar to the determination of the permanent gases yield in the Fortran Code. This would help in a more accurate tar measurement from the current model.

5.1.4 CO/CO$_2$, H$_2$/CO, CH$_4$/H$_2$ ratios for GB and RB

The specific gas ratios are obtained by dividing the values obtained for each species during the determination of the yield of permanent gases for Section 5.1.1. These ratios can also be calculated from the molar flowrate of each species from Aspen Plus®. The results with absolute and relative errors between the experimental and model values are presented in Table 21 and 22 for GB and RB respectively.

Table 21: Validation of CO/CO$_2$, H$_2$/CO and CH$_4$/H$_2$ Ratios from experiment and model with absolute and relative errors for tests with GB

TEST NO.	EXP RATIO	MODEL RATIO	ABSOLUTE ERROR [exp-model]	RELATIVE ERROR [abs(exp-model)/exp]
CO/CO$_2$				
1	0.992	1.012	-0.020	0.020
2	0.925	0.950	-0.025	0.027
3	1.036	1.005	0.031	0.029
4	0.950	1.026	-0.076	0.080
H$_2$/CO				
1	1.185	1.186	0.001	0.000
2	1.307	1.255	0.052	0.039
3	1.024	1.170	-0.146	0.142
4	0.914	1.340	-0.426	0.466
CH$_4$/H$_2$				
1	0.259	0.262	-0.003	0.011
2	0.240	0.248	-0.008	0.033
3	0.297	0.272	0.025	0.084
4	0.353	0.200	0.153	0.433

Table 22: Validation of CO/CO$_2$, H$_2$/CO and CH$_4$/H$_2$ Ratios from experiment and model with absolute and relative errors for tests with RB

TEST NO.	EXP RATIO	MODEL RATIO	ABSOLUTE ERROR [exp-model]	RELATIVE ERROR [abs(exp-model)/exp]
CO/CO$_2$				
5	0.929	1.003	-0.074	0.079
6	0.920	0.801	0.119	0.129
7	0.717	0.928	-0.211	0.294
8	0.706	1.057	-0.351	0.497
H$_2$/CO				
5	1.208	1.270	-0.062	0.051
6	1.174	1.330	-0.156	0.132
7	1.695	1.359	0.336	0.198
8	1.909	1.334	0.575	0.301
CH$_4$/H$_2$				
5	0.278	0.245	0.033	0.118
6	0.285	0.304	-0.019	0.060
7	0.208	0.284	-0.076	0.365
8	0.157	0.246	-0.089	0.566

The following observations can be made from Table 21 and 22:

➢ Overall, the ratios are predicted well by the model and practically match the experimental values within a maximum absolute error of 0.351 for CO/CO$_2$ (Test 8 RB), 0.575 for H$_2$/CO (Test 8 RB) and 0.153 (Test 4 GB) for CH$_4$/H$_2$.

➢ The average relative errors lie within 3.9% for CO/CO$_2$, 2.4% for H$_2$/CO and 4.2% for CH$_4$/H$_2$ for all tests with GB.

➢ The average relative errors lie within 24% for CO/CO$_2$, 34% for H$_2$/CO and 27% for CH$_4$/H$_2$ for all tests with RB.

➢ The deviation between the model and experimental values for the various gas ratios is lower for GB as compared to RB.

➢ A larger deviation is observed in H$_2$/CO and CH$_4$/H$_2$ ratios for Test 4 compared to other tests with GB due to overestimation of H$_2$ from the model for this test as shown in Section 5.1.1.1.

➢ Test 7 and 8 show higher deviations in CO/CO$_2$ and H$_2$/CO ratios due to comparatively larger differences from the experimental gases yield shown by the model for these tests.

The potential reasons for the cause of the differences in the yield of gases, causing deviations in the CO/CO$_2$, H$_2$/CO and CH$_4$/H$_2$ are discussed in Section 5.1.

5.1.5 Concluding Remarks

Overall, the model predicts the gas composition quite well. Apart from nitrogen, hydrogen is the most abundant component predicted for both GB and RB. The maximum deviation among the permanent gases yield with respect to all three categories (high temperature tests with GB, RB and low-temperature tests with RB) was observed for H_2 (high-temperature test with GB using F046), for CO (high-temperature test with RB using F046), and for CO (low-temperature tests with RB using F054). N_2 and H_2O values from the model agree fairly with the values measured through experiments, except with the largest deviation shown for a high-temperature test with RB using F054. N_2 values from the model is always below the experimental values with underestimation in case of tests with RB. The H_2O values from the model are always above the experimental results in case of tests with RB and for first three tests with GB. The model predicts the gas composition for high-temperature tests with better accuracy than the low-temperature tests, with the exception of overestimation of H_2 value obtained from the model for one of the high-temperature tests with GB using F046 bed material. It is difficult to determine whether tests with a particular bed material type gives lesser deviations from the model. The low-temperature tests are carried out with minimum supply of primary air to sustain the temperature of the bedzone and with certain amount of secondary air supplied to the freeboard region of the gasifier. The possible causes of differences observed with respect to the overestimation of CO for the low-temperature tests 7 and 8 in the model and experiment have been attributed to the possibility of diffusion of secondary air to the bedzone and gas-bed regions of the gasifier during the experiments and enhancing the combustion or oxidation reactions there, which does not occur in the model. Another possible cause has been attributed to the consideration of limited tar species in the model as compared to the various tar species undergoing cracking in the gasifier, which is facilitated under the influence of secondary air as seen in different literature studies [73]. Thus, a higher difference could be caused in the low-temperature tests with the cracking of these tars impacting the CO, CH_4 and H_2 yields. The CC, CGE and OE obtained from the model resemble the experimental values, except for a larger deviation observed for the low-temperature tests with secondary air. The consideration of GE in the calculation of CGE and OE is shown to result in a considerable improvement in the values, especially for tests with RB having a higher mass loss during the experiments. The tars have been predicted from the model with the use of phenol as tar species in the pyrolysis reactor block in the model, cracking into benzene and naphthalene. The consideration of limited tar species results in an underestimation as compared to the experimental values. The various gas ratios CO/CO_2, H_2/CO and CH_4/H_2 have been calculated from the model and are found to be in reasonable agreement with the experimental values, except for certain tests which have more deviations in the gas compositions predicted from the model. For the high temperature tests with GB, the model and experiment fairly follow the same trend for the first three tests with a slight deviation in CO_2 concentration. For the high-temperature tests with RB, the experiment and model also follow the same trend except for CO. For the low-temperature tests with RB, the same trend is followed except for CO and H_2O. A clear trend cannot be established for the CC, probably due to different conversion factors assumed for char density considered in the freeboard for the Boudouard, MSR and char reforming reaction in each test. The CGE and OE obtained from the model is always higher and follow the same trend in case of tests with RB. The OE follows the same trend as experiments for the first three tests in case of GB.

Overall, the model produces similar results as the experiments with certain deviations which are measured in terms of absolute and relative error compared to the values obtained from the experimental data. It can be concluded that the model would resemble the reality after taking into account various factors which could be the cause for this deviation.

The various reasons giving rise to differences between the experimental and model values include: -

➢ The reactions considered for gasification are an approximation of what happens in reality. In reality, many more reactions might be taking place in the gasifier. In addition to this, kinetic parameters for each reaction are taken from literature where reaction rates have been determined by experiments conducted for woody biomass at conditions similar to IHBFBSR setup. Minor differences in the kinetic parameters such as activation energy and rate constant could lead to different results in the model in terms of product gas composition, especially for WGS and MSR reactions.

➢ The PSD performed for biomass, char and ash is attempted to be carried out as accurately as possible. However, experimental errors in the process cannot be avoided. It could arise due to less time allowed than needed for vibrations, errors during measurement of weight of sieves or measuring container with biomass sample or passing of very fine particles through the sieves.

➢ Only phenol is modelled as the tar species in the Fortran code (giving mass yields of gas, liquid and solid fractions as output to pyrolysis block – RYield in Aspen Plus®). This is because of the reason that phenol is the most abundant species produced during pyrolysis in the temperature range of 700-900°C according to the observations made in the study from [64] and consideration of more tars was observed to result in an overestimation of tars from the model. However, in reality many tar species are generated from biomass pyrolysis which react and contribute to the gasification process and the overall composition of the product gas.

➢ Char is assumed to contain only carbon in the model, whereas it is seen that in reality, char also contain small amounts of oxygen, hydrogen, nitrogen and ash.

➢ The mass balances in Pyroprobe experiments do not close, and this is assumed to be contributed by gases, liquids and solids fraction generated during pyrolysis in the model. In reality, one fraction could contribute to the mass deviation to a greater extent or may not contribute at all to the mass deviation.

➢ The mass yields obtained from the Pyroprobe experiment have been normalized to 100% to account for the mass loss produced during Pyroprobe experiments and fitted on experimental data by the best fit curve. These values obtained for the coefficients of the various gases through this process may not be completely accurate as a result of normalization and extrapolation of experimental data. Moreover, the experimental data is obtained by performing pyrolysis on a small biomass sample which may not accurately depict the composition of the entire biomass feed to the gasifier. Certain assumptions taken for modelling the pyrolysis process in the model include: zero unreacted biomass during pyrolysis process and instant heating of biomass particle to the pyrolysis temperature with uniform temperature distribution over the biomass particle. In reality, local heat spots might be formed in the pyrolysis and gasification

section in addition to non-uniform distribution of reactants in the gasifier which can influence the kinetic rate of various reactions having an impact on the gas composition.

➢ Pyrolytic water cannot be measured from the experiments due to unavailability of Karl-Fischer apparatus required for the quantification of pyrolytic water. Therefore, an empirical relation for pyrolytic water is taken from literature to be used in the Fortran code which may deviate from actual amount of pyrolytic water formed.

➢ The model assumes gasification step to occur after the pyrolysis process. In reality, there could be an overlap between the gasification steps.

➢ The model is developed based on single-phase fluidization theory. A two-phase or three-phase model depicting more complex fluidization behaviour can predict the fluid dynamics phenomenon in the gasifier more accurately.

➢ Errors can also arise during performing the experiments: these include errors during measurement of tars and gases yield from the synthesis gas via HPLC or µ-GC, errors during analysis of liquid and solid fraction obtained from pyrolysis or errors during measurement of temperatures via thermocouple readings.

5.2 Recycle of fraction of the product gas to the burners and Sensitivity Analysis for evaluating process parameters for methanol production

This section evaluates the possibility of product gas recycle to the burners to generate heat, and to eliminate methane consumption for heat supply. It also does an analysis of the requirements or changes in process parameters for methanol production. Since a single test is chosen to evaluate this possibility as well as to perform sensitivity analyses for determining parameters required for optimal methanol production, first the H_2/CO ratio and $(H_2-CO_2)/(CO_2+CO)$ values are evaluated for each test from the model and presented in Table 23. As discussed in Section 4.2, based on this parameter, the selection of the test can be done.

Table 23: H_2/CO and $(H_2-CO_2)/(CO_2+CO)$ ratios from the model for different tests used for validation

Test no.	Experiment Date	H_2/CO	$(H_2-CO_2)/(CO_2+CO)$
1	07-10	1.186	0.099
2	12-10	1.255	0.098
3	14-10	1.170	0.088
4	19-10	1.340	0.184
5	25-11	1.270	0.136
6	27-11	1.330	0.063
7	04-12	1.359	0.135
8	15-12	1.334	0.199

It can be observed in Table 23 that the H_2/CO ratio is much closer to the desired ratio of 2:1 required to be achieved for optimal methanol production. Hence, it is decided to perform sensitivity analyses and evaluate the H_2/CO ratio by varying SB*, secondary air intake and primary air intake to observe the impact on other aspects: product gas composition, N_2, H_2O,

CC, OE, tar yields and on other ratios: CO/CO_2, CH_4/H_2. The effect of varying SB*, secondary air intake and primary air intake on the product gas temperature is also evaluated.

From Table 23, it can be seen that the H_2/CO ratio for Test 7 is the closest to the desired value of 2:1 ratio required for an optimal methanol yield. The values obtained for Test 4, 6 and 8 are also close. However, during the validation of the model, it was observed that the total amount of gas produced from Test 8 was higher than the gas produced from the other tests. Since the difference in H_2/CO ratio between these tests is not very significant, it is decided to choose Test 8 for performing the sensitivity analysis keeping in mind that less fraction of the product gas stream needs to be recycled back to the burners.

It could be observed that the total amount of gas produced from the different tests is not sufficient to be used for generating the required amount of heat in both burners. Hence, it is decided to recycle only a fraction of the product gas stream to one burner, thus eliminating the need for natural gas combustion in one of the two burners. It has been estimated that a value close to 84.88% of the product stream is needed to be recycled back to the bottom burner C-100 for generating 20 kW of heat in conditions pertaining to Test 8. In such case, the amount of gas available to be used for further gas cleaning and methanation reaction for the production of methanol is only 15.12% of the product gas obtained from the gasifier. Hence, it is decided to recycle the product gas to the top burner C-80 for producing 12 kW power. The fraction of product gas needed to be recycled for the top burner for Test 8 is 50.92% of the product gas. This has been assumed to be acceptable considering that 49.08% of the product gas is still left to be used for methanol production. However, it should be taken into account that the experiments produce a lower amount of gas due to mass losses defined by GE as described in Section 5.1.2. Also, this value is a rough estimate; as in reality other methods such as water scrubbing techniques could be performed prior to recycling. The recycle stream considers the combustion reactions Eq 4.12 till Eq 4.16. Along with benzene and naphthalene, if more tar species are included in the model in future, that could change the value of recycle fraction obtained for this test.

In addition to optimal value of H_2/CO ratio required for production of methanol from syngas, additional conditions of tar, particulates and alkali metals limit in syngas has to be met which can be achieved by subsequent gas cleaning procedures [58]. For this study, it is chosen to only analyse the H_2/CO as an important criterion to be taken into account during production of methanol.

Sensitivity analyses is performed for Test 8 by varying three parameters:

- ➢ SB*
- ➢ Secondary Air Intake
- ➢ Primary Air Intake

5.2.1 Impact of SB* Variation

The SB* has been varied by changing the steam flowrates (kg/hr) in the model and keeping other input parameters constant as per Test 8 input conditions. The process conditions for this analysis can be found in Table 24. The results of the impact of varying the SB* on product gas composition, N_2, H_2O, tars, CC, OE and various gas ratios along with the temperature of product gas are given in Appendix P. According to [44], the optimal range for varying SB* should lie between 0.5 and 1. A value lower than 0.5 will result in insufficient fluidization of

the bed material. A value higher than 1 will require energy to heat the incoming steam, and will reduce the energy efficiency of the gasifier setup. As the value of λ used for Test 8 is very low, it is considered to start from a minimum SB* of 0.5 corresponding to 3.6 kg/hr of steam mass flowrate. The maximum amount of steam that can be utilised as a gasification agent during the tests in the IHBFBSR is 15 kg/hr. The SB* corresponding to this value is 1.9. Though this is a very high value to be considered for SB*, it is still decided to run the sensitivity tests for this upper limit of the reactor to evaluate what happens to the product gas composition, N_2, H_2O CC, OE, tar yield and the various ratios: CO/CO_2, CH_4/H_2 along with H_2/CO ratio.

Table 24: Process Conditions to study Impact of Varying SB*

Variable	Symbol	Range	Unit
Steam Flowrate	M_{STEAM}	3.6-15	[kg/hr]
Steam to Biomass Ratio	SB*	0.5-1.9	--
Parameters	Symbol	Range/Type	Unit
Biomass Type	--	RB	--
Pyrolysis Reactor Temperature	T_{PYR}	722	[°C]
Bedzone Temperature	T_{CSTR1}	722	[°C]
Gas-Bed Temperature	T_{CSTR2}	754	[°C]
Freeboard Temperature	T_{PFR}	856	[°C]
Primary Air Flowrate	M_{AIR1}	1.9	[kg/hr]
Secondary Air Flowrate	M_{AIR2}	8	[kg/hr]
N_2 purge	M_{N2}	6.6	[kg/hr]
Outlet Pressure of Product Gas	P_{GAS}	70	mbar
Bed Material Type	--	F054	--

The effect of varying the SB* on product gas composition (permanent gases) and on N_2 and H_2O volume % in the product gas can be seen in Figure 36 respectively.
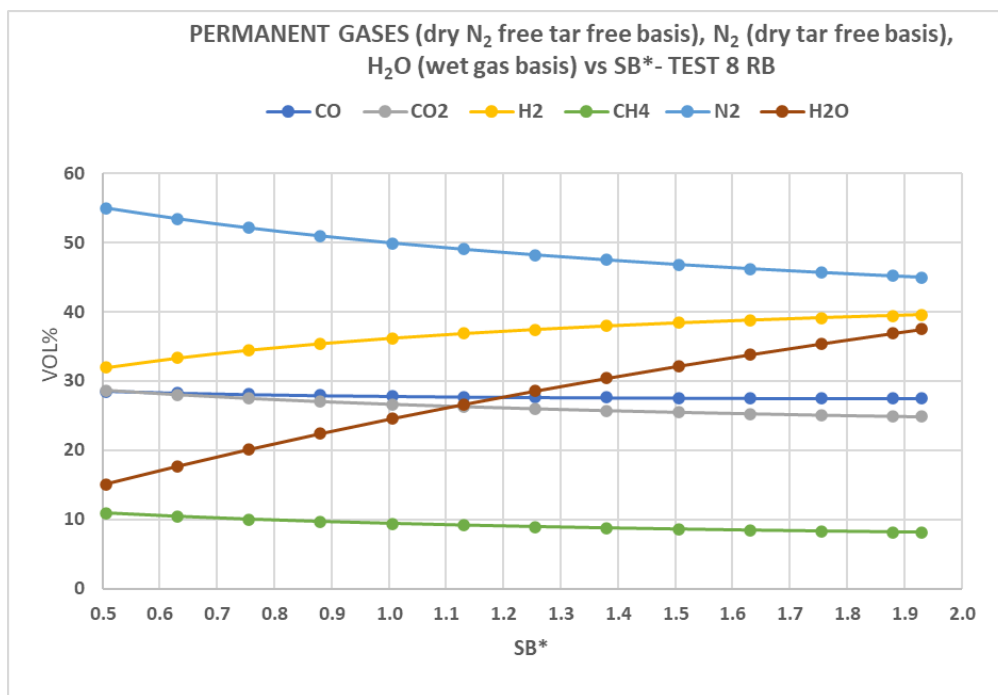
Figure 36: Impact of varying SB on Product Gas Composition, N_2 and H_2O volume % with process parameters kept constant at T_{PYR} and T_{CSTR1}=722°C, T_{CSTR2}=754°C, T_{PFR}=856°C, M_{AIR1}=1.9 kg/hr, M_{AIR2} =8 kg/hr, N_2 purge = 6.6 kg/hr and bed material = F054*

From Figure 36, it can be observed that as SB* is increased, there is significant increase in the H_2 yield, and moderate decrease in CO and CO_2 yield. The CH_4 yield shows slight decrease. The decrease in CO and increase in H_2 with increasing SB* matches similar observations made in Figure 16 as per [44], and the decrease in CH_4 and CO_2 with increase in SB* matches with the observations made in [60]. The decrease in CO, CH_4 and increase in H_2 with increase in SB* is also observed in the results for Test 1, 2 and 3 from the model and from the experiments given in Section 5.1.1.1. The effect of increasing the steam flowrate on the product gas composition is complex, and is influenced considerably by the chemical equilibrium attained in WGS reaction [60]. The addition of steam increases the H_2O concentration, and decreases the volume% of N_2 on dry tar free basis. The constant increase in H_2O yield is an indicator to the fact that less steam is actually being consumed for the reforming reactions than is added.

Figure 37 denotes the effect of varying SB* on CC and OE.
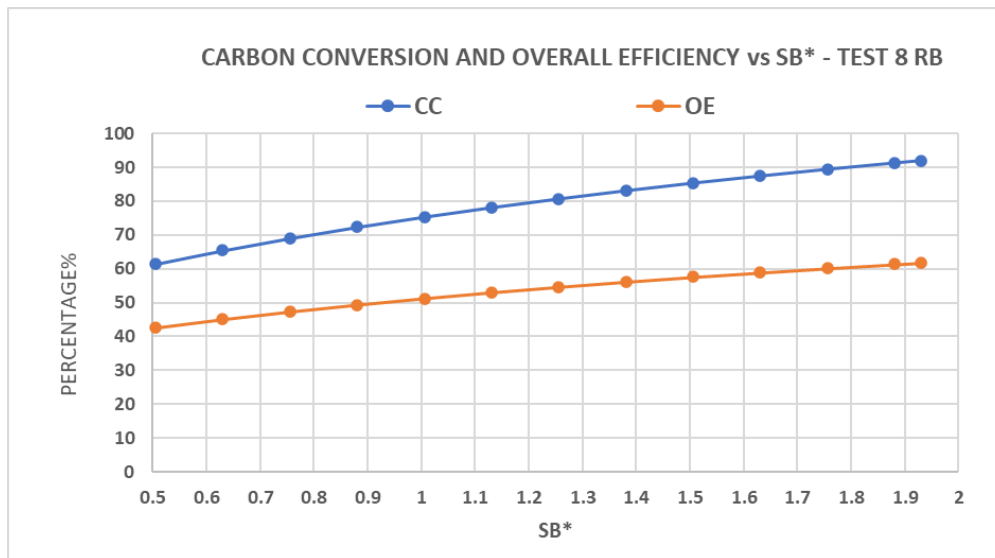
Figure 37: Impact of varying SB* on CC and OE with process parameters kept constant at T_{PYR} and T_{CSTR1}=722°C, T_{CSTR2}=754°C, T_{PFR}=856°C, M_{AIR1}=1.9 kg/hr, M_{AIR2} =8 kg/hr, N_2 purge = 6.6 kg/hr, bed material = F054

As seen in Figure 37, the increase of steam flowrate enhances the CC of the test as could be expected by promotion of char gasification upon added steam. Figure 37 shows an increasing trend for CC and OE with increase in SB*. The OE was calculated by considering the same heat input to the two preheaters, and similar burner efficiencies as the original parameters of the Test 8. However, as the steam flowrate increased, the power lost (represented by P-LOSS2 in Figure 26) decreased showing that more power was utilised in heating the incoming steam. The OE, nevertheless increased, probably as a result of increase in H_2 concentration contributing to the LHV of the product gas and the increase in the total gas flowrate due to rise in the temperature of the product gas and rise in H_2O concentration as the SB* increased. [62] however, shows a negative influence on CC and CGE with increase in SB*. The results for impact of variation of SB* to cause an increase in CC and OE as obtained for our case is still supported in literature findings such as [74].

Figure 38 denotes the effect of varying SB* on total volume of tars on a dry basis.
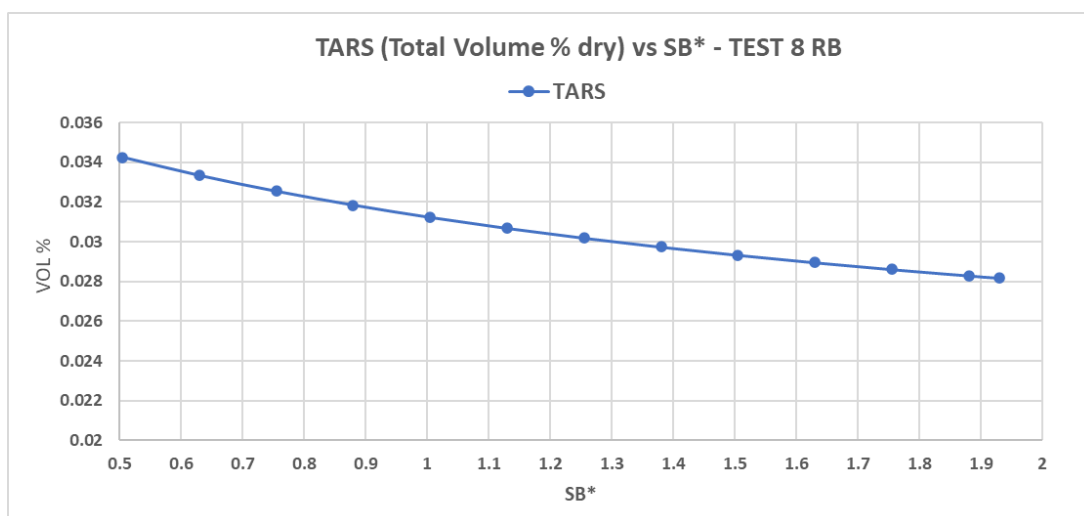
Figure 38: Impact of varying SB on tars (total volume% on dry basis) with process parameters kept constant at T_{PYR} and T_{CSTR1}=722°C, T_{CSTR2}=754°C, T_{PFR}=856°C, M_{AIR1}=1.9 kg/hr, M_{AIR2} =8 kg/hr, N_2 purge = 6.6 kg/hr, bed material = F054*

The total volume% of tars are found to decrease with increase in SB*, probably due to enhanced thermal cracking at higher temperatures. The rise of temperature of the product gas with increase in SB* is shown in Figure 39.
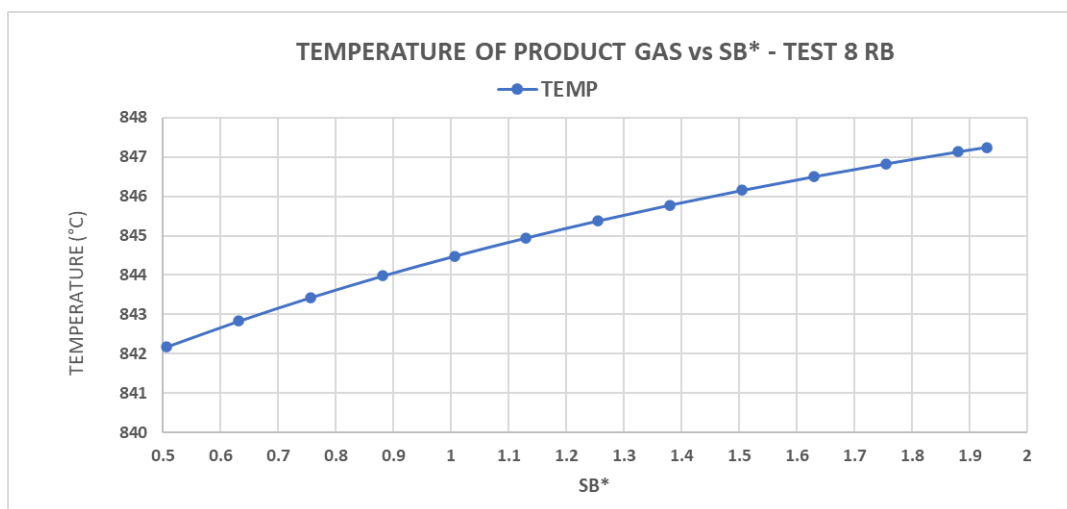
Figure 39: Impact of varying SB on temperature of product gas with process parameters kept constant at T_{PYR} and T_{CSTR1}=722°C, T_{CSTR2}=754°C, T_{PFR}=856°C, M_{AIR1}=1.9 kg/hr, M_{AIR2} =8 kg/hr, N_2 purge = 6.6 kg/hr, bed material = F054*

The increase in H_2 yield with increasing SB* and the moderate decrease in CO leads to an increasing H_2/CO ratio in the range for which the sensitivity analysis is performed; that can be observed from Figure 40. The highest H_2/CO ratio obtained from the sensitivity tests is 1.434 which corresponds to the highest steam flowrate limit of 15 kg/hr (SB* 1.9) to the IHBFBSR. The CO/CO_2 and CH_4/H_2 were observed to increase and decrease respectively at a moderate pace with increase of SB* as seen in Figure 40.
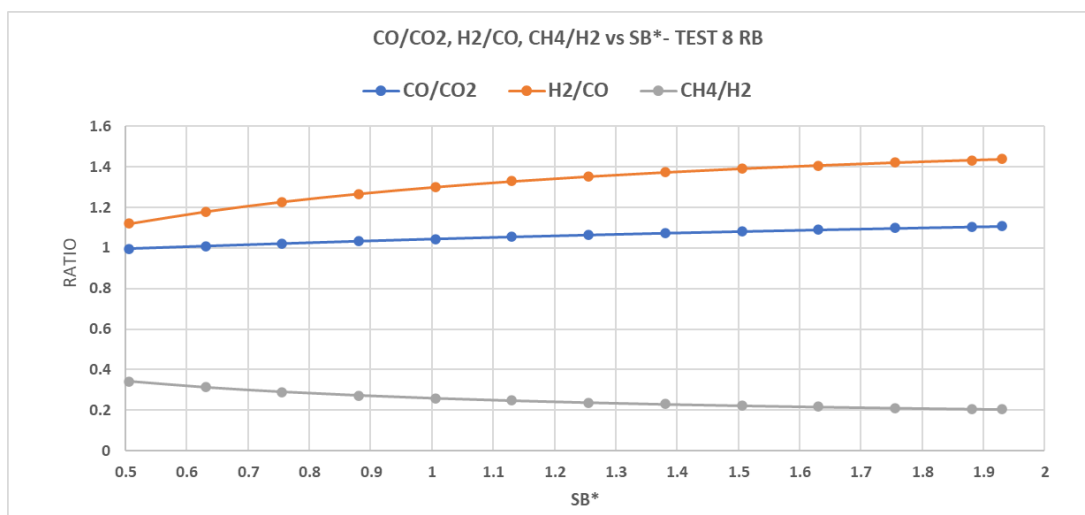
Figure 40: Impact of varying SB* on CO/CO₂, H₂/CO and CH₄/H₂ with process parameters kept constant at T_PYR and T_CSTR1=722°C, T_CSTR2=754°C, T_PFR=856°C, M_AIR1=1.9 kg/hr, M_AIR2 =8 kg/hr, N₂ purge = 6.6 kg/hr, bed material = F054

From running the simulations in Aspen Plus®, it is observed that the current power input of 6 kW to the second preheater in the model for heating steam is still sufficient to heat 15 kg/hr of steam. However, the current amount of heat supply to the preheater can be optimized by supplying only the required amount of heat to the preheaters or by removing one pre-heater. Moreover, it is also observed that beyond a SB* of 1.5, the pressure drop in the cyclone separators is very high due to the high gas flowrate. It is therefore advisable to increase the steam flowrate such that SB* obtained is within the range of 0.5-1 or a maximum of 1.5 for experiment with input parameters similar to this test and subsequently use a water gas shift reactor to increase the H_2/CO ratio of the synthesis gas required for the production of methanol.

5.2.1 Impact of Secondary Air Variation

The impact of secondary air intake on the product gas composition can be seen in Figure 41. The secondary air intake is varied such that the total equivalence ratio - λ_{total} (including the primary air intake) is within the range 0.041-0.51. The minimum amount of primary air supply of 1.9 kg/hr was required during the experiments to sustain the temperature of the bedzone while performing the gasification tests. At zero secondary air supply, this corresponds to a λ_{total} of 0.041 for Test 8. The maximum limit of the secondary air supply allowed to the IHBFBSR is 22 kg/hr which corresponds to a λ_{total} of 0.51. Hence, the secondary air intake is chosen to be varied between 0 -22 kg/hr. The process conditions for this analysis can be found in Table 25. The results of the impact of varying secondary air intake on product gas composition, N_2, H_2O, tars, CC, OE and various gas ratios along with temperature of product gas is given in Appendix Q.

Table 25: Process Conditions to study Impact of Secondary Air Intake

Variable	Symbol	Range	Unit
Secondary Air Intake	M_{AIR2}	0-22	[kg/hr]
Total Equivalent Ratio	λ_{total}	0.041-0.51	--
Parameters	**Symbol**	**Range/Type**	**Unit**
Biomass Type	--	RB	--
Pyrolysis Reactor Temperature	T_{PYR}	722	[°C]
Bed Temperature	T_{CSTR1}	722	[°C]
GasBed Temperature	T_{CSTR2}	754	[°C]
Freeboard Temperature	T_{PFR}	856	[°C]
Primary Air Flowrate	M_{AIR1}	1.9	[kg/hr]
Steam Flowrate	M_{STEAM}	8.8	[kg/hr]
N_2 purge	M_{N2}	6.6	[kg/hr]
Outlet pressure	P_{GAS}	70	mbar
Bed Material Type	--	F054	--

The effect of varying the secondary air intake on the product gas composition is seen in Figure 41.
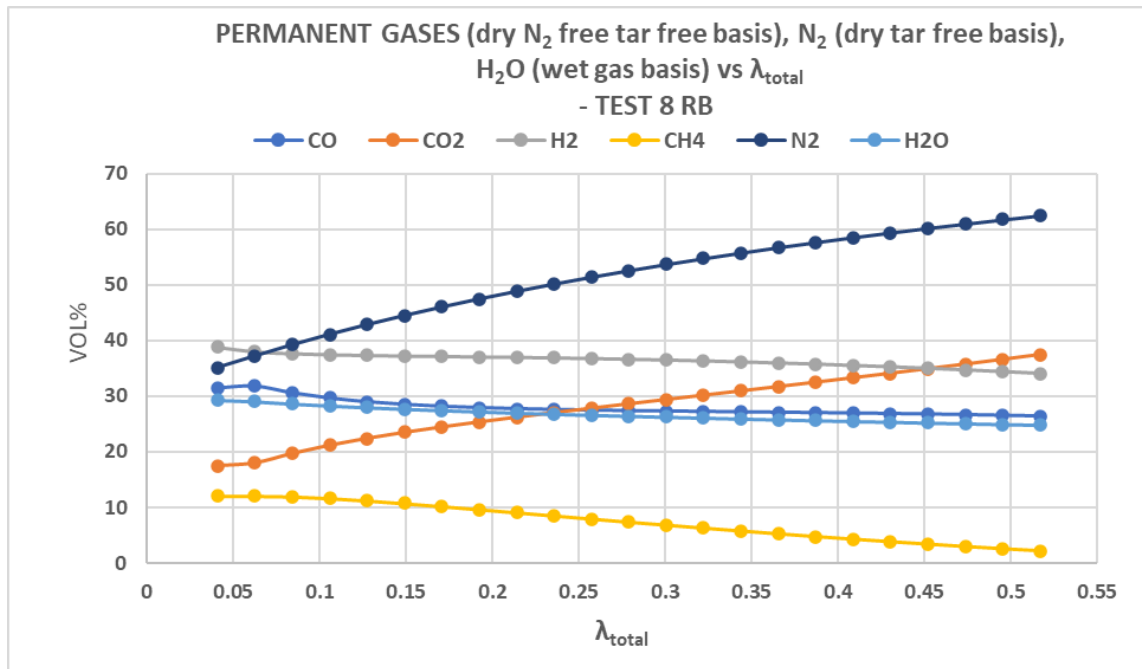
Figure 41: Impact of varying Secondary Air Intake on Product Gas Composition, N_2 and H_2O volume % with process parameters kept constant at T_{PYR} and T_{CSTR1}=722°C, T_{CSTR2}=754°C, T_{PFR}=856°C, M_{AIR1}=1.9 kg/hr, M_{STEAM} =8.8 kg/hr, N_2 purge = 6.6 kg/hr, bed material = F054

In Figure 41, it is seen that with the increase of secondary air intake, the overall oxygen concentration in the gasifier increases which is expected to increase the combustion products: CO_2 and H_2O yield in accordance with Figure 15 and due to enhanced oxidation of CO and H_2 to CO_2 and H_2O. The exception of H_2O decrease in this figure is attributed to the faster rate of increase in the total gas flow rate as compared to the relatively moderate increase observed in

the H_2O molar flowrate, thereby causing a decrease in the overall fraction of H_2O with respect to total gas as λ_{total} increases. The H_2O molar flowrate is observed to increase at a much faster rate, causing an increase in the overall volume fraction beyond the carbon limit for this test where the carbon conversion equals 100%. However, at a constant primary air supply of 1.9 kg/hr and by varying the secondary air, this is only possible at a secondary air supply higher than the limit of 22kg/hr and hence is not analysed for this test. N_2 is observed to increase with λ_{total} due to increase in secondary air supply and CH_4 is found to decrease steeply with increase in λ_{total}.

The effect of varying the λ_{total} on CC and OE is evaluated and presented in Figure 42.
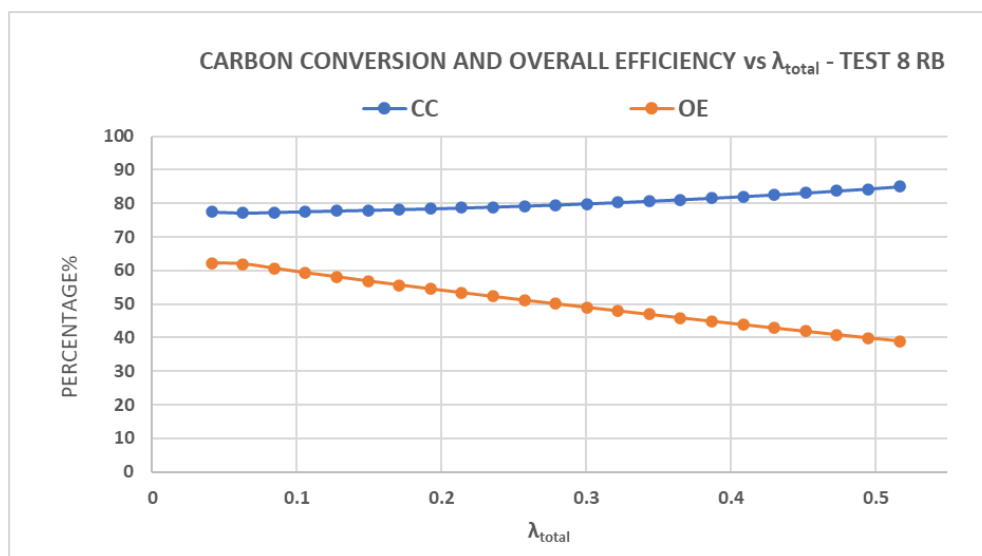
Figure 42: Impact of varying Secondary Air Intake on CC and OE with process parameters kept constant at T_{PYR} and T_{CSTR1}=722°C, T_{CSTR2}=754°C, T_{PFR}=856°C, M_{AIR1}=1.9 kg/hr, M_{STEAM} =8.8 kg/hr, N_2 purge = 6.6 kg/hr, bed material = F054

Figure 42 follows the same trend as for CC and CGE with increasing λ (without secondary air supply) in the reference model [16]. The CGE in the reference model is calculated by taking the burner power into account so it is a good indicator of the overall efficiency of the model. It should be noted that with constant primary air supply of 1.9 kg/hr, secondary air supply higher than the limit for the IHBFBSR (>22 kg/hr) needs to be supplied to achieve a 100% carbon conversion. Moreover, at this high supply of secondary air, the process would resemble combustion rather than gasification with excess of CO_2 and H_2O yield in the product stream resulting in a low-quality product.

In reality, secondary air intake has been observed to cause a significant rise in temperature of the dilute phase region, however reducing gas residence time [73]. Due to the rise in temperature, endothermic reactions like Boudouard, water gas reaction and tar cracking reactions are enhanced [73]. However, addition of secondary air beyond a certain value can result in low efficiency due to gas residence time becoming shorter [73]. The possible impact of increasing the secondary air supply on the total volume of tars and the temperature of the product stream is given in Figure 43 and 44 respectively.
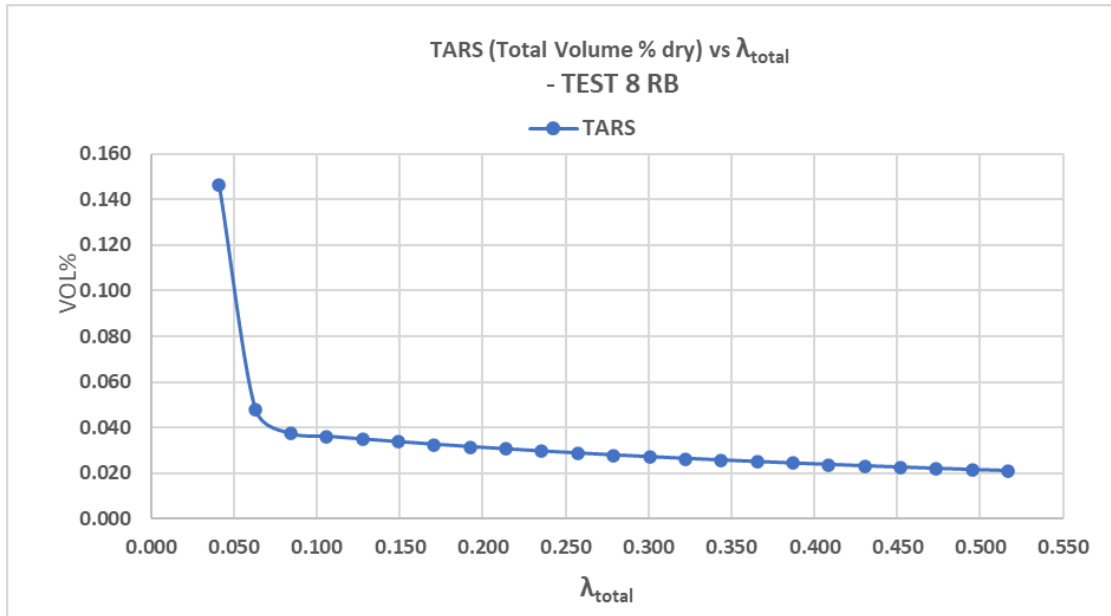
Figure 43: Impact of varying Secondary Air on Tars (total vol% dry) with process parameters kept constant at T_{PYR} and T_{CSTR1}=722°C, T_{CSTR2}=754°C, T_{PFR}=856°C, M_{AIR1}=1.9 kg/hr, M_{STEAM} =8.8 kg/hr, N_2 purge = 6.6 kg/hr, bed material = F054

From Figure 43, it is observed that increasing secondary air supply decreases the total volume of tars in the product gas.
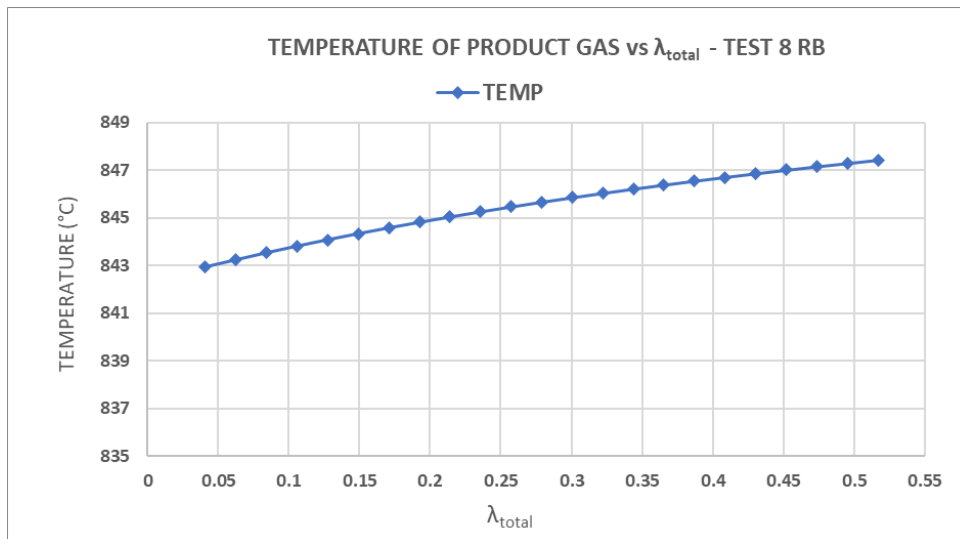
Figure 44: Impact of varying Secondary Air Intake on temperature of product stream with process parameters kept constant at T_{PYR} and T_{CSTR1}=722°C, T_{CSTR2}=754°C, T_{PFR}=856°C, M_{AIR1}=1.9 kg/hr, M_{STEAM} =8.8 kg/hr, N_2 purge = 6.6 kg/hr, bed material = F054

It can be seen from Figure 44 that the temperature of the product gas increases from 842.93°C to 847.23°C as a result of product gas composition variation due to the addition of secondary air intake.

Figure 45 represents the impact of varying secondary air on the various gas ratios: CO/CO_2, H_2/CO and CH_4/H_2.

Figure 45: Impact of varying Secondary Air Intake on CO/CO₂, H₂/CO and CH₄/H₂ with process parameters kept constant at T_{PYR} and T_{CSTR1}=722°C, T_{CSTR2}=754°C, T_{PFR}=856°C, M_{AIR1}=1.9 kg/hr, M_{STEAM} =8.8 kg/hr, N_2 purge = 6.6 kg/hr and bed material = F054

From Figure 45, it is seen that CO/CO_2 and CH_4/H_2 ratios decrease while H_2/CO ratio shows a moderately increasing trend with increase in λ_{total}, with a maximum value of 1.34 reached for a λ_{total} of 0.28. Beyond this point, the H_2/CO ratio decreases. This value of λ_{total} corresponds to a secondary air supply of 11 kg/hr at a constant primary air supply of 1.9 kg/hr. This is well within the limits of maintaining the maximum supply limit of 22 kg/hr of secondary air to the IHBFBSR; and is feasible. However, there is still the requirement of using a water gas shift reactor to increase the H_2/CO ratio to 2 for optimal methanol production.

5.2.1 Impact of Primary Air Variation

For observing the impact of primary air intake on the product gas composition, the same conditions as that considered for the previous sensitivity tests are taken into account. The primary air supply is varied and the secondary air intake is kept constant at a flowrate of 8 kg/hr.

The process conditions for this analysis can be found in Table 26. For the minimum value, a λ (without secondary air consideration) below 0.041 could not be employed during the experiments, because values lower than this were not able to maintain a constant temperature in the bedzone during gasification. The maximum amount of primary air supply allowed to the IHBFBSR is also 22 kg/hr which corresponds to a λ of 0.475. It is decided to vary the primary air flowrate within this range and evaluate its impact on the product gas composition, N_2, H_2O, CC, OE and the various ratios: CO/CO_2, H_2/CO, CH_4/H_2. The effect of adding primary air on the temperature of the product gas is also evaluated. The results of the impact of varying the primary air intake on product gas composition, N_2, H_2O, tars, CC, OE and various gas ratios along with the temperature of product gas is given in Appendix R.

Table 26: Process parameters to study impact of Primary Air Intake variation

Variable	Symbol	Range	Unit
Primary Air Intake	M_{AIR1}	1.9-22	[kg/hr]
Equivalent Ratio (Excluding Secondary Air Intake)	λ	0.041-0.475	--
Total Equivalent Ratio (Including Secondary Air)	λ_{TOTAL}	0.2-0.63	--
Parameters	**Symbol**	**Range/Type**	**Unit**
Biomass Type	--	RB	--
Pyrolysis Reactor Temperature	T_{PYR}	722	[°C]
Bed Temperature	T_{CSTR1}	722	[°C]
GasBed Temperature	T_{CSTR2}	754	[°C]
Freeboard Temperature	T_{PFR}	856	[°C]
Secondary Air Flowrate	M_{AIR2}	8	[kg/hr]
Steam Flowrate	M_{STEAM}	8.8	[kg/hr]
N₂ purge	M_{N2}	6.6	[kg/hr]
Outlet pressure	P_{gas}	70	mbar
Bed Material Type	--	F054	--

The effect of varying the primary air intake on the product gas composition is seen in Figure 46.
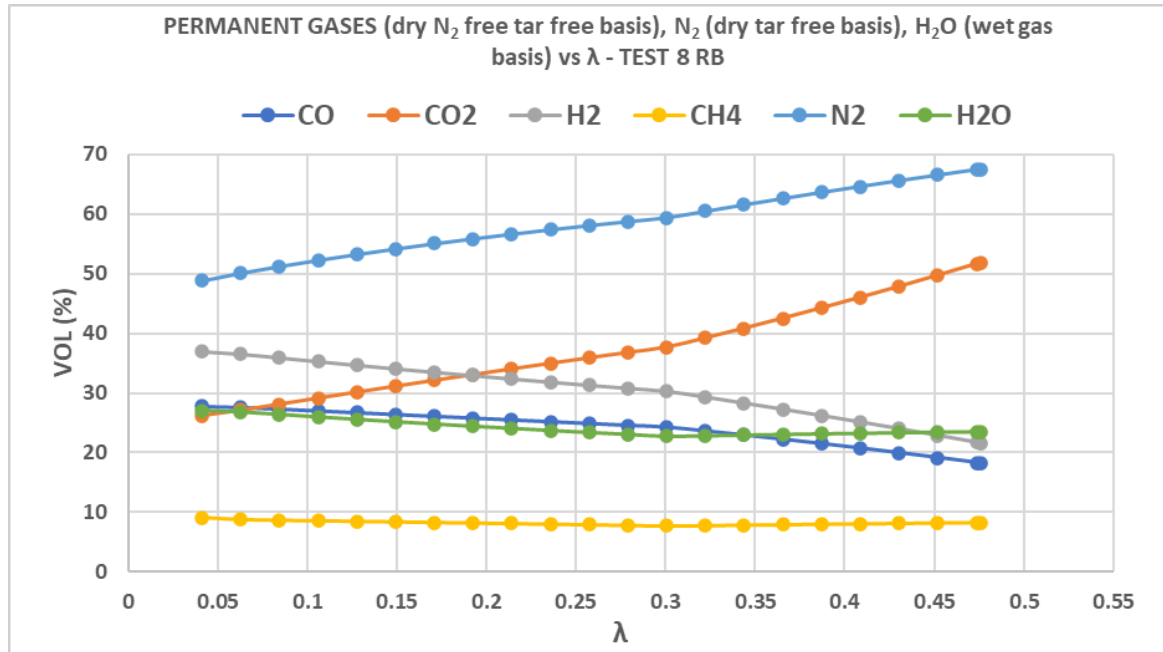
Figure 46: Impact of varying Primary Air Intake on Product Gas Composition, N_2 and H_2O volume % with process parameters kept constant at T_{PYR} and T_{CSTR1}=722°C, T_{CSTR2}=754°C, T_{PFR}=856°C, M_{AIR2}=8 kg/hr, M_{STEAM} =8.8 kg/hr, N_2 purge = 6.6 kg/hr and bed material = F054

The results of the sensitivity tests are in accordance with Figure 15 for the permanent gases. The H_2O is expected to increase with λ, however the rate of increase of total gas flow rate is much higher as compared to the increase in H_2O leading to a decrease in the volume fraction. However, beyond a λ of 0.32, the H_2O concentration begins to increase. This marks the carbon limit. Beyond this limit, the CO and H_2 decrease at a faster rate and CO_2 increases at a faster rate as seen in Figure 46.
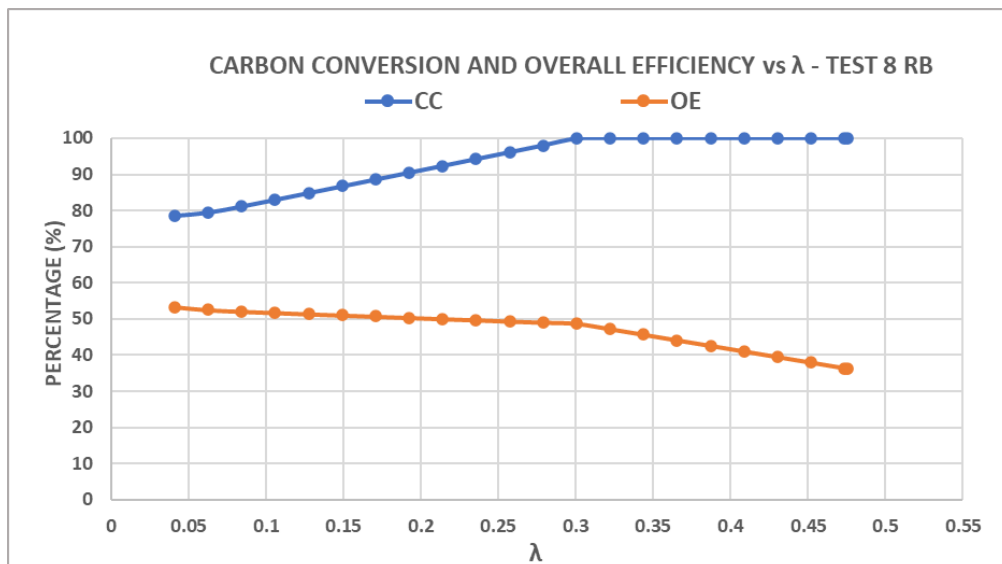
Figure 47: Impact of varying Primary Air Intake on CC and OE with process parameters kept constant at T_{PYR} and T_{CSTR1}=722°C, T_{CSTR2}=754°C, T_{PFR}=856°C, M_{AIR2}=8 kg/hr, M_{STEAM} =8.8 kg/hr, N_2 purge = 6.6 kg/hr and bed material = F054

From Figure 47, a 100% carbon conversion is achieved at a λ of 0.32 by keeping all other parameters constant as given in Table 26 or as specified below the figure. However, it should be noted that with a constant secondary air supply of 8 kg/hr and by keeping all other input parameters constant, and simultaneously increasing the primary air intake shows a very high pressure drop in the cyclone separators beyond a λ value of 0.15, due to the increased gas flowrate. It is advisable to change other parameters such as decreasing the secondary air intake to lower the pressure drop in the cyclone separators.

The effect of increasing the primary air intake on the total volume of tars and on product gas temperature is given in Figure 48 and 49.
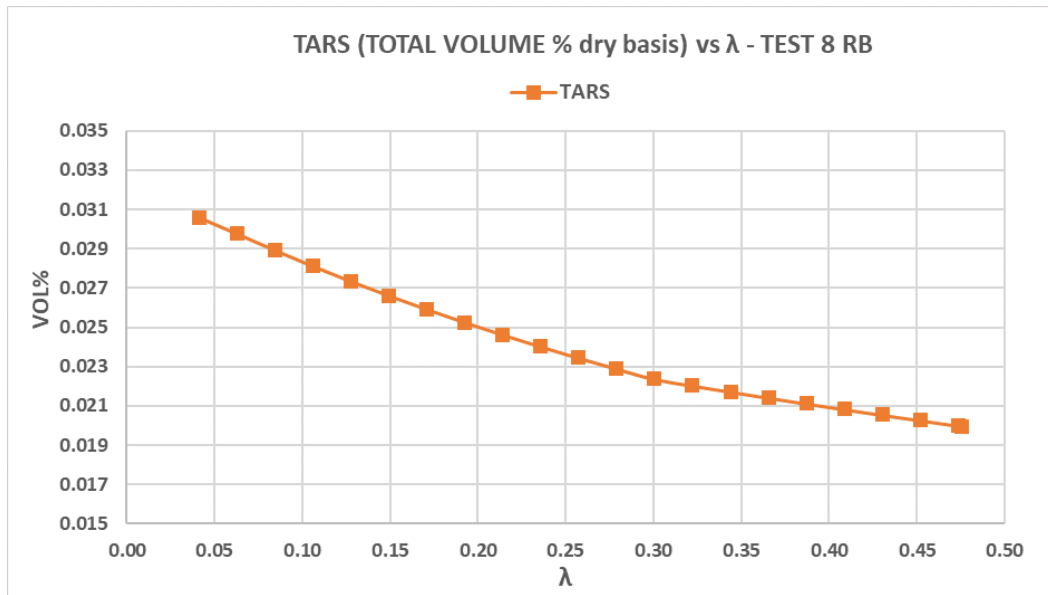
Figure 48: Impact of varying Primary Air Intake on Tars total vol% on dry basis with process parameters kept constant at T_{PYR} and $T_{CSTR1}=722^{\bullet}C$, $T_{CSTR2}=754^{\bullet}C$, $T_{PFR}=856^{\bullet}C$, $M_{AIR2}=8$ kg/hr, $M_{STEAM}=8.8$ kg/hr, N_2 purge = 6.6 kg/hr and bed material = F054
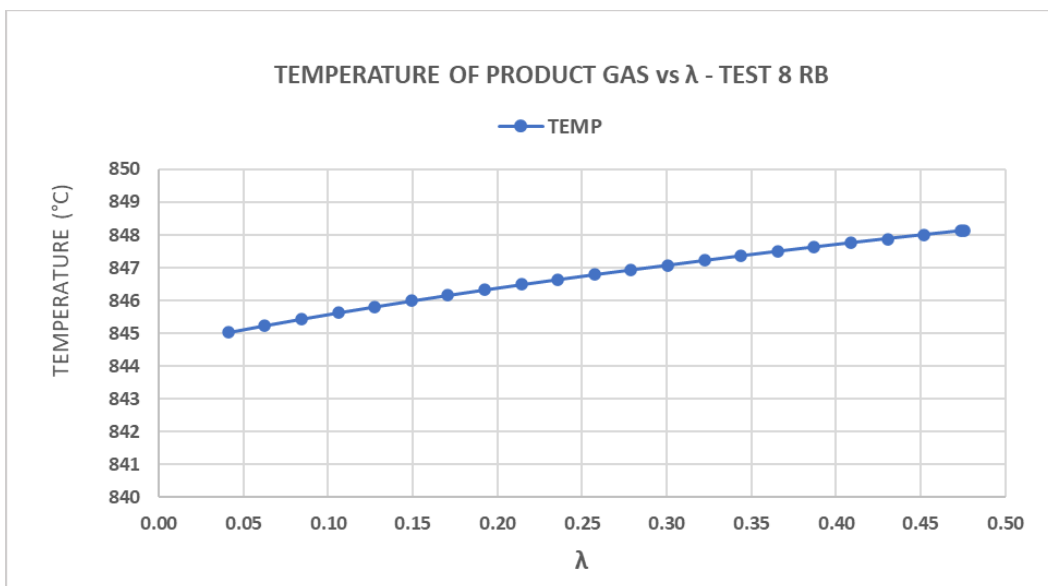
Figure 49: Impact of varying Primary Air Intake on temperature of product gas with process parameters kept constant at T_{PYR} and $T_{CSTR1}=722^{\bullet}C$, $T_{CSTR2}=754^{\bullet}C$, $T_{PFR}=856^{\bullet}C$, $M_{AIR2}=8$ kg/hr, $M_{STEAM}=8.8$ kg/hr, N_2 purge = 6.6 kg/hr and bed material = F054

As seen from Figure 48 and 49, with the increase of primary air inflow, the temperature of the product gas increases and the tar volume fraction in the total gas decreases.

The impact of varying the primary air flow on the various gas ratios is evaluated and presented in Figure 50.
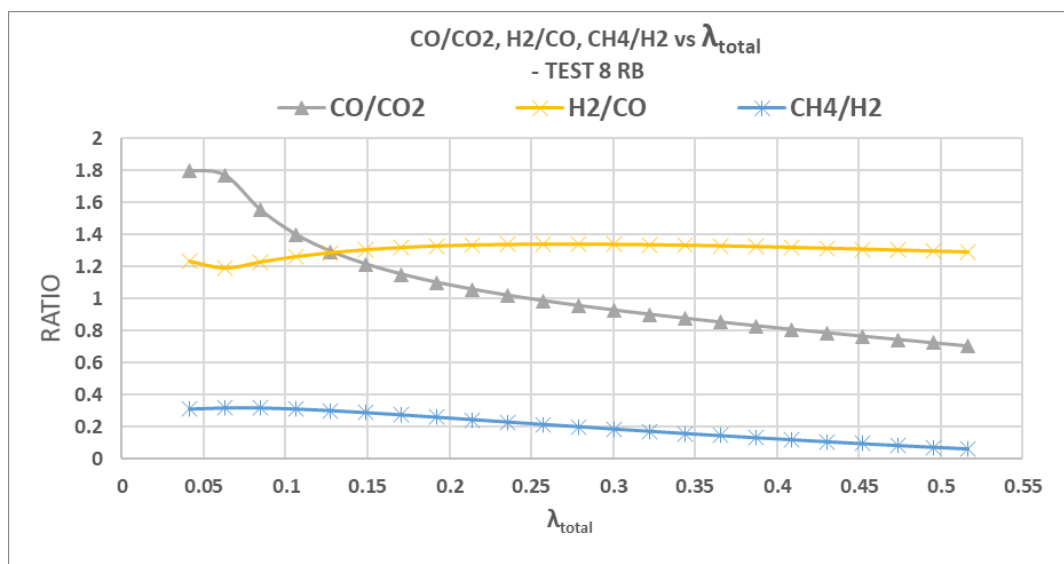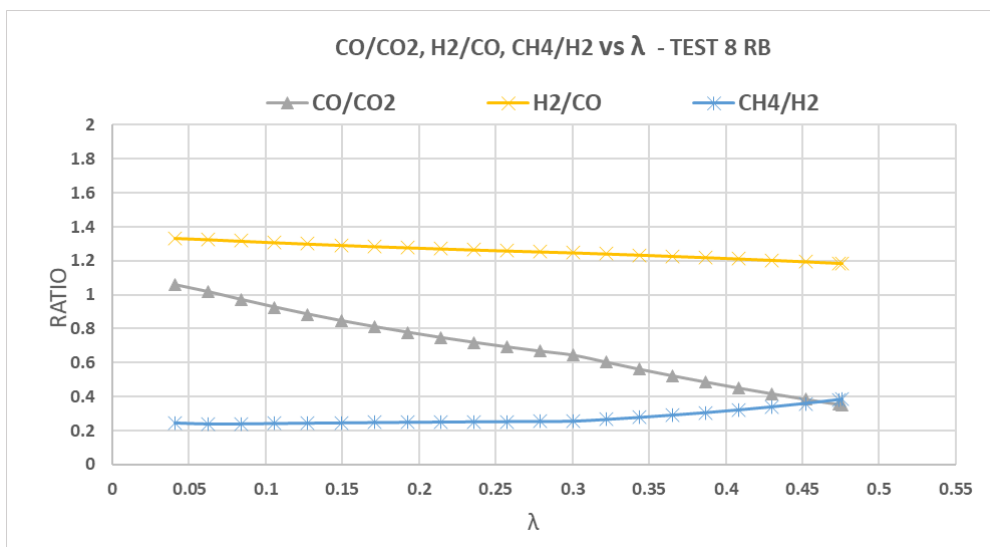

Figure 50: Impact of Primary Air Intake Variation on CO/CO₂, H₂/CO and CH₄/H₂ with process parameters kept constant at T_{PYR} and T_{CSTR1}=722°C, T_{CSTR2}=754°C, T_{PFR}=856°C, M_{AIR2}=8 kg/hr, M_{STEAM} =8.8 kg/hr, N_2 purge = 6.6 kg/hr and bed material = F054

It is observed that the H_2/CO ratio decreases at a moderate pace along with faster decrease in CO/CO_2 and moderate rate of increase in CH_4/H_2 ratio as the primary air intake is increased. Within the current range of λ applied for the sensitivity analysis, the highest ratio for H_2/CO is the starting/base case with the value of 1.334 obtained at a primary air supply of 1.9 kg/hr and a secondary air supply of 8 kg/h, corresponding to a λ of 0.041.

Because of limited time span, it was possible to run the sensitivity analysis for one test by varying a single input parameter and keeping the other parameters constant. It is suggested to conduct a more detailed sensitivity analysis by varying two or more parameters simultaneously, and observing the impact on the product gas composition, N_2, H_2O, CC, OE, tars, temperature of the product gas, and on the various gas ratios: H_2/CO, CH_4/H_2, CO/CO_2. Test 8 with which the sensitivity analysis was conducted is a low-temperature test with secondary air. It is also recommended to conduct sensitivity analysis for other tests such as the high temperatures tests without secondary air.

5.3 Heat and Mass Balance

In this section, the heat and mass balance calculate for Test 8 is reported. Figure 51 represents the heat and mass transfer streams between the different sections in the model.
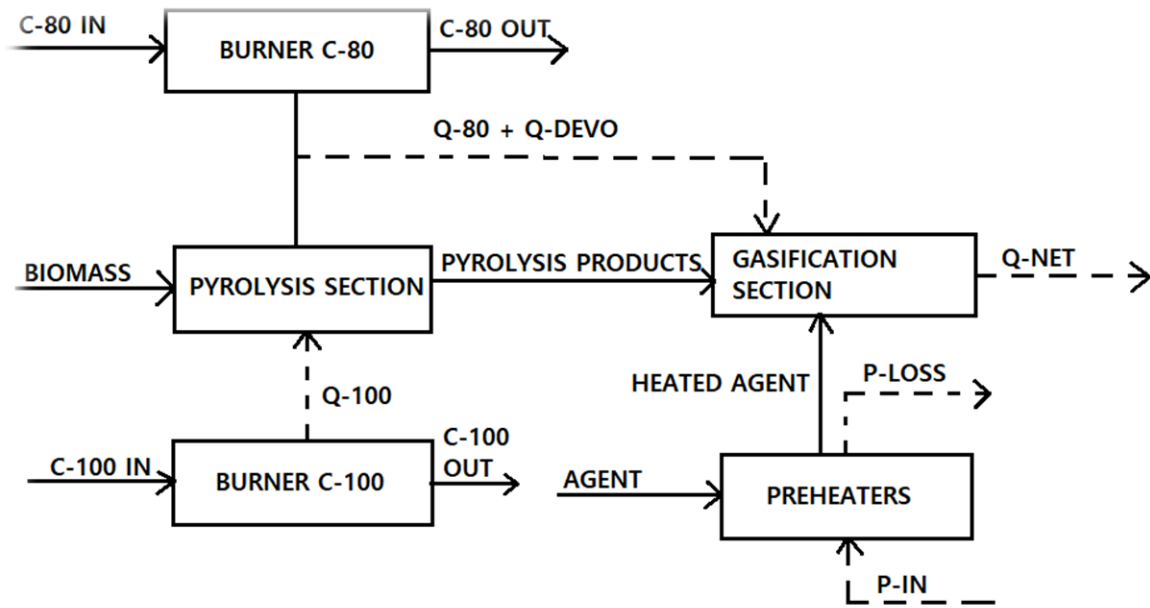
Figure 51: Heat and Mass Transfer in Model between different sections in the model. Dotted lines represent heat transfer; continuous lines represent mass transfer

5.3.1 Heat Analysis in Burners and Pre-Heaters

The two radiant tube burners in the IHBFBSR setup are used for providing heat for the endothermic gasification reactions by combustion of natural gas. The burners are located inside the actual experimental setup but in Aspen Plus®, they have been implemented outside the gasification section due to modelling limitations. In Figure 51, C-100 burner in the flowsheet supplies heat to the pyrolysis reactor block RYield. The heat generated from C-80 burner and RYield together provide heat to the gasification section. The energy required for heating up the gasification agent is supplied by the pre-heaters Preheat 1 and Preheat 2 given in Figure 26.

The C-80 and C-100 burners are designed to supply a nominal power of 12 kW and 20 kW respectively. The energy is generated by combustion reaction as shown in Eq 4.12. The amount of methane required to generate this power is calculated by Eq 5.2 [75].

$$P_{\text{burner}} = (T - T_0)\left[\left(F_{CH_4}C_{P,CH_4}\right) + 2\left(F_{CH_4}C_{P,O2}.(1 + \varepsilon_{O2})\right)\right] + 2 . 3.76\left(F_{CH_4}C_{P,N2}.(1 + \varepsilon_{O2})\right)]$$

$$(Eq 5.2)$$

P_{burner} represents the power supplied by the burners in kW. T_O represents the initial temperature of the reactants in K. F_{CH4} signifies the molar flowrate of methane required to be calculated for generating the necessary amount of power in kmol/s. $C_{P,i}$ denotes the calorific value of the components in kJ/kmol K. The excess amount of oxygen O_2, denoted by ε_{O2} is taken at 2% of the stoichiometric ratio required for combustion of methane. The amount of methane calculated for C-80 and C-100 burners to generate 12 kW and 20 kW power are 1.57 kg/hr and 2.62 kg/hr

respectively. The heat generated by combustion of methane is equal to the mass flow rate of methane multiplied by the HHV of methane which equals 55.5 MJ/kg as reported in [16]. Thus, the heat generated by the combustion of methane in each burner is given in Table 27.

Table 27: Heat generated by methane combustion in burners and heat supplied by burners

	C-80	C-100
Heat of reaction (kW)	25.25	40.39
Heat supplied by burner (kW)	12.00	20.00

It should be noted that 12 kW and 20 kW of power is supplied only when the burners are on. The duration for which the burners are on during the experiments is taken to be the burner efficiency. In most of tests conducted, the bottom burner C-100 remains on for an average of 95% duration; while, the top burner remains on for an average of 84% duration.

The heat balance for Test 8 is given in Table 28, as generated in Aspen Plus®. It should be noted that in the software, the heat balances close or the losses can be seen but in reality, there would be heat losses which are not accounted for.

Table 28: Heat Balance for Test 8

Input Heat (kW)		Heat utilised (kW)		Heat Lost (kW)		Heat Output (kW)
C-100	20.00	RYield	7.41			
C-80	12.00	CSTR$_1$+CSTR$_2$+PFR	2.06			22.53
P-IN1	4.5	PREHEAT 1	0.07	PLOSS-1	4.43	
P-IN2	6	PREHEAT 2	2.56	PLOSS-2	3.44	

It can be observed that the heat required for preheating the gasification agents is quite less as compared to the power at which it operates, especially in the first preheater. This can be an interesting opportunity to explore the option of adding a bypass line, which would allow the first preheater to be used for heating up of the reactor during start-up operations when large quantities of air and nitrogen are used, and allow bypass during operation. This way, the overall efficiency of the process can be increased.

5.3.2 Mass Balance

The mass balance for Test 8 calculates the total input mass flowrates of biomass and gasification agent along with nitrogen purge and total output mass flowrates of product gas, considering each component. It also calculates the input and output mass flowrates in C-80 and C-100 burner.

The mass balance for Test 8 is reported in Appendix S.

6. CONCLUSION AND RECOMMENDATION

The main objective of this research work was set out as to optimize and validate the kinetic model of the IHBFBSR developed by a former student with the results of the first air-steam gasification tests conducted at TU Delft and to evaluate the conditions under which the product gas obtained from the model can be used for one of the many downstream applications commonly implemented from biomass gasification. Production of methanol was chosen to be evaluated among the various end applications of biomass gasification due to the growing interest in this area and the use of methanol in different sectors related to energy, chemical, transportation and manufacturing. Since the model is based on allothermal gasification, a detailed literature review was done on the various allothermal gasifier technologies in commercial use. Moreover, as the study is focussed on modelling a gasifier setup in Aspen Plus® software, an attempt was made at reviewing different gasifier models developed in Aspen Plus® based on kinetic approach.

At the beginning of this research, the master thesis was consolidated into four main research questions. The master thesis now concludes by answering these questions.

6.1 Answering the Research Questions

The first question was: Does the optimized model predict the results of the product gas composition obtained from the IHBFBSR under various operating parameters with respect to the yield of permanent gases, N_2, tars, H_2O, various gas ratios CO/CO_2, H_2/CO, CH_4/H_2 and other key performance parameters such as CC, CGE and OE with reasonable accuracy?

The answer to this question is as follows:

It can be concluded from the results of the validation of the model with the first steam-air gasification tests that overall, the model predicts the gas composition quite well.

The maximum absolute deviations among the gases, considering all tests, are calculated to be 6 for CO (low temperature test with RB using F054), 4.8 for CO_2 (high temperature test with GB using F046), 9.6 for H_2 (high-temperature test with GB using F046) and 2.6 for CH_4 (low-temperature test with RB using F054). The average relative error for these gases among other tests are calculated to be 5.5% for CO and CO_2, 5.1% for H_2 and 10% for CH_4. The most plausible causes for these deviations have been thought of as:

- Possible catalytic reactions in the bed material due to accumulation of unreacted char (though the bed material is considered inert despite not being pure Al_2O_3)
- Non-uniformity in the efficiency of sampling line during the gasification tests, which can cause an additional difference in the product gas flowrates
- Possible diffusion of secondary air during the experiments to other regions of the gasifier during experiments enhancing oxidation reactions in the dense zone
- Enhanced thermal cracking of variety of tars produced during pyrolysis stage in the presence of secondary air influencing the composition of other gas species, especially CO, CH_4 and H_2, as compared to limited tar species considered in the model which might affect other gases yield.

The maximum absolute deviations for N_2 and H_2O concentration considering all the tests are 13.1 and 12.2 respectively for a high-temperature test with RB using F054. The average relative errors for N_2 and H_2O among other tests lie within 11% for N_2 and 8% for H_2O respectively. The most plausible causes for deviations have been thought of as:

- Inlet inaccuracies in nitrogen purge flows during experiments and possible leakage from bunkers and sampling line
- Since nitrogen is calculated based on the flowrates of other gases, a deviation in the values of these gases can also cause a difference in the N_2 values obtained from the model.
- More difficult experimental quantification of H_2O compared to other components

Generally, the model predicts the results of high-temperature tests with greater accuracy as compared to the low-temperature tests. The errors reported for the gases have been found to be within the ranges specified in other gasifier models in literature as discussed before.

Though the tars predicted from the model are underestimated due to the consideration of limited tar species in the model, it can provide an insight as to what can be useful for future analysis. It is recommended to analyse tars during Pyroprobe experiments and to use devolatilization curves generated for each type of tar in the model as a function of temperature, and use consequent tar oxidation and reforming reactions for an accurate determination of tars from model.

The CC, CGE and OE from the model resemble the calculations from the experimental values. The maximum deviation among these values is 16.5 for CC (low-temperature test with RB using F046), 15.2 for CGE (low-temperature test with RB using F054) and 9.4 for OE (high-temperature test with GB using F046). The average relative errors for CC, CGE and OE in other tests are found to be within 4.7%, 9.7 % and 10% respectively. The deviations are mainly found for the tests which have more differences from the experimental values in terms of gas compositions, and also for tests with secondary air. The possibility of secondary air diffusion to the bedzone and other regions of the gasifier enhancing char combustion in these areas during the experiments is also assumed as a possible reason for higher CC in those tests with secondary air.

The various gas ratios CO/CO_2, H_2/CO and CH_4/H_2 have been calculated from the model and are found to be in reasonable agreement with the experimental values within a maximum absolute error of 0.351 for CO/CO_2 (high-temperature test with RB using F054), 0.575 for H_2/CO (high-temperature test with RB using F054) and 0.153 (high-temperature test with GB using F046) for CH_4/H_2. The average relative errors among other tests for these ratios are 9%, 14.2% and 17% for CO/CO_2, H_2/CO and CH_4/H_2 respectively. Subsequent improvement in the deviations observed for the gas flowrates in these tests will lower the differences observed in the above-mentioned values.

Fairly, the experimental trend is observed in the gas compositions and N_2, H_2O concentrations from the model with slight deviations. High temperature tests with GB except CO_2, high-temperature tests with RB except CO, low-temperature tests with RB except CO and H_2O follow the trend. A clear trend cannot be established for CC, probably due to different conversion factors assumed for char density in the freeboard for the Boudouard, MSR and water gas reaction in each test. The CGE and OE obtained from the model is always higher

than the experiments and follow the same trend in case of tests with RB. The OE follows the same trend as experiments for the first three tests in case of GB.

Overall, the model does a good prediction of the performance of the IHBFBSR under various operating conditions, and can be a starting point for further improvement.

The second question was: Can the model be used as a basis for evaluating the best process conditions under which the product gas obtained from the IHBFBSR, can be used for downstream applications, which in this study is the production of methanol?

The impact of varying SB*, primary and secondary air flowrate on product gas composition, N_2, H_2O, tars, various gas ratios and key performance indicators is analysed. Although tar, particulate matter and alkali metals need to be within specified limits for optimum production of methanol, a preliminary evaluation is carried out based on the influence of the varying parameters on H_2/CO ratio, which is one of the most crucial factors deciding the optimal production of methanol. Among the tests having the values of H_2/CO ratio close to 2, which is the desirable value, the test with a higher output gas flowrate is chosen, keeping in mind, to evaluate the possibility of product gas recycle to the burners, that is facilitated with a higher gas flowrate. Based on the results of the sensitivity analysis, with the current process conditions applied for the specific[2] test, it is not possible to achieve the desired ratio by only changing the process parameters and without the use of a water gas shift reactor. The following recommendations can be made based on the results achieved: -

- ➢ By varying SB* and keeping other process parameters constant at Test 8 conditions, H_2/CO ratio increases with increase of SB*. By taking into account, high pressure drop observed in the cyclones beyond SB* of 1.5 due to higher gas flowrates upon steam addition and increase in product gas temperature, it is advisable to increase the steam flowrate within a SB* range of 0.5-1, as recommended in literature findings [44] or to a maximum of 1.5, considering experiments performed at process parameters similar to this test and subsequently use a water gas shift reactor.

- ➢ By varying secondary air flowrate and keeping other process parameters constant at Test 8 conditions, it is observed that increase of secondary air (λ_{total}) intake is not found to have a significant impact on H_2/CO ratio, which increases at a much moderate pace. The maximum value of H_2/CO ratio is 1.34 at a secondary air flowrate of 11 kg/hr corresponding to λ_{total} of 0.28. This is feasible to achieve.

- ➢ By varying primary air flowrate and keeping other process parameters constant at Test 8 conditions, H_2/CO ratios is found to decrease with increasing primary air (λ). The highest value of H_2/CO ratio is 1.334, which is obtained at the starting point with a primary air supply of 1.9 kg/hr.

This model can be used as a basis for giving the idea of the best process conditions which can be used to produce methanol after subsequent gas cleaning. However, a more detailed

---

[2] It must be noted that this statement is valid only for the process conditions pertaining to Test 8, and only taking SB*, primary air and secondary air flowrate variation indicators. Sensitivity Analysis for other tests can be conducted to find if it is possible to achieve the desired ratio by only changing the process parameters. Moreover, as seen during validation, it should be noted that the H_2/CO ratio from the model is not exactly equal to the experimental values.

sensitivity analysis considering variation of two or more parameters at the same time, and conducting the analysis for high-temperature tests should be considered to have a clear insight.

The third question was: Can the model be used for predicting the possibility of making the current IHBFBSR setup more sustainable by recycling a part of the product gas to produce heat that needs to be provided for the endothermic gasification reactions?

It is estimated from Test 8 conditions that 50.92% of the product gas needs to be recycled to the top burner C-80 for generating 12 kW of heat. This is more feasible to be implemented considering that 49.08% of the gas would still be available for further cleaning and subsequent steps required for methanol production or any other downstream applications. An estimated value of 84.88% recycle fraction is required for generating 20 kW heat in the bottom burner C-100. In that case, only 15.12% is available for the subsequent steps mentioned above. It can be derived that with the current process conditions applied, the gas yield is not sufficient to be recycled back to both the burners, and hence it can only result in a partially sustainable setup. It is recommended to evaluate best process conditions, which can give a higher gas yield and possibly make the setup completely sustainable.

However, these percentages should be taken as an estimate for the fact that experiments produce a lower amount of gas due to mass loss. Also in practical scenarios, techniques such as water scrubbing could be carried out before recycling the product gas. Also, consideration of more tar species will add to the reactions considered for recycle stream. These factors suggest a more detailed analysis to be performed for determining the amount of product gas recycle .

The fourth question was: Does the model provide any insight for improvements that can be implemented in the current gasifier setup?

From the heat analysis performed for the test used for sensitivity analyses and for evaluating the possibility of product gas recycle to the burners, it can be observed that very less amount of heat is utilised for heating the gasification agents as compared to the heat provided in the preheaters. For other tests with a higher primary air flowrate which is expected to have a higher heat utilisation in the first preheater, still the amount of heat used is quite less, compared to the heat supplied. This can provide an interesting opportunity to explore the possibility of adding a bypass line which can enable the first preheater to be used in the heating of the reactor during start-up operations where high amount of air and N_2 is used, and bypass the preheater during the heating of the agents for the experiments, especially for low-temperature ones. In this way, the overall efficiency of the process can be increased from not using the first preheater for heating the gasification agents.

6.2 Further Recommendations

The model has scope for improvement, which can be achieved through the points mentioned below: -

➢ Taking into account the oxidation, reforming and cracking of various tar species in the model will help improve the differences observed in the gas composition between the model and experiment. It is hence suggested to generate devolatilization curves for the different tars through an analysis after pyrolysis experiments as done for the gases to be used in the Fortran code.

➢ Char conversion is based on Shrinking Density Model, by assuming a negligible mass transfer limitation, with the assumption of char density conversion factors in the freeboard taken for the Boudouard, char reforming and MSR reactions. The conversion factors have been based on the agent flow. It is recommended to attempt other models for char conversion such as Shrinking Particle Model, and take into account the mass transfer limitations in the heterogenous reactions. It is also suggested that a varying composition for char with respect to temperature can be explored as given in the gasifier model developed in [42].

➢ A more detailed calculation of bed hydrodynamics and investigating aspects such as bubble size or velocity is recommended to understand the differences in behaviour of various bed material types under fluidisation.

➢ The possibility of catalytic activity due to accumulation of unreacted char in the bedzone during the gasification tests can be explored.

➢ Conducting experiments with varied biomass types and performing sensitivity analysis tests based on type of biomass.

➢ Consideration of a more detailed fluidization model such as two-phase/three-phase model to give a more accurate depiction of the fluid dynamic behaviour in the IHBFBSR.

➢ Since the model is based on the novel technology of using radiant tube burners for allothermal gasification, heat transfer between the radiant tubes and the gasification chamber can be studied and incorporated in the model.

➢ Further extension of the model can be done by considering simulation of methanol/SNG synthesis.

REFERENCES

[1] S. R.A. Kersten and W. De Jong, "Thermochemical Conversion - (Co)gasification and Hydrothermal Gasification," in *Biomass as a Sustainable Energy Source for the Future - Fundamentals of Biomass Conversion*, W. De Jong and R. J. Van Ommen, Eds., New Jersey, John Wiley & Sons, Inc., 2015, pp. 298-353.

[2] H. Hofbauer and M. Materazzi, "Waste gasification processes for SNG production," in *Substitute Natural Gas from Waste- Technical Assessment and Industrial Applications of Biochemical and Thermochemical Processes*, M. Materazzi and P. U. Foscolo, Eds., Academic Press, 2019, pp. 105-160.

[3] Macrotrends LLC, "World Population Growth Rate 1950-2020," Macrotrends LLC, 2020. [Online]. Available: https://www.macrotrends.net/countries/WLD/world/population-growth-rate. [Accessed 15 December 2020].

[4] W. De Jong and J. R. Van Ommen, "Introduction: Socioeconomic Aspects of Biomass Conversion," in *Biomass as a Sustainable Energy Source - Fundamentals of Conversion Processes*, W. De Jong and J. R. Van Ommen, Eds., New Jersey, John Wiley & Sons, Inc., 2015, pp. 3-33.

[5] Britannica, T. Editors of Encyclopedia, "Paris Agrrement," 27 January 2021. [Online]. Available: https://www.britannica.com/topic/Paris-Agreement-2015. [Accessed 25 May 2021].

[6] IRENA, "Renewable Energy: A Key Climate Solution," IRENA, 2017.

[7] World Bioenergy Association, "Global Bioenergy Statistics 2020," 2020.

[8] D. Mitchell, M. R. Allen, J. W. Hall, B. Muller, L. Rajamani and C. L. Quéré, "The myriad challenges of the Paris Agreement," *Phil. Trans. R. Soc. A,* vol. 376:20180066, 2 April 2018.

[9] International Energy Agency, "Global Energy & CO2 status report: The latest trends in energy and emissions in 2018," IEA , 2019.

[10] BP, "BP Statistical Review of World Energy 2020," 2020. [Online]. Available: https://www.bp.com/content/dam/bp/business-sites/en/global/corporate/pdfs/energy-economics/statistical-review/bp-stats-review-2020-full-report.pdf. [Accessed 15 December 2020].

[11] P. Basu, "Biomass Characteristics," in *Biomass Gasification and Pyrolysis*, Academic Press, 2010, pp. 27-63.

[12] International Energy Agency, "The Netherlands 2020 - Energy Policy Review," IEA, 2020.

[13] B. Strengers and H. Elzenga, "Availability and Applications of Sustainable Biomass. Report on a search for shared facts and views," PBL Netherlands Environmental Assessment Agency, The Hague, 2020.

[14] A. Gagliano, F. Nocera and M. Bruno, "Simulation Models of Biomass Thermochemical Conversion Processes, Gasification and Pyrolysis, for the Prediction of the Energetic Potential," in *Advances in Renewable Energies and Power Technologies*, I. Yahyaoui, Ed., Italy, Elsevier, 2018, pp. 39-85.

[15] S. Acar and A. Ayanoglu, "Determination of higher heating values (HHVs) of biomass fuels," *Energy Education Science and Technology Part A: Energy Science and Research,* vol. 28, no. 2, pp. 749-758, January 2012.

[16] M. Kwakkenbos, "Kinetic Modelling of Biomass Gasification in an Indirectly Heated Bubbling Fluidized Bed Steam Reformer," Delft University of Technology, 2020.

[17] Ö. Ç. Mutlu and T. Zeng, "Challenges and Opportunities of Modeling Biomass Gasification in Aspen Plus: A Comprehensive Review," *Chemical Engineering & Technology,* vol. 43, no. 9, June 2020.

[18] W. De Jong, "Biomass Composition, Properties and Characterization," in *Biomass as a Sustainable Energy Source for the Future*, W. De Jong and J. Van Ommen, Eds., New Jersey, John Wiley & Sons, Inc., 2015, pp. 36-65.

[19] D. Mohan, C. U. Pittman and P. H. Steele, "Pyrolysis of Wood/Biomass for Bio-oil: A Critical Review," *Energy & Fuels,* vol. 20, no. 3, pp. 848-889, 10 March 2006.

[20] IDC Technologies, "Coal," N.A.. [Online]. Available: http://www.idc-online.com/technical_references/pdfs/chemical_engineering/Coal.pdf. [Accessed 15 April 2021].

[21] A. Galvagno, M. Prestipino, V. Chiodo, S. Maisano, S. Brusca and R. Lanzafame, "Energy Performance of CHP System Integrated with Citrus Peel Air-Steam Gasification: a Comparative Study," in *72nd Conference of the Italian Thermal Machines Engineering Association, 6-8 September*, Italy, 2017.

[22] X. Liu, D. Yang, J. Lu, J. Guan and G. Qi, "Combustion characteristics and design of hot water boiler," in *IOP Conference Series: Earth and Environmental Science, 2nd International Conference on Advances in Energy Resources and Environment Engineering*, 2017.

[23] S. Xiong, B. Zhang, X. Jia, B. Xiao and M. He, "Feasibility Study on the Pyrolysis Production for Hydrogen-Riched Fuel Gas from the Wet Sewage Sludge," in *2009 3rd International Conference on Bioinformatics and Biomedical Engineering*, 2009.

[24] S. Rafie, N. Haider, N. Islam and A. B. M. Badruzzaman, "Assessing the Energy Values of Sewage Sludge from Pagla Sewage Treatment Plant," 6 March 2018.

[25] THEmeter.net, "bulk specific weight and density," 2010. [Online]. Available: http://www.themeter.net. [Accessed 29 April 2021].

[26] AVCalc LLC, "Density of Coal, Anthracite solid (material)," 2021. [Online]. Available: https://www.aqua-calc.com. [Accessed 29 April 2021].

[27] Engineering ToolBox, "Density of Various Wood Species," 2004. [Online]. Available: https://www.engineeringtoolbox.com/wood-density-d_40.html. [Accessed 23 May 2021].

[28] P. S. Lam, S. Sokhansanj, X. Bi, S. Mani, C. Lim, A. Womac, M. Hoque, J. Peng, T. JayaShankar, L. J. Naimi and S. Nayaran, "Physical characterization of wet and dry wheat straw and switchgrass – bulk and specific density," in *076058*, Minneapolis, Minnesota, 2007.

[29] S. Ma and S. Eckhoff, "Economy of Scale for Biomass Refineries: Bulk Densities, Transportation Cost, and Producer Incentives," *Transactions of the ASABE (American Society of Agricultural and Biological Engineers),* vol. 57, no. 1, pp. 85-91, March 2014.

[30] P. H. M.ˑ. d. Silva, F. Poggiani and J. P. Laclau, "Applying Sewage Sludge to Eucalyptus grandis Plantations: Effects on Biomass Production and Nutrient Cycling through Litterfall," *Applied and Environmental Soil Science,* 3 March 2011.

[31] A. Faaij, "Modern Biomass Conversion Technologies," *Mitigation and Adaptation Strategies for Global Change,* 18 June 2005.

[32] L. Pampillón-González and J. R. L. Canepa, "Biomass as an Alternative for Gas Production," in *Advances in Natural Gas Emerging Technologies*, INTECH, 2017, pp. 173-190.

[33] E4Tech, "Review of Technologies for Gasification of Biomass and Wastes," NNFCC, 2009.

[34] R. Singh, A. Prakash, B. Balagurumurthy and T. Bhaskar, "Hydrothermal Liquefaction of Biomass," in *Recent Advances in Thermo-Chemical Conversion of Biomass*, A. Pandey, T. Bhaskar, M. Stöcker and R. K. Sukumaran, Eds., Dehradun, Elsevier, 2015, pp. 269-291.

[35] P. Basu, "Introduction," in *Biomass Gasification and Pyrolysis*, Academic Press, 2010, pp. 1-25.

[36] P. Basu, "Pyrolysis and Torrefaction," in *Biomass Gasification and Pyrolysis*, Academic Press, 2010, pp. 65-96.

[37] M. F. A. Kamaroddin, T. A. T. Abdullah, R. Mat and N. A. S. Amin, "Effects of the Heat Carrier's Temperature and Particle Size on the Pyrolysis of Imperata cylindrica in a Transported Bed Reactor," *Applied Mechanics and Materials,* June 2014.

[38] P. Basu, "Tar Production and Destruction," in *Biomass Gasification and Pyrolysis*, Academic Press, 2010, pp. 97-116.

[39] L. Devi, K. J. Ptasinski and F. J. Janssen, "A review of the primary measures for tar elimination in biomass gasification processes," *Biomass and Bioenergy,* vol. 24, no. 2, pp. 125-140, February 2003.

[40] Y. S. Pradana and A. Budiman, "Bio-syngas derived from Indonesian oil palm empty fruit bunch (EFB) using middle-scale gasification," *Journal of Engineering Science and Technology,* no. 8, pp. 1-8, 7 August 2015.

[41] P. Basu, "Gasification Theory and Modelling of Gasifiers," in *Biomass Gasification and Pyrolysis*, Academic Press, 2010, pp. 117-165.

[42] L. Abdelouahed, O. Authier, G. Mauviel, J. P. Corriou, G. Verdier and A. Dufour, "Detailed Modeling of Biomass Gasification in Dual Fluidized Bed Reactors under Aspen Plus," *Energy & Fuels,* vol. 26, pp. 3840-3855, 1 May 2012.

[43] P. Basu, "Design of Biomass Gasifiers," in *Biomass Gasification and Pyrolysis*, Academic Press, 2010, pp. 167-228.

[44] P. Kaushal and R. Tyagi, "Advanced simulation of biomass gasification in a fluidized bed reactor," *Renewable Energy,* pp. 629-636, 2017.

[45] C. Vargas-Salgado, Elías Hurtado-Pérez, D. Alfonso-Solar and A. Malmquist, "Empirical Design, Construction, and Experimental Test of a Small-Scale Bubbling Fluidized Bed Reactor," *Sustainability,* vol. 13, no. 3, 20 January 2021.

[46] Butterworth-Heinemann, "Fluidisation," in *Coulson and Richardson's Chemical Engineering - Volume 2a: Particulate Systems and Particle technology*, 6 ed., vol. 2A, R. Chhabra and M. G. Basavaraj, Eds., 2019, pp. 449-554.

[47] G. Jovanovic, "Gas Flow in Fluidized beds of large particles: Experiment and Theory," Oregon State University, 1979.

[48] M. Bolhàr-Nordenkampf, R. Rauch, K. Bosch, C. Aichernig and H. Hofbauer, "Biomass CHP Plant Güssing – Using Gasification for Power Generation," 2003.

[49] A. v. d. Drift, R. Zwart, B. Vreugdenhil and L. Bleijendaal, "Comparing the options to produce SNG from biomass," in *18th European Biomass Conference and Exhibition, Lyon, France*, 2010.

[50] D. R. Rauch and D. J. Hrbek, "Country Report Austria," IEA Bioenergy 33, 2013.

[51] D. J. Hrbek, "Thermal Gasification of Biomass," IEA, Vienna, Austria, 2012.

[52] M. L. Rollins, L. Reardon, D. Nichols, P. Lee, M. Moore, M. Crim, R. Luttrell and E. Hughes, "Economic Evaluation of CO2 Sequestration Technologies Task 4, Biomass Gasification-Based Processing," 2002.

[53] Freidrich-Alexander Universitat Erlangen Nurmberg, "Heatpipe-Reformer Technology," 2021. [Online]. Available: https://www.evt.tf.fau.eu. [Accessed 22 April 2021].

[54] J. Karl, "Biomass heat pipe reformer-design and performance," *Biomass Conversion and Biorefinery,* vol. 4, no. 1, pp. 1-14, 25 October 2013.

[55] ECN, "MILENA Biomass Gasification process," 6 December 2011. [Online]. Available: https://www.milenatechnology.com/. [Accessed 22 April 2021].

[56] C. M. v. d. Meijden, "The MILENA gasification technology for the production of Bio-Methane," ECN, Petten, Netherlands, 2014.

[57] C. M. v. d. Meijden, H. J.Veringa, B. J. Vreugdenhil and B. v. d. Drift, "Bioenergy II: Scale-Up of the Milena Biomass Gasification Process," *International Journal of Chemical Reactor Engineering,* vol. 7, 4 November 2009.

[58] B. Sridharan, "System Study towards the Integration of Indirect Biomass Gasification,Methanol and Power Production," Delft University of Technology, 2017.

[59] T. Damartzis, S. Michailos and A. Zabaniotou, "Energetic assessment of a combined heat and power integrated biomass gasification–internal combustion engine system by using Aspen Plus®," *Fuel Processing Technology,* pp. 37-44, 2012.

[60] M. Hussain, L. D. Tufa, S. Yusup, H. Zabiri and S. A. Taqvi, "Aspen Plus® Simulation Studies of Steam Gasification in Fluidized Bed Reactor for Hydrogen Production Using Palm Kernel Shell," *Communications in Computer and Information Science,* pp. 628-641, August 2017.

[61] J. Yu, J. D. Smith, H. Golpour, A. Alembath, H. Al-Rubaye and X. Gao, "Validation and Application of a Kinetic Model for Downdraft Biomass Gasification Simulation," *Chemical Engineering & Technology,* June 2019.

[62] X. Meng, "Biomass gasification: the understanding of sulfur, tar, and char reaction in fluidized bed gasifiers," 2012.

[63] "Corundum Mineralogy and Gemology," N.A.. [Online]. Available: https://www.eoas.ubc.ca/courses/Dist-Ed/eosc118-webpromo/01-modB-les17-webpromo.html. [Accessed 22 April 2021].

[64] C. Tsekos, "Fast Pyrolysis of Woody Biomass in a Pyroprobe Reactor: Effect of Torrefaction on the Pyrolysis Products," Delft University of Technology, 2016.

[65] A. Go´mez-Barea and B. Leckner, "Modeling of biomass gasification in fluidized bed," *Progress in Energy and Combustion Science,* vol. 36, no. 4, pp. 444-509, 17 March 2010.

[66] I. Petersen and J. Werther, "Experimental investigation and modeling of gasification of sewage sludge in the circulating fluidized bed," *Chemical Engineering and Processing,* no. 44, pp. 717-736, 12 October 2004.

[67] S. Srinivas, R. P. Field and H. J. Herzog, "Modeling Tar Handling Options in Biomass Gasification," *Energy&Fuels,* no. 27, p. 2859−2873, 6 May 2013.

[68] C. L. Khairy Elsayed, "CFD modeling and multi-objective optimization of cyclone geometry using desirability function, artificial neural networks and genetic algorithms," *Applied Mathematical Modelling,* vol. 37, pp. 5680-5704, 14 December 2012.

[69] S. Wijitkosum and P. Jiwnok, "Elemental Composition of Biochar Obtained from Agricultural Waste for Soil Amendmen and Carbon Sequestration," *Applied Sciences, MDPI,* vol. 9, no. 19, 23 September 2019.

[70] L. Zhu and J. Fan, "Development of a Kinetic Model for Biomass Gasification in Dual Fluidized Bed Gasifier," *Journal of Chemical Engineering of Japan,* vol. 47, no. 12, pp. 855-863, 15 May 2014.

[71] K. M. Broer, "Partitioning of fuel bound nitrogen in biomass gasification," Ames, Iowa, 2014.

[72] L. Waldheim and T. Nilsson, "Heating Value of Gases from Biomass Gasification," *IEA Bioenergy Agreement,* no. TPS Termiska Processer AB, May 2001.

[73] L. Liu, Y. Huang, J. Cao, C. Liu, L. Dong, L. Xu and J. Zha, "Experimental study of biomass gasification with oxygen-enriched air in fluidized bed gasifier," *Science of the Total Environment,* vol. 626, pp. 423-433, 2018.

[74] N. Chatrattanaweta, W. Kanjanasorn, S. Authayanun, D. Saebea and Y. Patcharavorachot, "Biomass Steam Gasification of Sugarcane Leftover for Green Diesel Production," *Chemical Engineering Transactions,* vol. 70, pp. 1693-1698, 1 August 2018.

[75] J. O. Maloney, "Perry's Chemical Engineer's handbook," 8 ed., D. W.Green and R. H. Perry, Eds., Mc Graw Hill, 2008.

[76] C. J. Roos, "Clean Heat and Power Using Biomass Gasification for Industrial and Agricultural Projects," February 2010.

[77] W. B. Faulkner and B. W. Shaw, "Efficiency and pressure drop of cyclones across a range of inlet velociies," *Applied Engineering in Agriculture,* vol. 22, no. 1, pp. 155-161, 2006.

[78] D. L. Pyle and C. A. Zaror, "Heat Transfer and Kinetics in the Low Temperature Pyrolysis of Solids," *Chemical Engineering Science,* vol. 39, no. 1, pp. 147-158, 6 May 1983.

APPENDICES

Appendix A- Advantages and Disadvantages of Fixed Bed, Fluidized Bed and Entrained Flow Gasifiers

Table 1: Advantages and Disadvantages of various gasifier configurations

[76] [1]

Type of Reactor	Advantages	Disadvantages
Downdraft	- Low tar content in product gas - Less start-up time required compared to downdraft	- High maintenance cost
Updraft	- Better heat utilisation compared to downdraft, resulting in high CGE - Suitable for high ash, high moisture biomass	- High tar and methane content in product gas; high methane concentration might be undesirable for specific products such as syngas
Crossdraft	- Low tar content in product gas - Least start-up time required compared to updraft and downdraft	- Unsuitable for high ash fuels - Reactor walls have to withstand high temperatures
BFB	- Fuel flexibility - Uniform mixing	- High tar and particulate matter in product gas - Bed sintering due to presence of ash and alkali metals
CFB	- Fuel flexibility - Low tar in product gas - Easy for scale-up - High carbon conversion due to solids recycle	- Corrosion problems - Potential for agglomeration due to ash melting - Particulate matter in product gas
DFB	- Choice of fuel flexibility - Does not require biomass pre-treatment - Higher efficiency compared to BFB/CFB - Low emissions - Low nitrogen dilution of product gas	- Difficult for scaling up - Product gas contains more tar - Difficult to operate under pressure - High capital cost - Steam in product gas results in dilution

		- External heat supply required during biomass gasification
EF	- Low tar in product gas - Fuel flexibility - Can be used for large capacities	- Severe pre-treatment (size reduction) of fuel required - High exergy loss due to high temperature - Complicated to operate - Ash slagging

Appendix B- Comparison of various allothermal gasifier technologies with the IHBFBSR in terms of process parameters, carbon conversion and energy/cold gas efficiency

Table 2: Comparison of the various allothermal gasifiers in commercial use with the IHBFBSR

Gasifier Technology	FICFB TUV (Austria) [49] [33] [48] [50] [51]	SilvaGas Gasifier (USA) [33] [52]	Heat Pipe Reformer (Germany) [54] [53]	Milena ECN (Netherlands) [33] [55] [56] [57]	IHBFBSR TU Delft, NL
Gasification chamber	BFB	TB	Pressurized FB Reformer	CFB	BFB
Combustion chamber	CFB	CFB	FB	BFB	Radiant Tube Burners
Temperature	900-1000°C	800-850°C	800-900°C	850-925°C	700-850°C
Pressure	Atmospheric	Atmospheric	2-10 bar	Atmospheric	Atmospheric
Agent	Steam	Steam	Steam	Steam	Steam or Steam + Air
Energy Efficiency	81.3% (electrical + thermal efficiency)	80% (overall efficiency)	75% (cold gas efficiency)	78% (Cold Gas Efficiency)	50-80% (cold gas efficiency), depending on operating parameters, obtained from latest experiments
Carbon Conversion	90%	Exact value not found but carbon conversion specified as high in literature	100%	80-85%	85-95%, depending on operating parameters, obtained from latest experiments
Heating value of Product Gas (MJ/Nm³)	12-15	15.5 – 17.3	- medium calorific value gas but exact value not found	10-16	- From latest experiments, LHV ranging from 3.8-5.8 on db
Lab Scale Operation	10 kW in 1993 at TUV	10-12 odt/day in 1980 at BCL, Ohio	A 20 kW_{th} plant followed by two 120 kW_{th} in 2001 at TU Munich	25 kW plant in 2004 at ECN	50 kW at TU Delft NL
Pilot Scale Operation	100 kW in 1997 at TUV	- 40 MW_{th} (200 odt/day) commercial plant at the Mc Neil power station, Burlington, Vermont in 1997	500 kW_{th} input developed by Agnion Inc. in 2008 at Pfaffenhofen, Germany	800 kW_{th} in 2008 at ECN	

Demo Plant	-8 MW (4.5MW$_{th}$, 2MW$_{el}$ output) CHP plant with gas engine at Gussing, Austria in 2002	- Capacity of demo plant increased to 350 odt/day	-1.3 MW$_{th}$ input plant built in 2012 at Grassau, Germany	- 4 MWth input biomethane plant in Alkmaar, NL	
Other Commercial Scale Plants/ Scale-up	- 8.5 MW (2.8 MW$_{el}$ output) CHP with gas engine and integrated ORC plant in Oberwart, Austria in 2008 -14 MW (5 MW$_{el}$ output) CHP with gas engine and integrated ORC plant in Senden, Germany in 2011 - 32 MW (20 MW output) Bio-SNG plant in Goteborg, Sweden in 2013 - 50 KW (30 MW) hydrogen production unit in Vienna, Austria in 2012 (scale-up planned)	-BTL plant in Rialto, California producing 600 barrels synthetic diesel and 35 MWe renewable electric power estimate (scale-up planned)	- 100 kW design using membranes for in-situ hydrogen removal (tested) - 50 MW lignite-based design (scale-up planned)	- 1 MWe gasifier in India using soya residue (ongoing) - 2-4 MWe CHP plants from waste wood - 50 MWth – 500 MWth bio-methane plant in 2012 (scale-up planned)	
Advantages	- Low carbon in fly ash residue from combustor, hence it is processed similarly to ash	- Less expensive compared to other gasifiers - Variety of feedstocks can be accepted	- High heat transfer coefficient - Reduced heat transfer area	- Less steam required compared to other gasifiers - No external heat supply required	- Heat transfer from inside to outside is expected to result in low heat loss
Disadvantages	- Wood chips are supplied by local wood farmers hence availability/sup-ply is an issue - Resistance for accepting varied feedstocks - High steam to biomass ratio required for gasification	- Not any specific disadvantage mentioned in literature	- Hydrogen diffusion from generated syngas from reformer vessel to heat	- Not any specific disadvantage found in literature	- Bed removal limitation

Appendix C- Study on various gasifier models developed in Aspen Plus® based on kinetic approach

Table 3: Description of the various gasifier models based on kinetic approach in Aspen Plus®

	Model 1 [61]	Model 2 [42]	Model 3 [44]	Model 4 [59]	Model 5 [62]
Feedstock	Biomass	Biomass	Biomass	Biomass	Biomass
Gasification Agent	Air	Steam/Recycled syngas	Steam/O_2	Air	Steam/Air
Simulator	Aspen Plus + Fortran subroutines	Aspen Plus + Fortran subroutines	Aspen Plus + Fortran subroutines	Aspen Plus + Fortran subroutines	Aspen Plus + Fortran subroutines
Type of Gasifier	Downdraft	DFB	BFB	BFB	CFB
Method used in Aspen Plus® & Stream Class	- Not specified	- RK Method	- Not specified	Peng-Robinson	-Not specified
General Assumptions	- Biomass is non-conventional - CO, H_2, CH_4, CO_2, O_2, N_2, H_2S, H_2O, char and ash considered from pyrolysis - char assumed to be conventional solid carbon only	- Biomass and char are non-conventional -Bed material is assumed to be inert - N and S neglected in ultimate analysis - Pyrolysis and secondary reaction zones assumed to be adiabatic	- Isothermal process at steady state - H_2, CO, CO_2, CH_4, H_2O, tar and char considered during pyrolysis - Spherical bed particles with uniform diameter - Char assumed to be conventional solid carbon only - Fuel does not contain N and S.	- Isothermal process at steady state - H_2, CO, CO_2, CH_4, H_2O are formed during pyrolysis - Instantaneous devolatilization - Uniform distribution of gases in the reactor - Char is assumed to contain carbon and ash N and S reactions are not considered.	-Biomass is non-conventional component - RStoic reactor block is used for CH_4, C_2H_4, C_6H_6 - CH_4, C_2H_4 yields are calculated experimentally, and from empirical relations, assumed to be 8% and 4.5% of carbon in biomass, respectively - H_2S, HCl are formed from S and Cl in biomass -PSD is not considered - Char is assumed to be pure carbon -Instantaneous

					- devolatilization - Steady state isothermal process
Drying Section	- Modelled by RStoic which converts moisture in biomass to steam - Controlled by Fortran subroutines	- Modelled by heater, controlled by Fortran which calculates heat required to evaporate moisture	- Modelled by RStoic block	- Modelled by RStoic reactor. Heat is provided for removal of moisture by using heat released from cooling the product gas	- Not specified
Pyrolysis Section	- Modelled by RYield + RGibbs block. RYield decomposes biomass based on mass balance from ultimate and proximate analysis. Char is separated from the outlet stream and volatile components fed to RGibbs reactor to form gases + tar	- Pyrolysis products mass yields given as function of reactor temperature; correlations derived from experiments and tar analysis - Char mass yield considers variation in composition according to temperature - Modelled by RYield block	- Kinetics of pyrolysis considered - Composition of pyrolysis products proportional to the reaction rate - Fortran subroutines connected to RYield block to simulate pyrolysis process - Char is separated from product stream and the volatile matter converted to products in RGibbs following the equilibrium approach	- Modelled by RYield + RGibbs reactor. The product yields from pyrolysis are based on proximate and ultimate analysis of feed. The RGibbs block carrying out reactions of volatile components from pyrolysis by equilibrium method.	-Modelled by RYield converting biomass into its constituents
Bed Hydrodynamics	--	- Not specified	- BFB is divided into dense zone and freeboard - Uniform mixing is assumed in both regions - Voidage in dense zone assumed to be constant	- No hydrodynamic considerations	-Riser divided into bed, upper, exit zone. - Constant voidage in bedzone and variation with the height of the upper zone.
Gasification Section	- Gasifier is divided into four equal sections for better accuracy.	- Modelled by RPlug reactor for homogenous gas-phase and heterogenous char reactions	- Modelled by two RCSTR's representing bedzone and freeboard	- Modelled by RGibbs + RCSTR block. RCSTR models the homogenous	-Char gasification and combustion reactions occur in the

	Each section is made of one CSTR + one PFR. RCSTR is used for heterogenous reactions RPlug is used for homogenous reactions.		- Homogenous and heterogenous reactions, along with primary tar cracking take place in both reactors - Kinetics defined in Fortran subroutine and coupled to RCSTR	gas phase and tar oxidation reactions. The char gasification reactions are modelled in RGibbs.	bed zone modelled by RCSTR Homogeneous reactions occur in the upper and the exit zone, modelled by RCSTR and RPlug block respectively.
Reactions Kinetics	- Taken from experimental studies in literature and similar simulation works	- Kinetics taken from references, with calculations done for tar catalytic conversion over char and soot gasification - CH_4 gas phase conversion assumed negligible - Toluene and benzene cracking rates assumed similar to naphthalene cracking rates	- Kinetics taken from references	- Kinetics taken from references	- From literature partly and partly from TGA experiments
Tar Model	Considered as 5 main compounds – acetone, phenol, toluene, naphthalene, propionic acid	4 lumped groups of tar – benzene, toluene, naphthalene, phenol	- Tar defined as "primary tar" cracking into CO, CO_2, CH_4, H_2 and secondary tar during gasification.	- 20% weight of biomass is converted to tar containing 60% benzene, 20% toluene and 20% naphthalene by weight	-60% carbon in biomass converts to benzene
Gas Cleaning	-Not specified	-Not specified	- Modelled by cyclone separator	- Nitrogen and sulphur removed by separator, unreacted char removed by cyclone separator	- Modelled by ideal separator
Parametric Study	ER, feed composition, temperature, moisture content	Syngas composition and tar concentration	SB, syngas composition, temperature	ER, Temperature	-SB, Temperature
Model Validation	Model validated with experiment	Model validated with data of FERCO and	Model validated with experimental results of steam-gasification of	Model validated with experimental results of	Model validated with experimental

	al results of hazelnut and pinewood gasification in a downdraft gasifier	TNEE pilot plants	biomass in a pilot-scale BFB gasifier	steam-gasification of olive kernel in a BFB at Aristotle University	results of steam-gasification in 100 kW$_{th}$ CFB at TU Delft (now dismantled)
Model Validation Results	- CO, H$_2$ and CH$_4$ prediction lie in the range of 7%, 19% and 33% average error respectively, which is less compared to the average errors seen in other models. - Simulation results show tar fraction as 1-3% volume fraction of gas phase with acetone making up 50% of tar composition followed by benzene and naphthalene	- CH$_4$ in close agreement with data of pilot plants; CO overpredicted and CO$_2$ underpredicted - Total tars in good agreement with data of pilot plants - Permanent gases yield and LHV values in good agreement with data of pilot plants	- Gas compositions and tar concentration in close agreement with experimental values	- Gas compositions at similar ER and temperatures show an average error from 2.1% to 8%	- Gas compositions predicted well by the model - CGE and CC obtained from model are higher with maximum difference of 12.3 for CC and 19.1 for CGE (absolute error)
Reasons for deviation/Further recommendations	Temperature calculation is done for last section of gasifier from energy conservation law; for other sections it is assumed at a set operationa	- WGS reaction kinetic modified; CO and CO$_2$ values are in good agreement with modified kinetics, the modified kinetics could be used for DFB gasifiers above 850°C and below 950°C - Possible catalytic effects of bed to be considered	- Results can be further improved by considering fluid mixing, mass transfer limitations and complex bed hydrodynamics	- Results can be further improved by considering catalytic effects of olivine used in pilot plant	- Shrinking Core Model and Volume Reaction Model used; more complicated models such as rand pore recommended for char combustion and gasification

	l temperatur e which may not be equal to real temperatur es - Focus on accuracy of WGS kinetics		108		

Appendix D- Reference Model Flowsheet and Fortran Code in Pyrolysis section
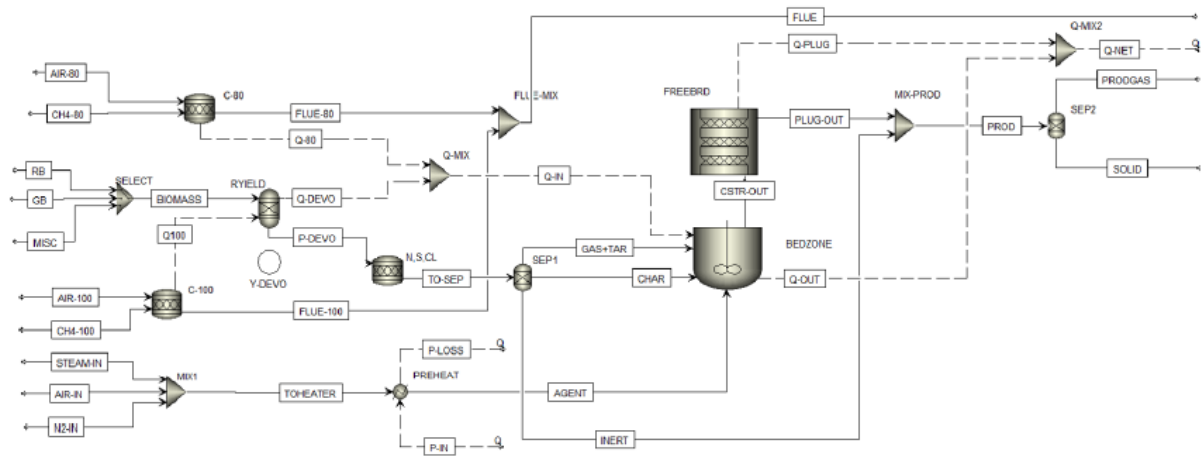
Figure 1: Flowsheet Diagram for the Reference Model

FORTRAN CODE FOR PYROLYSIS SECTION

It was determined in [16] that the pyrolysis section has a heat transfer limitation. Nevertheless, it was not taken into account and was modelled as a chemical rate limited process.

The solid fraction obtained from pyrolysis is assumed to contain char and ash. The ash percentage obtained from proximate analysis of the biomass feed is subtracted from the solid fraction yield obtained from Pyroprobe results to calculate the char yield. The char is modelled as conventional solid carbon (graphite) in Aspen plus®. The liquid fraction is assumed to consist of the pyrolytic water, tars, and moisture. The water vapour generated in pyrolysis step is the sum of moisture content determined by proximate analysis and the pyrolytic water. The pyrolytic water is implemented in the model as a function of the pyrolysis temperature as per data taken from literature for slow pyrolysis at similar pyrolysis conditions of the IHBFBSR. It has been stated in [16] that the value of pyrolytic water is not influenced to a considerable extent based on slow or fast pyrolysis conditions. The empirical relation considered for pyrolytic water is given in Eq 1 taken from [42].

$$Y^{ar}_{pyr-H_2O} = 5.157.10^{-5}T^2 - 1.186.10^{-1}T + 84.91 \qquad \text{(Eq 1)}$$

Based on the experimental percentage of the gas, solid, liquid fraction and of specific gaseous components from pyrolysis, the yield curves have been generated as a function of pyrolysis temperature for each biomass. The coefficients of the mass yield of pyrolysis products as a function of temperature are derived from the best fit curves described by a 4th degree polynomial in MATLAB®. The mass yields of H_2, CO_2, CH_4, CO, liquid fraction and solid fraction as a function of temperature are described by the polynomial function in Eq 2 [16]. Here Y_i denotes the mass yields of particular component i; a, b, c, d, e are the coefficients obtained from MATLAB®.

$$Y_i = aT^4 + bT^3 + cT^2 + dT + e \qquad \text{(Eq 2)}$$

The pyrolysis model assumes instantaneous heating of the homogenous biomass particle to the pyrolysis temperature with uniform temperature distribution throughout the particle. It also considers that the gasification step proceeds only after complete devolatilization of the feed takes place.

Appendix E - Experimental Results of Pyroprobe apparatus

Table 4: Experimental Results of Pyroprobe apparatus [16]

Biomass	Mass [mg]	Particle size [μm]	F_{N2} [ml/min]	Heating rate [°C/s]	Holding time [s]	T_{real} [°C]	T_{set} [°C]	Sample name
RB	30 ±0.5	80	10±0.5	600	11.5	600	744	RB_11_4_600
								RB_11_4_600
					11.9	700	876	RB_12_4_700
								RB_17_4_700
					12.5	800	1008	RB_18_4_800
								RB_25_4_800
					12.9	900	1141	RB_26_4_900
								RB_26_4_900
					13.5	1000	1273	RB_2_5_1000
								RB_3_5_1000
GB	30 ±0.5	80	10	600	11.5	600	744	GB_8_5_600
								GB_9_5_600
					11.9	700	876	GB_9_5_700
								GB_10_5_700
					12.5	800	1008	GB_10_5_800
								GB_10_5_800
					12.9	900	1141	GB_15_5_900
								GB_16_5_900
					13.5	1000	1273	GB_16_5_1000
								GB_17_5_1000

Sample name	Treal [°C]	test	Gas	Tar	Char	Mass balance	H2	CO	CH4	CO2
RB_11_4_600		_3	6.64%	34.90%	39.60%	81.13%	0.004%	1.73%	0.06%	4.84%
RB_11_4_600		_4	6.19%	33.00%	40.67%	79.86%	0.003%	1.70%	0.04%	4.44%
	600	average	6.41%	33.95%	40.13%	80.49%	0.003%	1.72%	0.05%	4.64%
		stdev	0.32%	1.34%	0.76%	0.90%	0.00%	0.02%	0.02%	0.28%
RB_12_4_700		_1	10.06%	37.46%	25.08%	72.60%	0.03%	4.80%	0.53%	4.70%
RB_17_4_700		_3	9.60%	39.07%	27.48%	76.16%	0.02%	3.57%	0.32%	5.70%
	700	average	9.83%	38.27%	26.28%	74.38%	0.03%	4.18%	0.42%	5.20%
		stdev	0.32%	1.14%	1.70%	2.52%	0.01%	0.87%	0.15%	0.70%
RB_18_4_800	800	_2	17.12%	32.78%	18.87%	68.77%	0.097%	9.385%	1.421%	6.215%
RB_25_4_800		_4	0.19379	32.12%	18.87%	70.37%	0.137%	11.523%	1.683%	6.036%
		average	18.25%	32.45%	18.87%	69.57%	0.12%	10.45%	1.55%	6.13%
		stdev	1.60%	0.47%	0.00%	1.13%	0.03%	1.51%	0.19%	0.13%
RB_26_4_900	900	_3	30.70%	20.40%	13.71%	64.81%	0.340%	19.071%	3.210%	8.076%
RB_26_4_900		_4	30.09%	21.59%	15.61%	67.30%	0.334%	18.696%	3.194%	7.866%
		average	30.39%	21.00%	14.66%	66.06%	0.34%	18.88%	3.20%	7.97%
		stdev	0.43%	0.84%	1.35%	1.76%	0.00%	0.27%	0.01%	0.15%
RB_2_5_1000	1000	_3	29.25%	22.52%	17.55%	69.32%	0.437%	20.382%	3.577%	8.277%
RB_3_5_1000		_4	30.13%	21.93%	15.95%	68.00%	0.497%	17.930%	3.419%	7.407%
		average	29.69%	22.22%	16.75%	68.66%	0.47%	19.16%	3.50%	7.84%
		stdev	0.62%	0.42%	1.13%	0.93%	0.04%	1.73%	0.11%	0.62%

Sample name	Treal [°C]	test	Gas	Tar	Char	Mass balance	H2	CO	CH4	CO2
GB_8_5_600	600	_1	5.28%	30.70%	46.36%	82.33%	0.00%	1.23%	0.06%	3.99%
GB_9_5_600		_3	5.24%	32.00%	45.67%	82.91%	0.00%	1.41%	0.06%	3.77%
		average	5.26%	31.35%	46.01%	82.62%	0.00%	1.32%	0.06%	3.88%
		stdev	0.03%	0.92%	0.49%	0.40%	0.00%	0.12%	0.00%	0.16%
GB_9_5_700	700	_1	9.41%	40.20%	26.91%	76.52%	0.01%	3.30%	0.31%	5.79%
GB_10_5_700		_2	10.52%	41.33%	26.00%	77.85%	0.02%	4.18%	0.45%	5.87%
		average	9.96%	40.77%	26.46%	77.18%	0.02%	3.74%	0.38%	5.83%
		stdev	0.78%	0.80%	0.64%	0.93%	0.00%	0.62%	0.09%	0.06%
GB_10_5_800	800	_1	17.86%	31.89%	21.26%	71.01%	0.12%	9.90%	1.53%	6.32%
GB_10_5_800		_2	18.68%	32.78%	20.53%	71.99%	0.11%	10.25%	1.55%	6.78%
		average	18.27%	32.34%	20.90%	71.50%	0.11%	10.07%	1.54%	6.55%
		stdev	0.58%	0.63%	0.52%	0.69%	0.01%	0.25%	0.02%	0.33%
GB_15_5_900	900	_1	26.81%	20.33%	18.00%	65.14%	0.28%	16.50%	2.85%	7.17%
GB_16_5_900		_2	26.84%	21.40%	18.39%	66.64%	0.28%	16.66%	2.87%	7.03%
		average	26.82%	20.87%	18.20%	65.89%	0.28%	16.58%	2.86%	7.10%
		stdev	0.02%	0.76%	0.28%	1.06%	0.00%	0.11%	0.01%	0.10%
GB_16_5_1000	1000	_1	27.04%	20.67%	17.67%	65.37%	0.28%	16.77%	2.88%	7.10%
GB_17_5_1000		_2	26.47%	20.60%	17.28%	64.35%	0.27%	16.42%	2.82%	6.96%
		average	26.76%	20.64%	17.47%	64.86%	0.28%	16.60%	2.85%	7.03%
		stdev	0.40%	0.05%	0.28%	0.72%	0.00%	0.25%	0.04%	0.10%

Appendix F- Coefficient values for Normalized Solid, Liquid and Gaseous fraction from MATLAB®

Table 5: Coefficients for the pyrolysis products (normalized) yield as a function of temperature

RB		for y=aT^4+bT^3+cT^2+dT+e		T in[K]	
Component	a	b	c	d	e
Char	2.67080E-09	-1.14340E-05	1.85000E-02	-1.34588E+01	3.76080E+03
Tar	8.67920E-09	-3.48420E-05	5.16000E-02	-3.34258E+01	8.02860E+03
Gas	-1.13750E-08	4.63830E-05	-7.03000E-02	4.70054E+01	-1.17210E+04
H_2	-2.11250E-10	8.83940E-07	-1.40000E-03	9.40800E-01	-2.39994E+02
CO	-7.14580E-09	2.89470E-05	-4.35000E-02	2.88940E+01	-7.14920E+03
CH_4	-1.31500E-09	5.34260E-06	-8.10000E-03	5.35260E+00	-1.32560E+03
CO_2	-2.67080E-09	1.10710E-05	-1.71000E-02	1.16597E+01	-2.96450E+03
GB		for y=aT^4+bT^3+cT^2+dT+e		T in[K]	
Component	a	b	c	d	e
Char	4.35000E-09	-1.99590E-05	3.43000E-02	-2.62405E+01	7.55620E+03
Tar	1.31670E-09	-2.63780E-06	-9.15590E-04	4.43360E+00	-2.14460E+03
Gas	-5.63330E-09	2.24530E-05	-3.32000E-02	2.16450E+01	-5.26900E+03
H_2	-1.95830E-10	8.11350E-07	-1.20000E-03	8.48900E-01	-2.14922E+02
CO	-3.47080E-09	1.35090E-05	-1.94000E-02	1.22023E+01	-2.85070E+03
CH_4	-8.16670E-10	3.22350E-06	-4.70000E-03	3.01040E+00	-7.16190E+02
CO_2	-1.15830E-09	4.94660E-06	-7.90000E-03	5.62910E+00	-1.49960E+03

Appendix G- Fortran Code Implemented For New Model in Aspen Plus®

```
IF (SELECT.EQ. 1) THEN

    H2 = -1.958333E-10*T**4 + 8.1135E-7*T**3 - 0.001249466*T**2
   ++ 0.848914*T -214.9224
    CO2 = -1.1583333E-09*T**4 + 4.9465667E-06*T**3 - 0.007909678*T**2
   ++ 5.6290514*T - 1499.6015
    CO = -3.4708333E-09*T**4 + 1.3509317E-05*T**3 - 0.019383356*T**2
   ++ 12.2022899*T - 2850.65
    CH4 = -8.166667E-10*T**4 + 3.223467E-06*T**3 - 0.00470016*T**2
   ++ 3.010361*T - 716.1900
    SOLID = 4.3500E-09*T**4 - 1.9958533E-05*T**3 + 0.034324832*T**2
   +- 26.240484*T + 7556.209
    LIQUID = 1.3166667E-09*T**4 - 2.6378E-06*T**3
   +- 0.00091558757*T**2 + 4.4336308*T - 2144.5671
    N2 = 0.3
    S = 0.01
    ASH = 0.73
    O2 = 0.0
    LGASSES = 0
    CHAR = SOLID - ASH
    PW= 5.157E-05*T**2 - 11.86E-02*T + 84.91
    MOIST = 5.08
    H2O = PW + MOIST
    PHENOL = (LIQUID - H2O)
    CL2 = 0
    TCSTR = T
    TSTOIC = T
    FR = 4.72E-3*exp (37737 / (8.31445985 * T))
    BETAC = -((1+2*FR) / (1+FR))
    BETACO = 2*((-BETAC) - 1)
    BETACO2 = 2 + BETAC
```

ELSE IF (SELECT.EQ. 2) THEN

H2 = -2.1125E-10*T**4 + 8.83935E-07*T**3

+- 1.373465E-03*T**2 + 9.408256E-01*T -2.399939E+02

CO2 = -2.6708333E-09*T**4 + 1.1070717E-05*T**3

+- 1.7087881E-02*T**2 + 11.659741E+00*T - 2.9644706E+03

CO = -7.1458333E-09*T**4 + 2.8947417E-05*T**3 -4.3539045E-02*T**2

++ 2.8893979E+01*T -7.14979E+03

CH4 = -1.315E-09*T**4 +5.3426467E-06*T**3 -8.0538438E-03*T**2

++ 5.352608E+00*T -1.3255625E+03

SOLID = 2.6708333E-09*T**4 -1.143405E-05*T**3 +1.8493951E-02*T**2

+- 1.3458835E+01*T + 3.7608329E+03

LIQUID = 8.6791667E-09*T**4 -3.4841817E-05*T**3

++ 5.1611559E-02*T**2 -3.3425752E+01*T +8.0285895E+03

N2 = 0.06

S = 0.01

ASH = 0.49

O2 = 0.0

LGASSES = 0

CHAR = SOLID - ASH

PW = 5.157E-05*T**2 - 11.86E-02*T + 84.91

MOIST = 5.57

H2O = PW + MOIST

PHENOL = (LIQUID - H2O)

CL2 = 0

TCSTR = T

TSTOIC = T

FR = 4.72E-3*exp (37737 / (8.31445985 * T))

BETAC = -((1+2*FR) / (1+FR))

BETACO = 2*((-BETAC) - 1)

BETACO2 = 2 + BETAC

END IF

Appendix H- Kinetics for chemical reactions used in the model

Table 6: Different Kinetic Reactions Used in the Model and the reaction rate parameters [65] [67] [66]

Reaction no.	Reaction name	Gasifier section	Reaction Equation
1	Boudouard	Gas-Bed + Freeboard	$C + CO_2 \rightarrow 2CO$
2	Water Gas Shift	Gas-Bed + Freeboard	$CO + H_2O \rightarrow CO_2 + H_2$
OXIDATION			
3	Char Oxidation	Bedzone + Freeboard	$\alpha C + O_2 \rightarrow 2(\alpha\text{-}1)\ CO + (2\text{-}\alpha)\ CO_2$
4	Hydrogen Oxidation	Bedzone + Freeboard	$H_2 + 0.5O_2 \rightarrow H_2O$
5	Carbon Monoxide Oxidation	Bedzone + Freeboard	$CO + 0.5O_2 \rightarrow CO_2$
6	Methane Oxidation	Bedzone + Freeboard	$CH_4 + 0.5O_2 \rightarrow CO + 2H_2$
7	Benzene Oxidation	Freeboard	$C_6H_6 + 3O_2 \rightarrow 6CO + 3H_2$
8	Naphthalene Oxidation	Freeboard	$C_{10}H_8 + 7O_2 \rightarrow 10CO + 4H_2O$
REFORMING			
9	Water Gas/Char Gasification	Gas-Bed + Freeboard	$C + 1.2\ H_2O \rightarrow 0.8CO + 0.2CO_2 + 1.2H_2$
10	Methane Reforming	Gas-Bed + Freeboard	$CH_4 + H_2O \rightarrow CO + 3\ H_2$
11	Phenol Reforming	Gas-Bed + Freeboard	$C_6H_5OH + 3H_2O \rightarrow 2CO + CO_2 + 2.95CH_4 + 0.05C + 0.1H_2$
12	Benzene Reforming	Gas-Bed + Freeboard	$C_6H_6 + 2H_2O \rightarrow 1.5C + 2.5CH_4 + 2CO$
CRACKING			
13	Phenol Cracking	Gas-Bed	$C_6H_5OH \rightarrow CO + 0.4\ C_{10}H_8 + 0.15C_6H_6 + 0.1\ CH_4 + 0.75H_2$

The reaction rate for most of the homogenous gas-phase and char oxidation reaction are described by Power Law kinetics. The heterogenous char reforming reaction, WGS and MSR reaction are described by LHHW kinetics. The kinetics considered for these reactions are specified in Table 5. Activation energy Ea,i is defined in kJ/kmol. The unit of Reaction Constant k_i depends on the order of reaction i. The unit of reaction rate r_i for an n-th order reaction is given by $[(m^3/kmol)^{n-1}(m/s)]$.

For a reaction with A and B as reactants converting to C and D as products, Eq 3 can be written:

$$aA + bB \rightarrow CC + dD \qquad\qquad \text{(Eq 3)}$$

The rate law kinetic expression is given in Eq 4.

$$r_i = k_i[A]^a[B]^b \qquad \text{(Eq 4)}$$

where k_i is the reaction rate constant given by the Arrhenius's Law in Eq 5.

$$k_i = A_i exp\left[\frac{-E_{ai}}{R_g T}\right] \qquad \text{(Eq 5)}$$

The LHHW kinetic expression rate considered for the same reaction in Eq 3 is calculated as described in Eq 6.

$$r_i = \frac{k_i[A]^a}{1 + k_a[A]^a + k_c[C]^c + k_d[D]^d} \qquad \text{(Eq 6)}$$

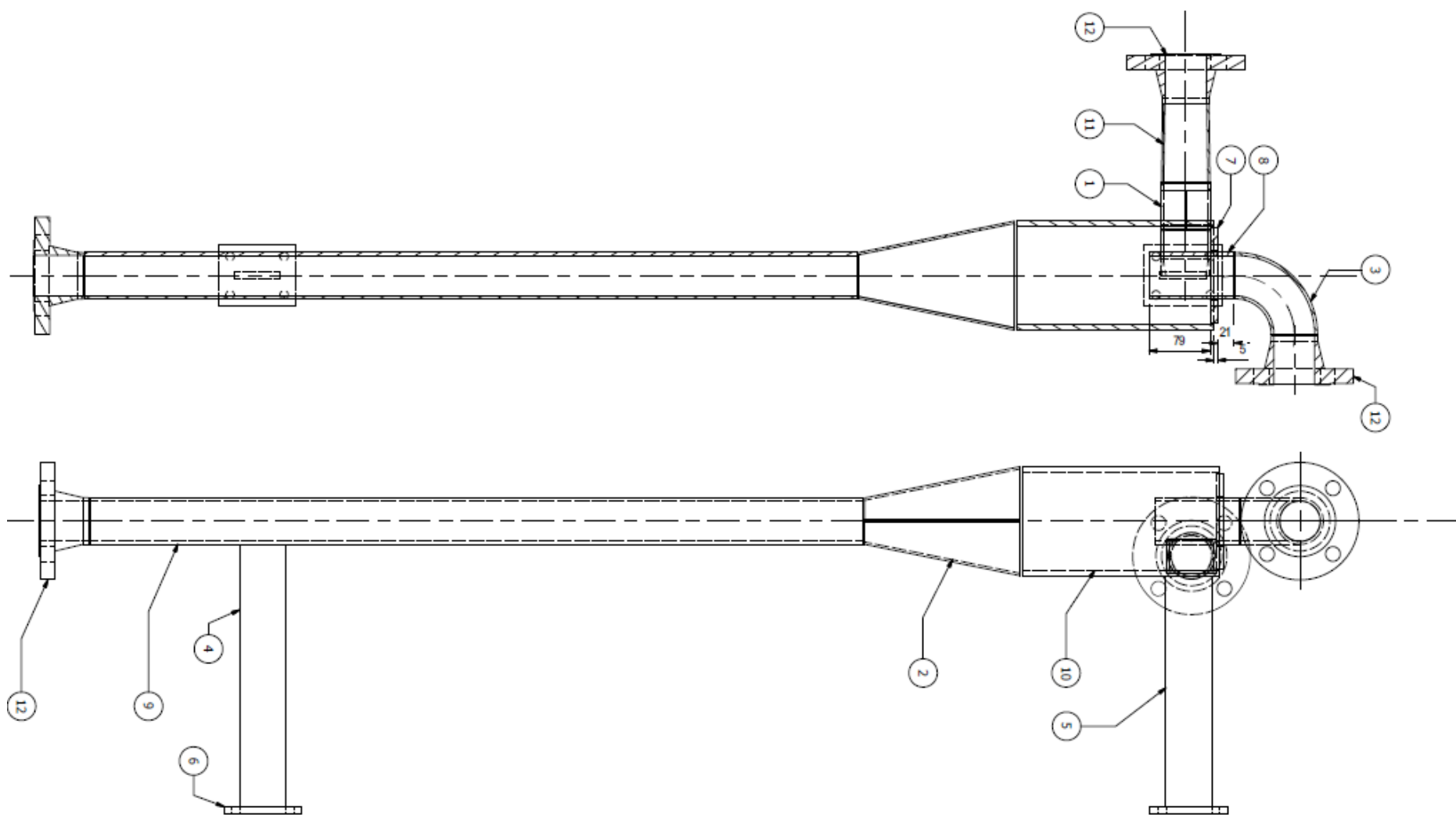The reaction rate constants for Eq 6 are described by Arrhenius's Law given in Eq 5.

Reaction no.	Reaction name	Reaction Kinetics	Source
1	Boudouard $C + CO_2 \rightarrow 2CO$	$r_1 = \dfrac{k_1 F_1[CO_2]}{1 + k_{CO2}[CO_2] + k_{CO}[CO]}$ $k_1 = 4.89.10^{10} \exp(-\dfrac{268000}{RT})$ $F_1 = \dfrac{\rho_{char}(1-X)}{MW_{char}}$ $k_{CO2} = 66$ $k_{CO} = 120 \exp(-\dfrac{25500}{RT})$	[66]
2	Water Gas Shift $CO + H_2O \rightarrow CO_2 + H_2$	$r_2 = k_2[CO][H_2O] - \dfrac{[CO_2][H_2]}{k_{eq}}$ $k_2 = 2778 \exp(-\dfrac{12560}{RT})$ $k_{eq} = 0.022 \exp(\dfrac{34730}{RT})$	[66]
Oxidation			
3	Char oxidation $\alpha C + O_2 \rightarrow 2(\alpha-1) CO + (2-\alpha) CO_2$	$r_3 = k_3.6/d_p[O_2]$ $k_3 = 595.7T \exp(-\dfrac{149400}{RT})$ $d_p = 0.006\,m$ $\alpha = \dfrac{1+2f_r}{1+f_r}$ $f_r = 4.72.10^{-3} \exp(-\dfrac{37737}{RT})$	[66]
4	Hydrogen Oxidation $H_2 + 0.5O_2 \rightarrow H_2O$	$r_4 = k_4.[O_2][H_2]$ $k_4 = 1.08.10^{13} \exp(-\dfrac{125525}{RT})$	[66]
5	Carbon Monoxide Oxidation $CO + 0.5O_2 \rightarrow CO_2$	$r_5 = k_5.[O_2]^{0.3}[H_2O]^{0.5}[CO]$ $k_5 = 4.78.10^8 \exp(-\dfrac{66900}{RT})$	[65]

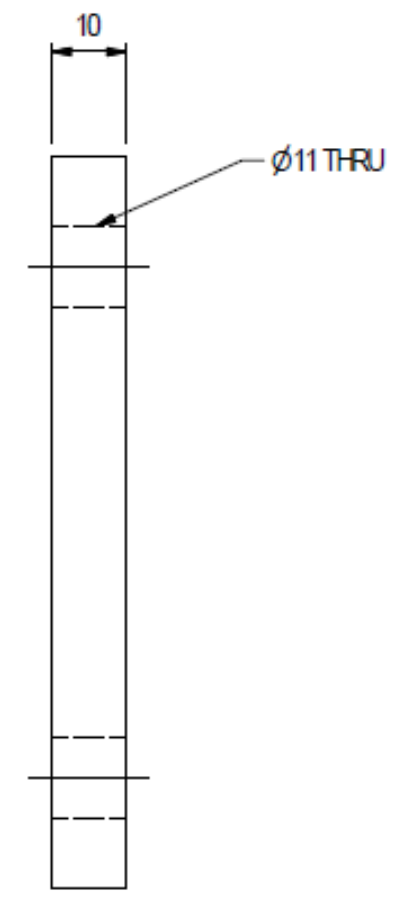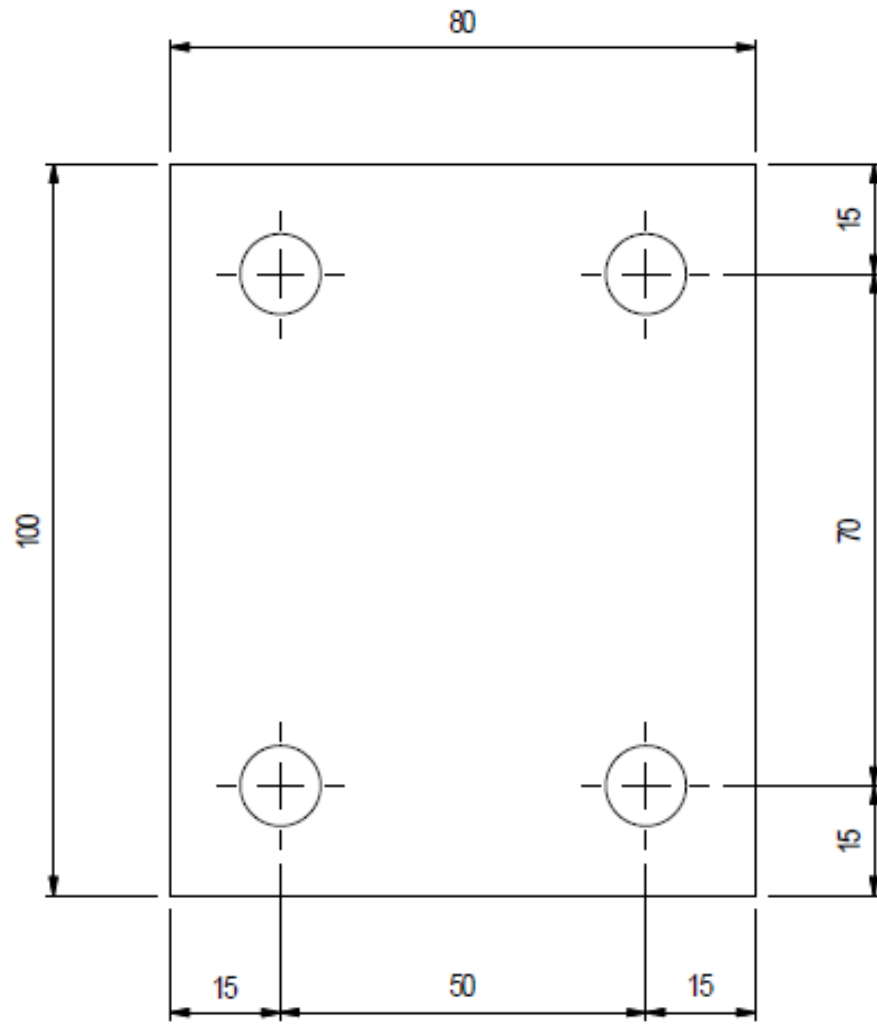|			
6	Methane Oxidation $CH_4 + 0.5O_2 \rightarrow CO + 2H_2$	$r_6 = k_6.\,[O_2]^{0.25}[CH_4]^{0.5}$ $k_5 = 4.4.\,10^{11} \exp(-\dfrac{126000}{RT})$	[65]
7	Benzene Oxidation $C_6H_6 + 3O_2 \rightarrow 6CO + 3H_2$	$r_7 = k_7.\,[C_6H_6][O_2]$ $k_6 = 1.58.\,10^{15} \exp(-\dfrac{202641}{RT})$	[66]
8	Naphthalene Oxidation $C_{10}H_8 + 7O_2 \rightarrow 10CO + 4H_2O$	$r_8 = k_8.\,[C_{10}H_8]^{0.5}[O_2]$ $k_8 = 9.2.\,10^6 T \exp(-\dfrac{80000}{RT})$	[67]
Reforming			
9	Water Gas/Char Gasification $C + 1.2\,H_2O \rightarrow 0.8CO + 0.2CO_2 + 1.2H_2$	$r_{10} = \dfrac{k_{10}F_{10}[H_2O]}{1 + k_{H_2O}[H_2O] + k_{CO}[CO] + k_{H_2}[H_2]}$ $k_{10} = 2.39.\,10^5 \exp(-\dfrac{129000}{RT})$ $F_{10} = \dfrac{\rho_{char}\,(1-X)}{MW_{char}}$ $k_{H_2O} = 31{,}6 \exp(-\dfrac{30100}{RT})$ $k_{H_2} = 5.36 \exp(-\dfrac{59800}{RT})$ $k_{CO} = 0.0825 \exp(-\dfrac{96100}{RT})$	[66]
10	Methane reforming $CH_4 + H_2O \rightarrow CO + 3\,H_2$	$r_{10} = k_{10}[CH_4][H_2O] - \dfrac{[CO][H_2]^3}{k_{eq}}[C(s)]$ $k_{10} = 4.916.\,10^{-4}T^2.\dfrac{1}{M_C\rho_{char}d_P}\exp\left(-\dfrac{36150}{RT}\right)$ $k_{eq} = 3.106.\,10^8 \exp\left(-\dfrac{208800}{RT}\right)$	[66]
11	Phenol Reforming $C_6H_5OH + 3H_2O \rightarrow 2CO + CO_2 + 2.95CH_4 + 0.05C + 0.1H_2$	$r_{11} = k_{11}[C_6H_5OH]$ $k_{11} = 1.\,10^8 \exp\left(-\dfrac{100000}{RT}\right)$	[67]
12	Benzene Reforming $C_6H_6 + 2H_2O \rightarrow 1.5C + 2.5CH_4 + 2CO$	$r_{12} = k_{12}.\,[H_2O]^{0.2}[C_6H_6]^{1.3}[H_2]^{-0.4}$ $k_{12} = 3.39.\,10^{16} \exp\left(-\dfrac{443000}{RT}\right)$	[67]

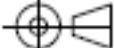| 13 | Phenol Cracking $C_6H_5OH \rightarrow CO + 0.4$ $C_{10}H_8 + 0.15C_6H_6 +$ $0.1\ CH_4 + 0.75H_2$ | $r_{13} = k_{13}[C_6H_5OH]$ $k_{11} = 1.10^7 \exp\left(-\dfrac{100000}{RT}\right)$ | [67] |

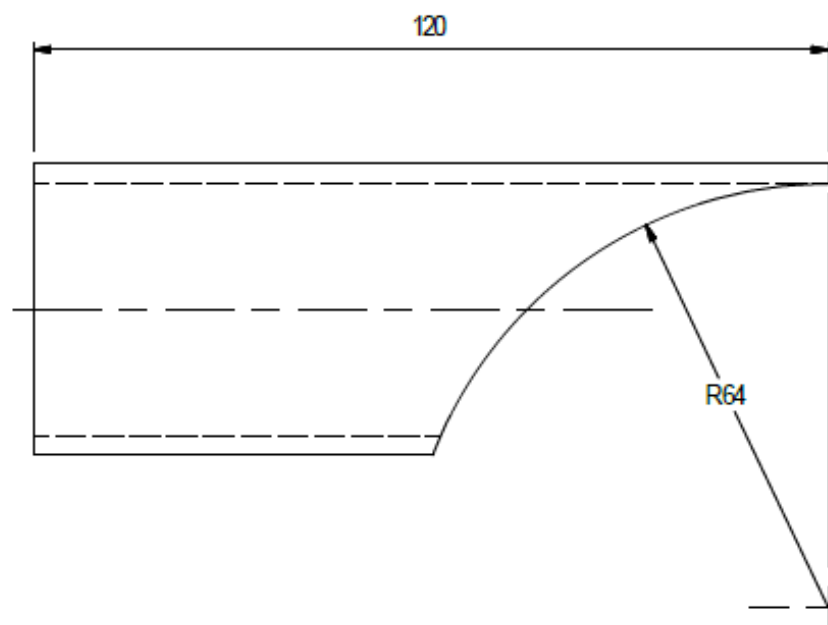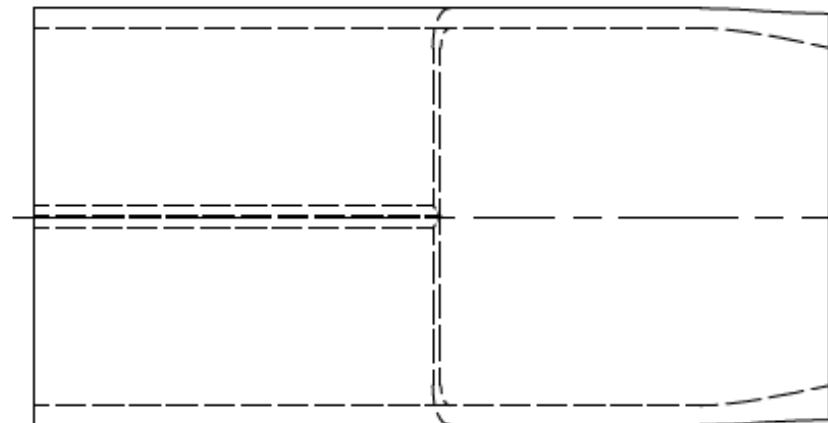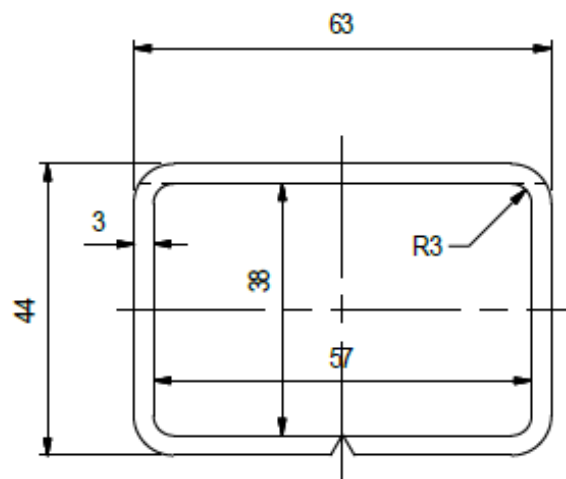The consideration of char density for Reaction 1, 9 and 10 is explained in Appendix L.

Appendix I- Cyclone Separator data from Datasheet provided by Petrogas Gas-Systems
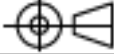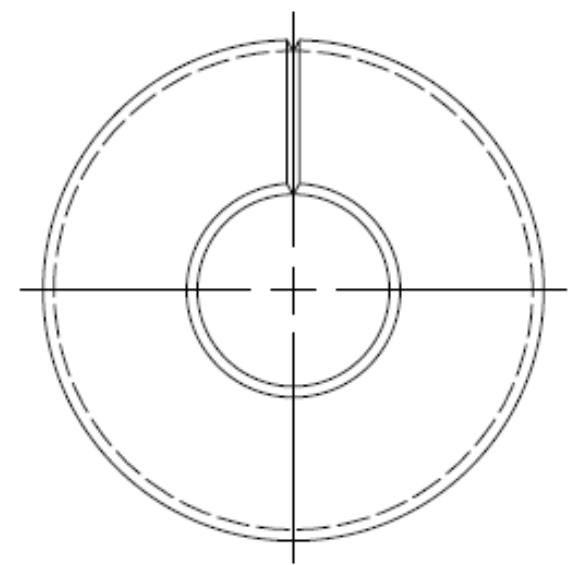
Item	Qty	Title	OD	ID	TH	Height	Length	Material	Cert.	Comments	Item N°	Spec. N°
12	3	WN FLG RF-2-STD-150-SA-182 F310						SA-182 F310	Yes		AE0035941	ASME B16.5
11	1	TRANSDUCER			3 mm			SA-240 310S	Yes		AE0039783	
10	1	SMLS PIPE-5-STD	141.3 mm		6.55 mm		256 mm	SA-312 TP310S	Yes		AE0039778	
9	1	SMLS PIPE-2-STD	60.32 mm		3.91 mm		1000 mm	SA-312 TP310S	Yes		AE0039780	
8	1	SMLS PIPE-2-STD	60.32 mm		3.91 mm		110 mm	SA-312 TP310S	Yes		445276	
7	1	ROUND PLATE	124.2 mm	64 mm	10 mm			SA-240 310S	Yes		AE0039782	
6	2	PLATE			10 mm	80 mm	100 mm	S.S.304	No		AE0040059	
5	1	FLAT BAR60 x 10			10 mm	60 mm	300.0 mm	SA-240 310S	No		AE0040057	
4	1	FLAT BAR60 x 10			10 mm	60 mm	340.0 mm	SA-240 310S	No		AE0040060	
3	1	ELBOW-LR-90°-2 x 0.154-SA-403 WP310S-ST						SA-403 WP310S	Yes		AE0039786	ASME B16.9
2	1	CONE			3 mm			SA-240 310S	Yes		AE0039777	
1	1	CHANNEL						SA-240 310S	Yes		AE0039784	

TITLE

CYCLONE SEPARATOR

R&D BIOMASS STEAM REFORMING

This drawing and the copyright thereof is owned by us. Without our written permission this drawing may neither be copied nor submitted to third parties. If no order follows drawing and enclosure will be returned to us.

PROJECT	16501	Date
DRAWN	JoGr	04/21/2017
CHECKED	JaMu	04/21/2017
APPROVED BY	ArTr	04/21/2017

ROUGHNESS ACC. NPR 3637

GENERAL TOLERANCES ACC. ISO 2768-m

PETROGAS GAS SYSTEMS Gouda — The Netherlands

ITEM NUMBER : AE0039779

DOCUMENT NUMBER: AE0039781   Sh 2 /2
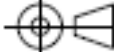
SCALE 1 / 5

SIZE A1

REV 00

Revisions   Drawn   Appr.

121

80

10

Ø11 THRU

15

100

70

15

15

50

15

122

Item	Qty	Title	OD	ID	TH	Height	Length	Material	Cert.	Comments	Item N°	Spec. N°
1	1	PLATE			10 mm	80 mm	100 mm	S.S.304	No		AE0040059	

TITLE
PLATE

R&D BIOMASS STEAM REFORMING

ROUGHNESS
ACC. NPR 3637

GENERAL TOLERANCES
ACC. ISO 2768-m

PROJECT	16501	Date
DRAWN	JoGr	04/19/2017
CHECKED	JaMu	04/21/2017
APPROVED BY	ArTr	04/21/2017

PETROGAS
GAS SYSTEMS
Gouda — The Netherlands

ITEM NUMBER : AE0040059

DOCUMENT NUMBER: AE0040061   Sh 1 /1

SCALE 1 : 1

SIZE A3

REV 00

Revisions   Drawn   Appr.

63

3

44

38

57

R3

120

R64

124

Item	Qty	Title	OD	ID	TH	Height	Length	Material	Cert.	Comments	Item N°	Spec. N°
1	1	CHANNEL						SA-240 310S	Yes		AE0039784	

TITLE
CHANNEL

R&D BIOMASS STEAM REFORMING

PROJECT	16501	Date
DRAWN	JoGr	04/19/2017
CHECKED	JaMu	04/21/2017
APPROVED BY	ArTr	04/21/2017

ROUGHNESS
ACC. NPR 3637

GENERAL TOLERANCES
ACC. ISO 2768-m

PETROGAS
GAS SYSTEMS
Gouda — The Netherlands

ITEM NUMBER :
AE0039784
DOCUMENT NUMBER:
AE0040062   Sh 1 /1

SCALE
1 : 1

SIZE
A3

REV
00

Revisions   Drawn   Appr.

201

Ø141

Ø60.2

126

Item	Qty	Title	OD	ID	TH	Height	Length	Material	Cert.	Comments	Item N°	Spec. N°
1	1	CONE			3 mm			SA-240 310S	Yes		AE0039777	

TITLE

CONE

R&D BIOMASS STEAM REFORMING

ROUGHNESS ACC. NPR 3637	GENERAL TOLERANCES ACC. ISO 2768-m

PROJECT	16501	Date
DRAWN	JoGr	04/19/2017
CHECKED	JaMu	04/21/2017
APPROVED BY	ArTr	04/21/2017

PETROGAS
GAS SYSTEMS
Gouda — The Netherlands

ITEM NUMBER :
AE0039777

DOCUMENT NUMBER:
AE0040063   Sh 1 /1

SCALE	SIZE	REV
1 / 2	A3	00

Revisions   Drawn   Appr.

100

3

Ø60.3

3

63

44

3

Item	Qty	Title	OD	ID	TH	Height	Length	Material	Cert.	Comments	Item N°	Spec. N°
1	1	TRANSDUCER			3 mm			SA-240 310S	Yes		AE0039783	

TITLE

TRANSDUCER

R&D BIOMASS STEAM REFORMING

This drawing and the copyright thereof is owned by us. Without our written permission this drawing may neither be copied nor submitted to third parties. If no order follows drawing and enclosure will be returned to us.

PROJECT	16501	Date
DRAWN	JoGr	04/19/2017
CHECKED	JaMu	04/21/2017
APPROVED BY	ArTr	04/21/2017

ROUGHNESS ACC. NPR 3637

GENERAL TOLERANCES ACC. ISO 2768-m

PETROGAS
GAS SYSTEMS
Gouda – The Netherlands

ITEM NUMBER : AE0039783

DOCUMENT NUMBER: AE0040065 Sh 1 /1

SCALE 1 : 1

SIZE A3

REV 00

Revisions   Drawn   Appr.

256

Ø141.3

44

5

63

3

45

44

130

Item	Qty	Title	OD	ID	TH	Height	Length	Material	Cert.	Comments	Item N°	Spec. N°
1	1	SMLS PIPE-5-STD	141.3 mm		6.55 mm		256 mm	SA-312 TP310S	Yes		AE0039778	

TITLE

SMLS PIPE-5-STD

R&D BIOMASS STEAM REFORMING

PROJECT	16501	Date
DRAWN	JoGr	04/19/2017
CHECKED	JaMu	04/21/2017
APPROVED BY	ArTr	04/21/2017

ROUGHNESS
ACC. NPR 3637

GENERAL TOLERANCES
ACC. ISO 2768-m

PETROGAS
GAS SYSTEMS
Gouda – The Netherlands

Revisions   Drawn   Appr.

ITEM NUMBER :
AE0039778

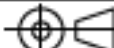DOCUMENT NUMBER:
AE0040066   Sh 1 /1

SCALE	SIZE	REV
1 / 2	A3	00

Ø124.2

Ø64.3

10

132
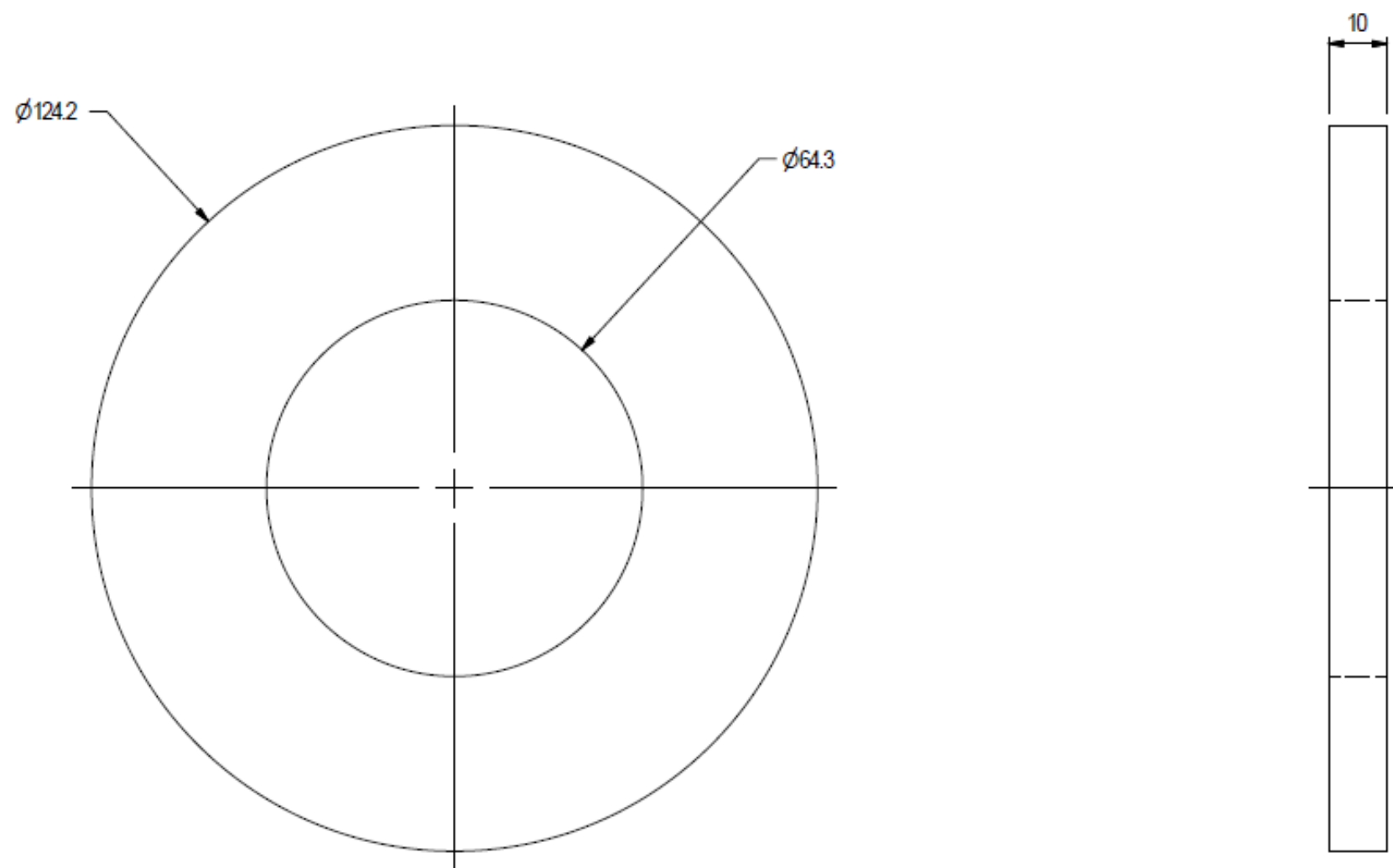
Item	Qty	Title	OD	ID	TH	Height	Length	Material	Cert.	Comments	Item N°	Spec. N°
1	1	ROUND PLATE	124.2 mm	64.3 mm	10 mm			SA-240 310S	Yes		AE0039782	

TITLE

ROUND PLATE

R&D BIOMASS STEAM REFORMING

ROUGHNESS
ACC. NPR 3637

GENERAL TOLERANCES
ACC. ISO 2768-m

PROJECT	16501	Date
DRAWN	JoGr	04/19/2017
CHECKED	JaMu	04/21/2017
APPROVED BY	ArTr	04/21/2017

PETROGAS
GAS SYSTEMS
Gouda — The Netherlands

ITEM NUMBER :
AE0039782

DOCUMENT NUMBER:
AE0040067   Sh 1 /1

SCALE
1 : 1

SIZE
A3

REV
00

Revisions	Drawn	Appr.

Appendix J - PSD Curves of Inlet and Outlet Streams of cyclones

The PSD curves for the streams at the inlet and outlet of the cyclone separator can be analysed to get an insight on the effect of cyclone efficiency selection on PSD of the solids in the inlet and outlet stream. This analysis is done for the first test with GB.

GB and RB are defined by their PSD as given in Table 8. The PSD curves for GB and RB are generated in Aspen Plus® and given in Figure 2, 3, 4 and 5.
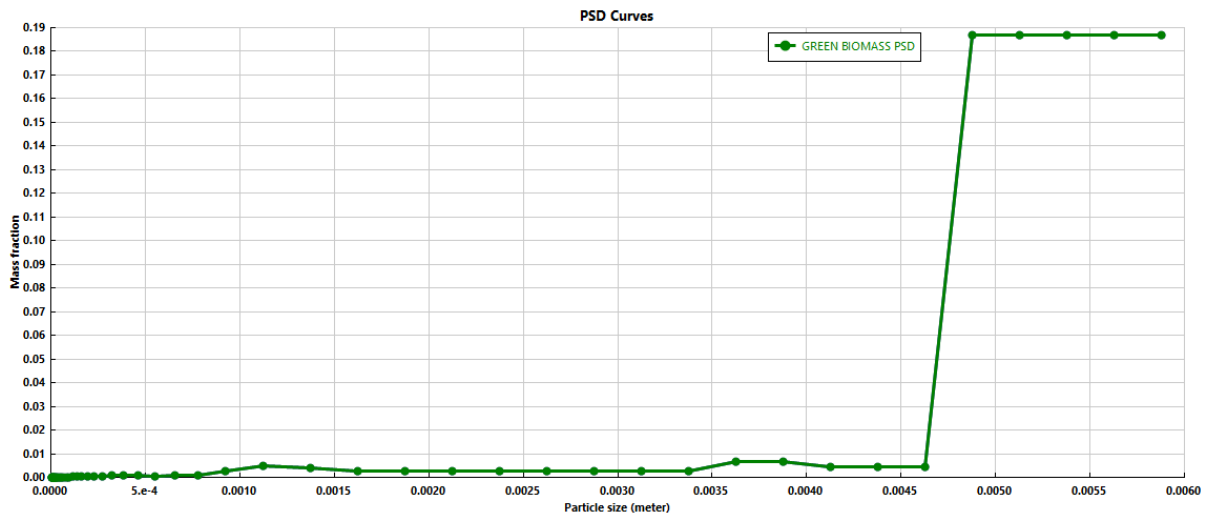
Figure 2: PSD of GB representing mass fraction of particles w.r.t particle size
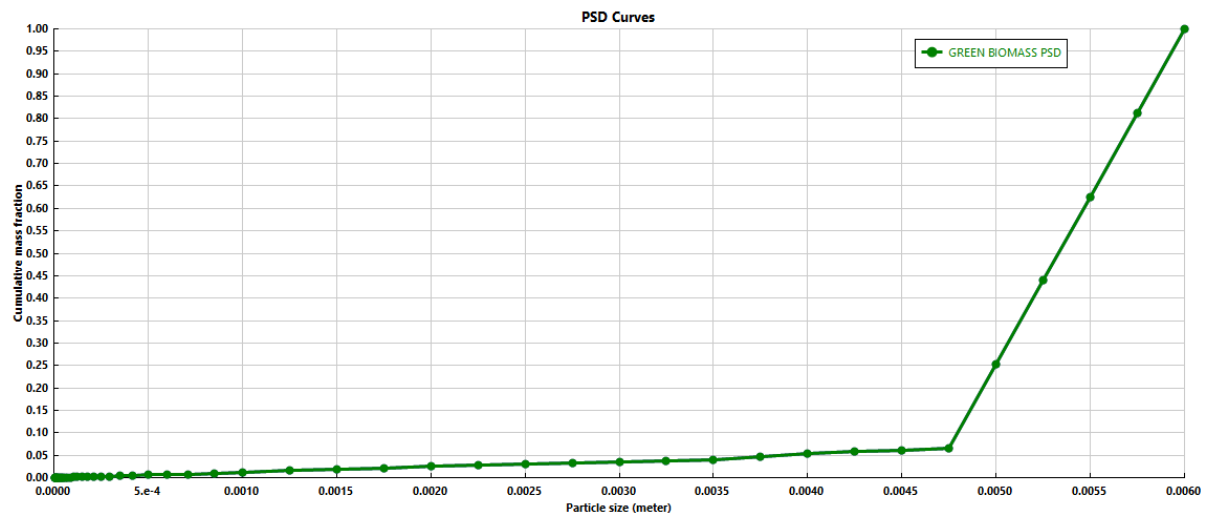
Figure 3: PSD of GB representing cumulative mass fraction of particles w.r.t particle size
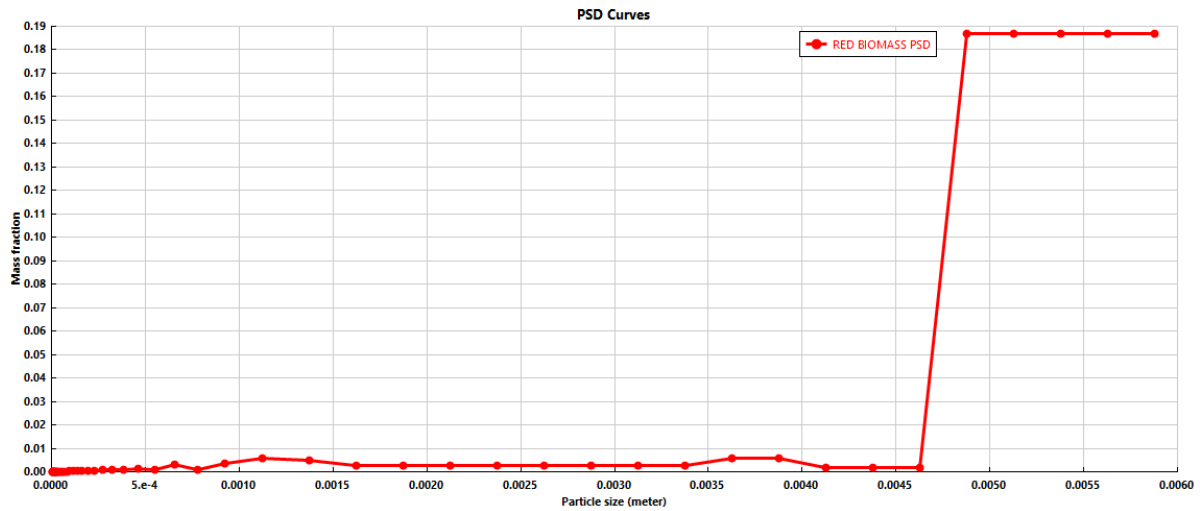
Figure 4: PSD of RB representing mass fraction of particles w.r.t particle size
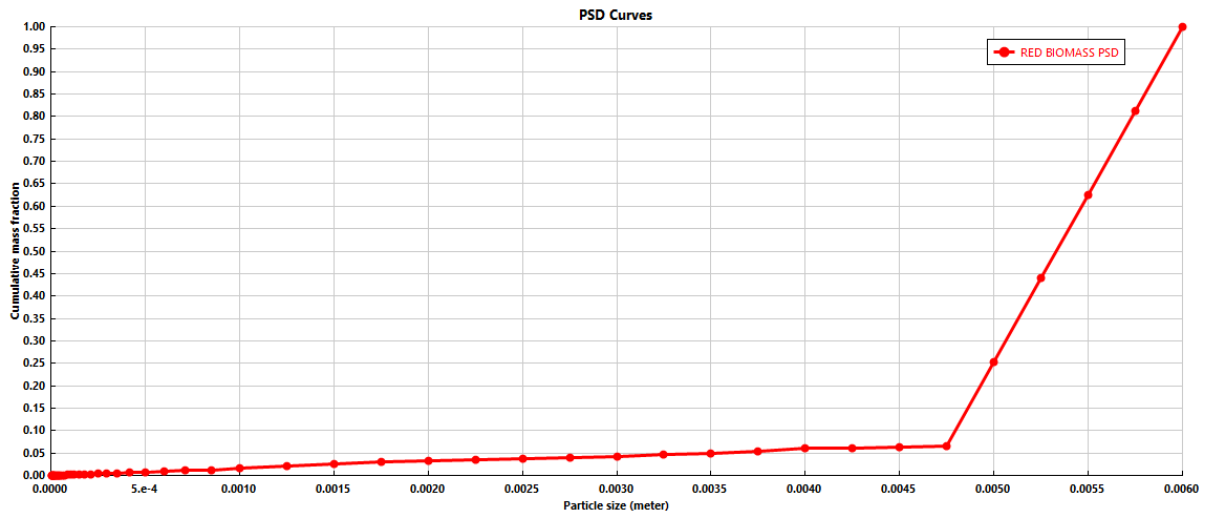
Figure 5: PSD of RB representing cumulative mass fraction of particles w.r.t particle size

Two scenarios were considered in Section 4.1.8. The PSD curves generated for char and ash for those scenarios are presented below.

SCENARIO 1

The product stream passes through Cyclone 1. The efficiency of the cyclones is selected in a manner such that the overall efficiency of both the cyclone separators is 100%. In this scenario, it is expected that both the cyclones will remove the char and ash particles equally. The PSD curves for the inlet stream and outlet stream of the cyclones are presented in the figures below. Figure 6 shows the PSD for char and ash in terms of mass fraction at the inlet of the first cyclone separator in Aspen Plus®.

135
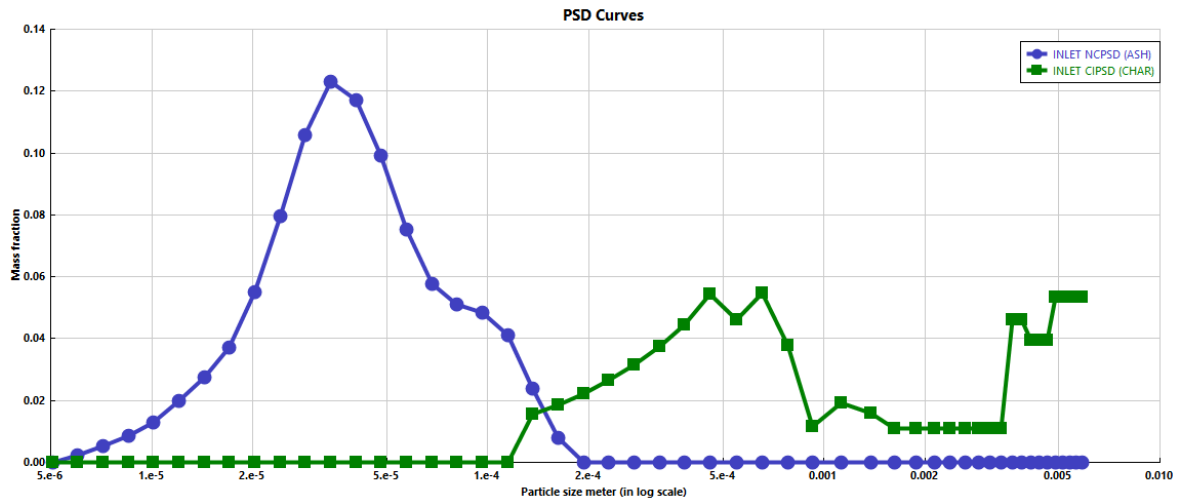
Figure 6: PSD for inlet stream at Cyclone 1 representing mass fraction of particles w.r.t particle size for Scenario 1 for char and ash, run w.r.t to Test 1 input parameters (GB)

Figure 7 shows the PSD for char and ash in terms of cumulative mass fraction at the inlet of the first cyclone separator in Aspen Plus®.
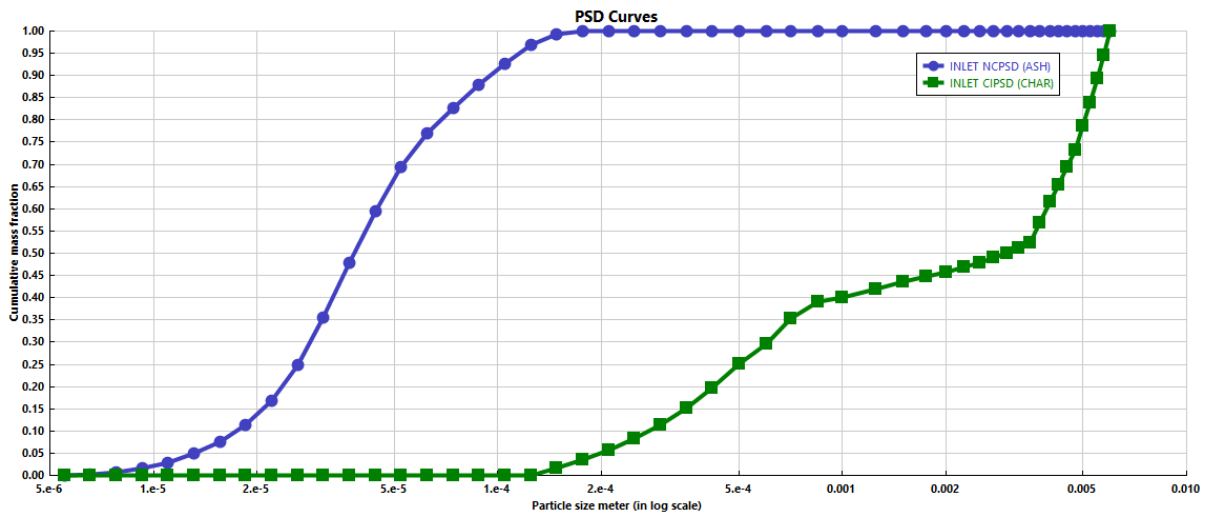
Figure 7: PSD of inlet stream at Cyclone 1 representing cumulative mass fraction of particles w.r.t particle size for Scenario 1 for char and ash, run w.r.t to Test 1 input parameters (GB)

Figure 8 shows the PSD for char and ash in terms of mass fraction at the outlet of the first and second cyclone separator in Aspen Plus®.

136
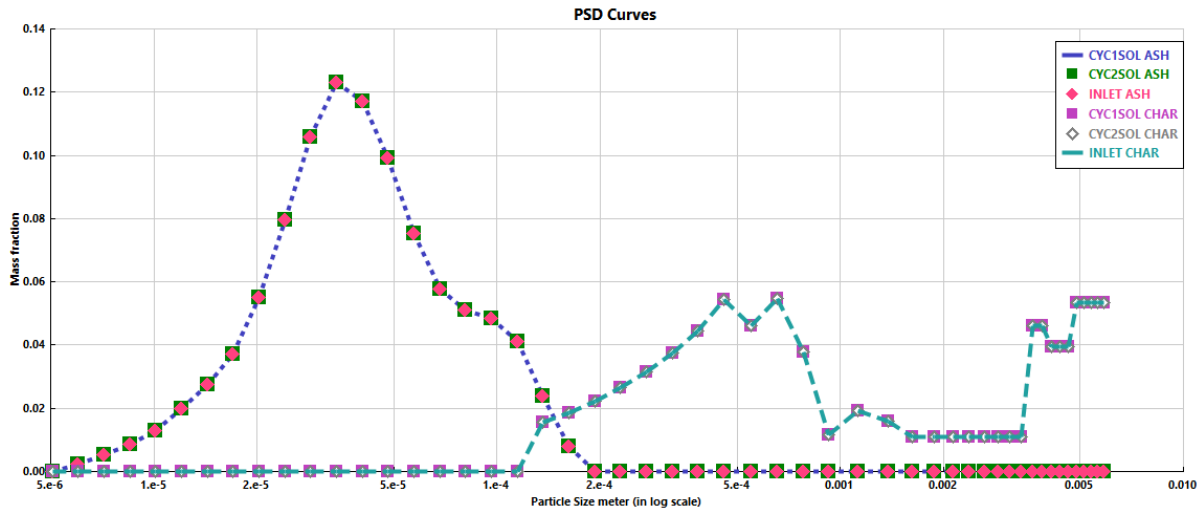
Figure 8: PSD of outlet stream of both cyclones overlapping with the PSD of inlet stream for Ash and Char represented by mass fraction of particles w.r.t particle size for Scenario 1, run w.r.t to Test 1 input parameters (GB)

Figure 9 shows the PSD for char and ash in terms of cumulative mass fraction at the outlet of the first and second cyclone separator in Aspen Plus®.
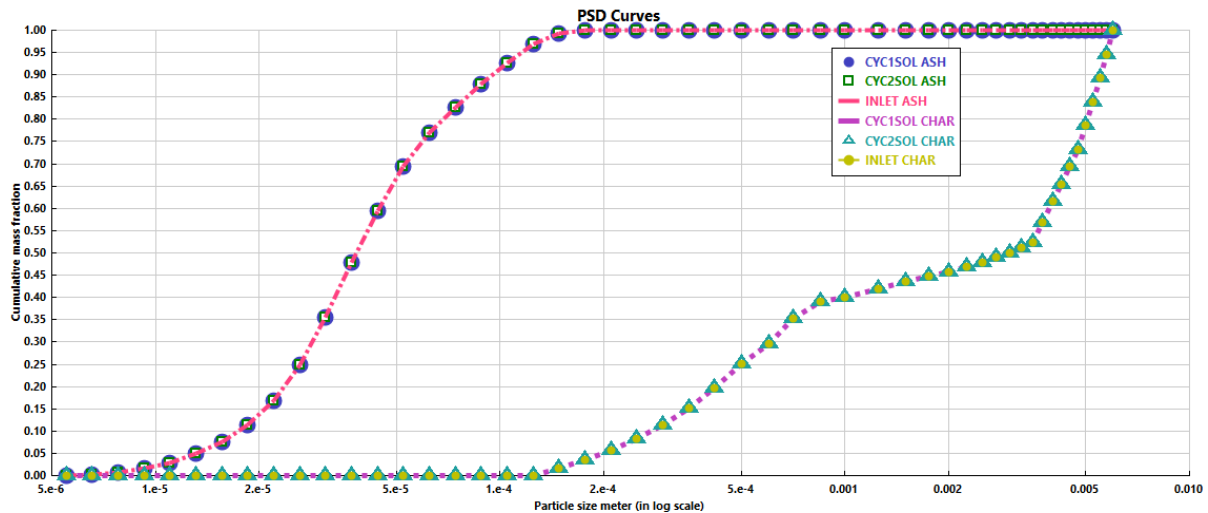
Figure 9: PSD of outlet stream of both cyclones overlapping with PSD of inlet stream for Ash and Char represented by mass fraction of particles w.r.t particle size for Scenario 1, run w.r.t to Test 1 input parameters (GB)

The efficiency selected for the first cyclone in this case is 50%. It can be observed from the PSD curves in Figure 8 and 9 that the outlet streams of both cyclones have overlapping PSD curve with that of the inlet stream. The cyclone is designed in such a way that when the product stream obtained from the gasifier passes through the first cyclone, 50% weight fraction of all char and ash (50% from all the particle size ranges representing the solids i.e., char and ash) get removed from the first cyclone. This stream containing remaining 50% weight fraction then passes through the second cyclone to be removed completely. The solids stream from first cyclone contains 50% weight fraction of the solids. The remaining part containing the rest 50% weight fraction of the solids passes through the second cyclone and gets removed in the solid stream of the second cyclone. Hence, the overall PSD of char and ash at the inlet and outlet

streams remains the same, resulting in overlapping PSDs for the inlet and outlet streams of each of the cyclone separator.

SCENARIO 2

The efficiency of the first cyclone is selected such that all solids having particle size above 3125 μm is removed 100% by the first cyclone and the solids having particle size below 3125 μm is removed up to 50% efficiency. The gaseous outlet stream of the first cyclone contains the remaining solids which get filtered by the second cyclone. Figure 10 shows the PSD for char and ash in terms of mass fraction w.r.t particle size in log scale at the outlet of the first and second cyclone separator in Aspen Plus®.
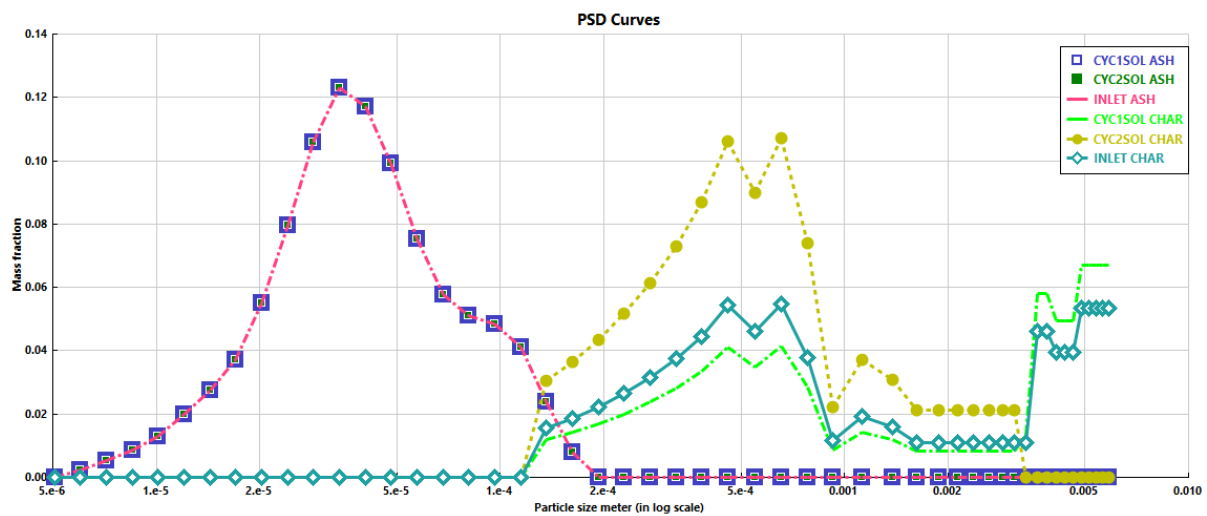
Figure 10: PSD of outlet stream of both cyclones for Char and Ash at 50% efficiency removal for particle size less than 3125 μm representing mass fraction of particles w.r.t particle size for Scenario 2 for char and ash, run w.r.t to Test 1 input parameters (GB)

Figure 11 shows the PSD for char and ash in terms of cumulative mass fraction w.r.t particle size in log scale at the outlet of the first and second cyclone separator in Aspen Plus®.
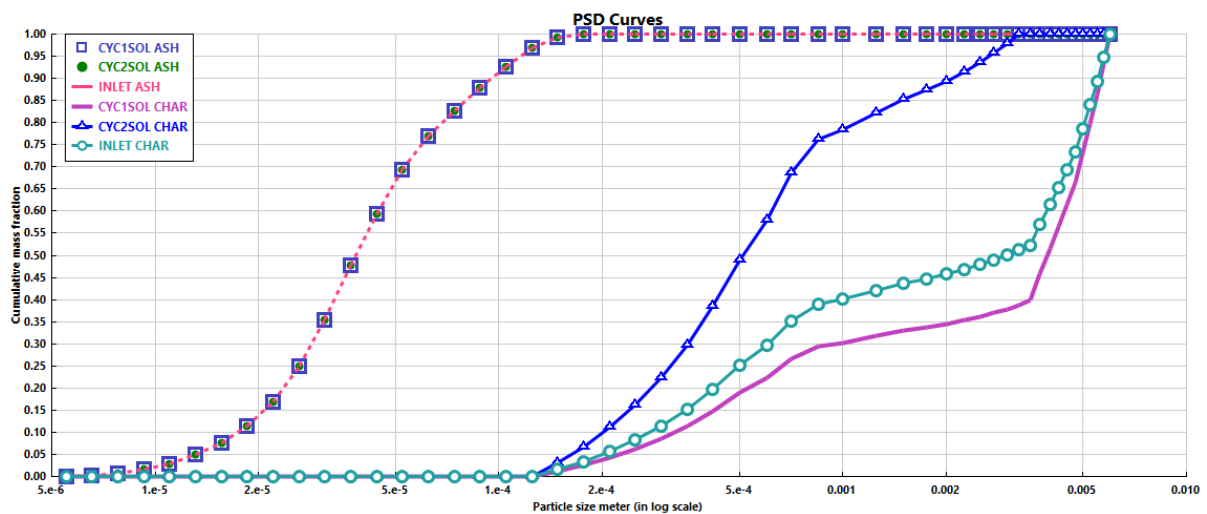
Figure 11: PSD of outlet stream of both cyclones for Char and Ash at 50% efficiency removal for particle size less than 3125 μm 1 representing cumulative mass fraction of particles w.r.t particle size for Scenario 2 for char and ash, run w.r.t to Test 1 input parameters (GB)

138

By observing the PSD for ash and char in Table 9 and 10, it can be seen that size ranges from 124.5 µm to 294 µm for ash and sizes of char particles fall in the category of 124 µm to 6000 µm. Approximately 50% weight fraction of char for GB comes from size range above 3000 µm. In this scenario, the PSDs for ash in the inlet and outlet streams of the cyclones overlap as 50% from each particle size range for ash is equally removed by the first cyclone and then it passes to the second cyclone. So, the individual weight fractions of each particle size range at the inlet and outlet stream for ash remains same. However, the PSD for char shows variation in the inlet and outlet streams as seen in Figure 10 and 11. This is because all the weight fractions of char having particle size range above 3125 µm is removed completely by the first cyclone, and the remaining weight fractions are removed only by a 50% efficiency by the first cyclone which then passes to the second cyclone.

For the simulations, Scenario 1 is selected.

The first cyclone and the second cyclone give a pressure drop of 0.025 bar and 0.039 bar respectively in both the scenarios. This is slightly higher than the pressure drop found in literature for cyclone separators (below 0.0225 bar at inlet velocities below 20 m/s) [77]. The reason for this can be attributed to the cyclone geometry and high inlet velocity of the product gas. The velocities at the inlet of Cyclone 1 and 2 for Test 1 are estimated to be above 100 m/s. Because the outlet pressure of the product gas obtained from the gasifier is at reduced pressures as compared to the atmospheric pressure, it results in a high inlet velocity of the gas, thereby increasing the pressure drop experienced in the cyclone.

Appendix K- Aspen Plus® flowsheet diagram with recycle stream
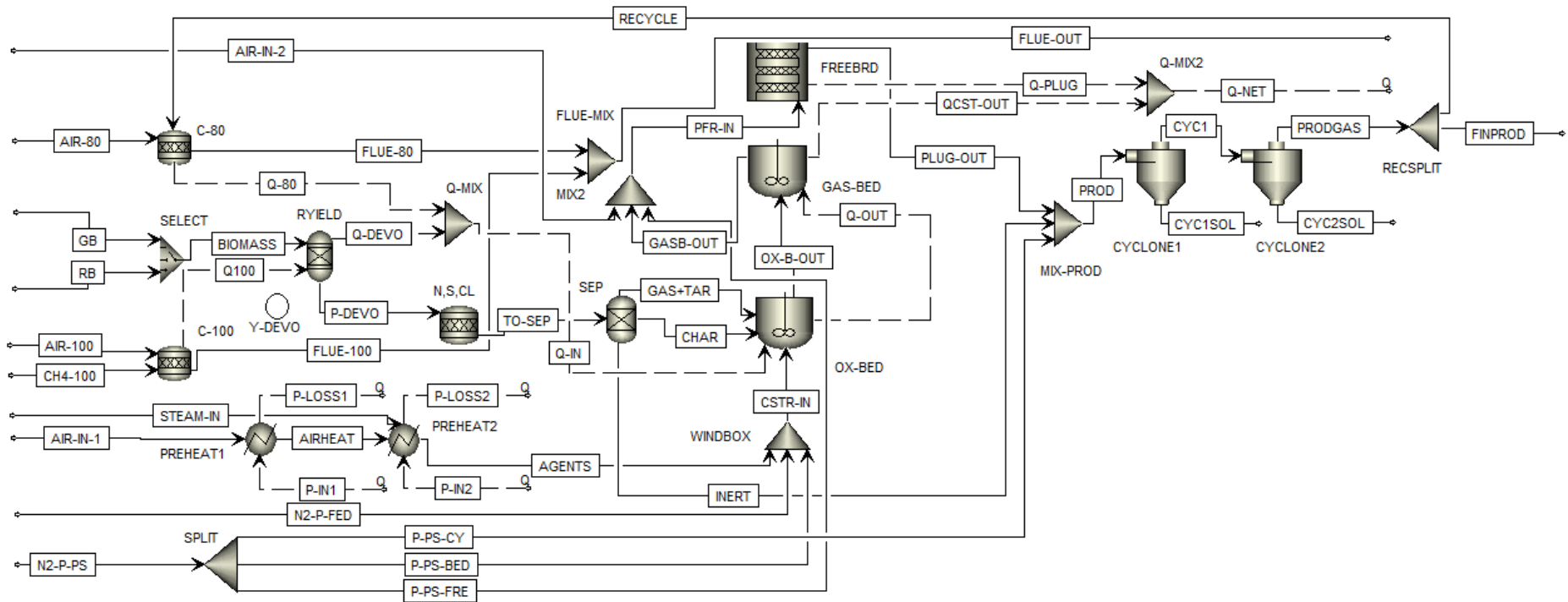
Appendix L- Density Factors for Char conversion

The density factors used for char conversion have been assumed in the freeboard for Reaction no. 1, 9 and 10 in Appendix H for different tests have been based on the gasification agent flow. If less agent is supplied to the reactor, the char particle is assumed to shrink less and vice-versa. Considering a char density of 250 kg/m^3 from [78], and density factors from 0.05 to 0.95 representing 95% reduction and 5% reduction in char density respectively, while reaching the freeboard from the bedzone, the values of pre-exponential factor for Reaction 1, 9 and 10 after considering the density factors of char in the freeboard are given in Table 7. Table 8 provides the density factors chosen for each test used for validation of model.

Table 7: Pre-exponential Factors for R1, R9 and R10 under different density conversion factors of char

	bouduard (k) [R1]	fb-bouduard (k)[R1]	char-ref (k) -[R9]	fb-char-ref (k) -[R9]	CH4-rf (k) [R10]	CH4-rf (k) [R10]
density=250 and considering 0.05 (95% density reduction)	6.62E+11	3.31E+10	2.49E+06	1.24E+05	2.73E-05	5.46E-04
density=250 and considering 0.10 (90% density reduction)	6.62E+11	6.62E+10	2.49E+06	2.49E+05	2.73E-05	2.73E-04
density=250 and considering 0.15 (85% density reduction)	6.62E+11	9.93E+10	2.49E+06	3.73E+05	2.73E-05	1.82E-04
density=250 and considering 0.20 (80% density reduction)	6.62E+11	1.32E+11	2.49E+06	4.98E+05	2.73E-05	1.37E-04
density=250 and considering 0.25 (75% density reduction)	6.62E+11	1.66E+11	2.49E+06	6.22E+05	2.73E-05	1.09E-04
density=250 and considering 0.30 (70% density reduction)	6.62E+11	1.99E+11	2.49E+06	7.47E+05	2.73E-05	9.10E-05
density=250 and considering 0.35 (65% density reduction)	6.62E+11	2.32E+11	2.49E+06	8.71E+05	2.73E-05	7.80E-05
density=250 and considering 0.40 (60% density reduction)	6.62E+11	2.65E+11	2.49E+06	9.96E+05	2.73E-05	6.83E-05
density=250 and considering 0.45 (55% density reduction)	6.62E+11	2.98E+11	2.49E+06	1.12E+06	2.73E-05	6.07E-05
density=250 and considering 0.50 (50% density reduction)	6.62E+11	3.31E+11	2.49E+06	1.24E+06	2.73E-05	5.46E-05
density=250 and considering 0.55 (45% density reduction)	6.62E+11	3.64E+11	2.49E+06	1.37E+06	2.73E-05	4.97E-05
density=250 and considering 0.60 (40% density reduction)	6.62E+11	3.97E+11	2.49E+06	1.49E+06	2.73E-05	4.55E-05
density=250 and considering 0.65 (35% density reduction)	6.62E+11	4.30E+11	2.49E+06	1.62E+06	2.73E-05	4.20E-05
density=250 and considering 0.70 (30% density reduction)	6.62E+11	4.63E+11	2.49E+06	1.74E+06	2.73E-05	3.90E-05
density=250 and considering 0.75 (25% density reduction)	6.62E+11	4.97E+11	2.49E+06	1.87E+06	2.73E-05	3.64E-05
density=250 and considering 0.80 (20% density reduction)	6.62E+11	5.30E+11	2.49E+06	1.99E+06	2.73E-05	3.41E-05
density=250 and considering 0.85 (15% density reduction)	6.62E+11	5.63E+11	2.49E+06	2.12E+06	2.73E-05	3.21E-05
density=250 and considering 0.90 (10% density reduction)	6.62E+11	5.96E+11	2.49E+06	2.24E+06	2.73E-05	3.03E-05
density=250 and considering 0.95 (5% density reduction)	6.62E+11	6.29E+11	2.49E+06	2.36E+06	2.73E-05	2.87E-05

Table 8: Density factors assumed for char conversion in each Test

Test no.	Density Factors
1	0.30
2	0.20
3	0.30
4	0.20
5	0.35
6	0.40
7	0.50
8	0.40

Appendix M - Absolute and Relative Errors for Permanent Gases, N_2, H_2O for GB and RB

Component	Absolute Error [exp-model]	Relative error [[abs(exp-model)/exp]
Test 1		
CO	-0.1	0.00
CO_2	0.4	0.01
H_2	-0.1	0.00
CH_4	-0.1	0.00
N_2 dry	0.7	0.01
H_2O	0.0	0.00
Test 2		
CO	-0.6	0.02
CO_2	0.1	0.00
H_2	0.6	0.02
CH_4	-0.1	0.01
N_2 dry	2.5	0.04
H_2O	-1.0	0.03
Test 3		
CO	1.7	0.05
CO_2	0.8	0.02
H_2	-2.5	0.08
CH_4	0.1	0.01
N_2 dry	3.1	0.06
H_2O	-0.6	0.02
Test 4		
CO	2.5	0.08
CO_2	4.8	0.15
H_2	-9.6	0.34
CH_4	2.3	0.23
N_2 dry	9.0	0.16
H_2O	2.8	0.09
Test 5		
CO	-0.3	0.01
CO_2	1.8	0.06
H_2	-2.1	0.06
CH_4	0.5	0.06
N_2 dry	13.1	0.22
H_2O	-12.2	0.67
Test 6		
CO	2.6	0.09
CO_2	-1.1	0.03
H_2	-0.7	0.02

CH₄	-0.8	0.09
N₂ dry	7.2	0.13
H₂O	-4.1	0.15
Test 7		
CO	-3.6	0.16
CO₂	3.2	0.10
H₂	2.6	0.06
CH₄	-2.2	0.27
N₂ dry	12.8	0.20
H₂O	-4.4	0.18
Test 8		
CO	-6.1	0.28
CO₂	4.4	0.14
H₂	4.3	0.10
CH₄	-2.5	0.40
N₂ dry	10.3	0.17
H₂O	-3.1	0.13

Appendix N- Burner Efficiencies for calculation of OE

The efficiency of the burner is based on the total time during the gasification tests when the burner remains on. If the bottom burner remains on for 97% of the time, then the total power delivered will be 20*0.97 = 19.4 kW.

Q Preheaters[kW]	Top Burner kW	Bottom Burner (kW)	Q Burners [kW]	Qin (MJ)	Bottom Burner on	Top Burner on
10.5	12	20	29.20	142.93	0.97	0.82
			29.40	105.83	0.96	0.84
			27.23	98.04	0.81	0.91
			28.30	101.89	0.87	0.92
			32.00	115.20	1.00	1.00
			31.06	111.81	0.95	1.00
			26.11	94.01	1.00	0.51
			28.04	100.96	1.00	0.67

Appendix O- Absolute and Relative Errors for CC, CGE and OE for GB and RB

CC, CGE, OE	EXP %	MODEL % (With GE)	ABSOLUTE ERROR (EXP - MODEL)	RELATIVE ERROR ABS (EXP-MODEL)/EXP	MODEL % (Without GE)	ABSOLUTE ERROR (EXP -MODEL)	RELATIVE ERROR ABS (EXP-MODEL)/EXP
Test 1							
CC	87.4	83.4	4.0	0.04	--	--	--
CGE	77.3	79.4	-2.1	0.02	79.4	-2.1	0.02
OE	42.1	43.4	-1.3	0.03	43.4	-1.3	0.03
Test 2							
CC	83.5	81.7	1.8	0.02	--	--	--
CGE	70.5	71.80	-1.3	0.01	76.9	-6.4	0.09
OE	43.6	44.4	-0.8	0.01	47.6	-4.0	0.09
Test 3							
CC	90.9	81.5	9.4	0.10	--	--	--
CGE	69.2	73.7	-4.5	0.06	77.9	-8.7	0.12
OE	44.0	46.9	-2.9	0.06	49.6	-5.6	0.12
Test 4							
CC	93.9	87.8	6.1	0.06	--	--	--
CGE	61.0	75.9	-14.9	0.24	85.7	-24.7	0.40
OE	38.3	47.7	-9.4	0.24	53.8	-15.5	0.40
Test 5							
CC	89.4	91.5	-2.1	0.02	--	--	--
CGE	49.9	51.9	-2.0	0.04	84.5	-34.6	0.69
OE	30.0	31.3	-1.3	0.04	50.9	-20.9	0.69
Test 6							
CC	89.0	82.0	7.0	0.08	--	--	--
CGE	56.1	58.6	-2.5	0.04	74.8	-18.7	0.33
OE	34.2	35.7	-1.5	0.04	45.6	-11.4	0.33
Test 7							
CC	88.3	71.8	16.5	0.18	--	--	--
CGE	46.6	59.5	-12.9	0.27	86.1	-39.5	0.85
OE	27.8	35.4	-7.6	0.27	51.2	-23.4	0.84
Test 8							
CC	84.8	78.7	6.1	0.07	--	--	--
CGE	54.5	69.7	-15.2	0.27	92.4	-37.9	0.69
OE	31.6	40.2	-8.6	0.27	53.4	-21.8	0.68

Appendix P- Sensitivity Analysis Results (SB*)

Steam Flowrate (kg.hr)	SB*	CO (VOL %)	CO$_2$ (VOL %)	H$_2$ (VOL %)	CH$_4$ (VOL %)	N$_2$ (VOL %)	H$_2$O (VOL %)	TARS (VOL %)	CC (%)	OE (%)	CO/CO$_2$	H$_2$/CO	CH$_4$/H$_2$	TEMP (°C)
3.6	0.51	28.51	28.62	31.96	10.91	54.98	15.09	0.034	61.43	42.54	0.996	1.121	0.342	842.18
4.6	0.63	28.25	27.99	33.34	10.42	53.44	17.66	0.033	65.41	45.06	1.009	1.180	0.313	842.83
5.6	0.76	28.06	27.46	34.47	10.02	52.11	20.09	0.033	69.02	47.31	1.022	1.228	0.291	843.43
6.6	0.88	27.92	27.00	35.40	9.67	50.95	22.39	0.032	72.31	49.37	1.034	1.268	0.273	843.98
7.6	1.01	27.82	26.62	36.19	9.38	49.93	24.56	0.031	75.33	51.27	1.045	1.301	0.259	844.48
8.6	1.13	27.73	26.28	36.86	9.13	49.02	26.62	0.031	78.12	53.03	1.055	1.329	0.248	844.95
9.6	1.26	27.67	25.98	37.44	8.91	48.21	28.56	0.030	80.70	54.65	1.065	1.353	0.238	845.38
10.6	1.38	27.62	25.71	37.94	8.72	47.48	30.41	0.030	83.11	56.16	1.074	1.374	0.230	845.78
11.6	1.51	27.58	25.48	38.39	8.55	46.83	32.16	0.029	85.35	57.57	1.083	1.392	0.223	846.15
12.6	1.63	27.55	25.26	38.78	8.40	46.22	33.83	0.029	87.45	58.88	1.091	1.407	0.217	846.50
13.6	1.76	27.53	25.07	39.13	8.27	45.67	35.41	0.029	89.43	60.15	1.098	1.421	0.211	846.83
14.6	1.88	27.52	24.89	39.44	8.15	45.17	36.92	0.028	91.28	61.32	1.105	1.434	0.207	847.13
15	1.93	27.51	24.82	39.56	8.10	44.98	37.50	0.028	92.00	61.77	1.108	1.438	0.205	847.25

Appendix Q- Sensitivity Analysis Results (Secondary Air)

Secondary Air (kg/hr)	λ_{total}	CO	CO2	H2	CH4	N2	H2O	TARS	CC	OE	CO/CO2	H2/CO	CH4/H2	TEMP
		(vol %)	(vol %)	(vol %)	(vol %)	(vol %)	(vol %)	(vol %)	(%)	(%)				°C
0	0.04	31.52	17.52	38.86	12.10	35.11	29.31	0.146	77.474	62.150	1.80	1.23	0.31	842.93
1	0.06	31.89	18.03	37.99	12.09	37.20	29.06	0.048	77.149	61.932	1.77	1.19	0.32	843.23
2	0.08	30.65	19.72	37.65	11.98	39.22	28.65	0.037	77.348	60.629	1.55	1.23	0.32	843.53
3	0.11	29.68	21.19	37.46	11.67	41.10	28.30	0.036	77.574	59.314	1.40	1.26	0.31	843.81
4	0.13	29.00	22.42	37.33	11.25	42.85	27.99	0.035	77.778	58.102	1.29	1.29	0.30	844.08
5	0.15	28.52	23.50	37.23	10.75	44.49	27.71	0.034	77.977	56.847	1.21	1.31	0.29	844.34
6	0.17	28.17	24.47	37.15	10.21	46.03	27.46	0.033	78.185	55.673	1.15	1.32	0.27	844.58
7	0.19	27.91	25.36	37.07	9.65	47.48	27.23	0.032	78.407	54.496	1.10	1.33	0.26	844.81
8	0.21	27.72	26.22	36.98	9.09	48.85	27.01	0.031	78.652	53.361	1.06	1.33	0.25	845.04
9	0.24	27.57	27.03	36.88	8.51	50.15	26.81	0.030	78.921	52.240	1.02	1.34	0.23	845.25
10	0.26	27.45	27.83	36.77	7.95	51.38	26.62	0.029	79.214	51.141	0.99	1.34	0.22	845.46
11	0.28	27.36	28.61	36.64	7.39	52.55	26.44	0.028	79.535	50.058	0.96	1.34	0.20	845.66
12	0.30	27.28	29.39	36.49	6.84	53.67	26.27	0.027	79.881	48.994	0.93	1.34	0.19	845.85
13	0.32	27.20	30.17	36.33	6.30	54.73	26.11	0.026	80.255	47.938	0.90	1.34	0.17	846.03
14	0.34	27.13	30.94	36.15	5.78	55.75	25.95	0.026	80.657	46.905	0.88	1.33	0.16	846.21
15	0.37	27.06	31.72	35.95	5.26	56.71	25.80	0.025	81.086	45.861	0.85	1.33	0.15	846.38
16	0.39	26.99	32.50	35.74	4.77	57.64	25.65	0.024	81.542	44.844	0.83	1.32	0.13	846.55
17	0.41	26.91	33.30	35.50	4.29	58.53	25.50	0.024	82.028	43.834	0.81	1.32	0.12	846.70
18	0.43	26.82	34.10	35.25	3.83	59.38	25.36	0.023	82.542	42.835	0.79	1.31	0.11	846.86
19	0.45	26.73	34.92	34.97	3.38	60.20	25.22	0.023	83.088	41.852	0.77	1.31	0.10	847.01
20	0.47	26.62	35.75	34.68	2.95	60.99	25.09	0.022	83.665	40.875	0.74	1.30	0.09	847.15
21	0.50	26.50	36.60	34.36	2.55	61.74	24.96	0.021	84.276	39.915	0.72	1.30	0.07	847.29
22	0.52	26.36	37.46	34.02	2.16	62.47	24.82	0.021	84.921	38.966	0.70	1.29	0.06	847.43

Appendix R- Sensitivity Analysis Results (Primary Air)

Primary Air Flowrate (kg/hr)	λ	CO (vol %)	CO₂ (vol %)	H₂ (vol %)	CH₄ (vol %)	N₂ (vol %)	H₂O (vol %)	TARS (vol %)	CC (%)	OE (%)	CO/CO₂	H₂/CO	CH₄/H₂	TEMP OF PRODUCT GAS (°C)
1.9	0.041	27.72	26.22	36.98	9.09	48.85	27.01	0.031	78.65	53.36	1.06	1.33	0.25	845.04
2.9	0.063	27.57	27.11	36.56	8.76	50.14	26.76	0.030	79.53	52.53	1.02	1.33	0.24	845.25
3.9	0.084	27.29	28.12	35.95	8.64	51.26	26.36	0.029	81.21	52.09	0.97	1.32	0.24	845.44
4.9	0.106	26.99	29.13	35.32	8.55	52.30	25.95	0.028	83.04	51.73	0.93	1.31	0.24	845.63
5.9	0.128	26.69	30.14	34.70	8.47	53.27	25.55	0.027	84.89	51.38	0.89	1.30	0.24	845.82
6.9	0.149	26.38	31.13	34.10	8.39	54.19	25.16	0.027	86.75	51.04	0.85	1.29	0.25	845.99
7.9	0.171	26.08	32.11	33.51	8.30	55.06	24.78	0.026	88.61	50.70	0.81	1.29	0.25	846.16
8.9	0.192	25.77	33.07	32.94	8.21	55.88	24.42	0.025	90.48	50.37	0.78	1.28	0.25	846.33
9.9	0.214	25.47	34.03	32.39	8.12	56.66	24.06	0.025	92.35	50.03	0.75	1.27	0.25	846.49
10.9	0.236	25.17	34.96	31.84	8.03	57.40	23.72	0.024	94.23	49.70	0.72	1.27	0.25	846.64
11.9	0.257	24.87	35.88	31.32	7.93	58.10	23.39	0.023	96.10	49.37	0.69	1.26	0.25	846.79
12.9	0.279	24.57	36.79	30.80	7.84	58.77	23.07	0.023	97.98	49.05	0.67	1.25	0.25	846.94
13.9	0.301	24.28	37.69	30.30	7.74	59.41	22.76	0.022	99.86	48.72	0.64	1.25	0.26	847.08
14.9	0.322	23.64	39.22	29.34	7.80	60.49	22.84	0.022	100.00	47.26	0.60	1.24	0.27	847.22
15.9	0.344	22.95	40.86	28.32	7.87	61.57	22.95	0.022	100.00	45.69	0.56	1.23	0.28	847.36
16.9	0.365	22.24	42.53	27.28	7.94	62.62	23.06	0.021	100.00	44.14	0.52	1.23	0.29	847.50
17.9	0.387	21.51	44.26	26.22	8.01	63.64	23.16	0.021	100.00	42.59	0.49	1.22	0.31	847.63
18.9	0.409	20.75	46.03	25.14	8.08	64.64	23.25	0.021	100.00	41.02	0.45	1.21	0.32	847.76
19.9	0.430	19.97	47.85	24.03	8.15	65.61	23.34	0.021	100.00	39.47	0.42	1.20	0.34	847.88
20.9	0.452	19.16	49.73	22.89	8.22	66.54	23.43	0.020	100.00	37.92	0.39	1.19	0.36	848.00
21.9	0.474	18.33	51.66	21.73	8.28	67.46	23.51	0.020	100.00	36.36	0.35	1.19	0.38	848.12
22	0.476	18.24	51.86	21.61	8.29	67.55	23.52	0.020	100.00	36.21	0.35	1.18	0.38	848.13

Appendix S- Mass Balance for Test 8

Table 8: Mass Balance at the burners and mass balance of biomass + gasifying agent + N₂ purge = product gas output +char

Input Mass Flowrate (kg/hr)		Output Mass Flowrate (kg/hr)	
C-80 burner		C-80 burner	
Methane	1.57	Methane	0.00
O_2	6.40	O_2	0.12
N_2	21.08	N_2	21.08
Air ($O_2 + N_2$)	27.48	CO_2	4.32
		H_2O	3.53
Total	29.05	Total	29.05
C-100 burner		C-100 burner	
Methane	2.63	Methane	0.00
O_2	10.66	O_2	0.21
N_2	35.12	N_2	35.12
Air ($O_2 + N_2$)	45.79	CO_2	7.19
		H_2O	5.89
Total	48.41	Total	48.41
Biomass		Biomass	
RB	8.00	RB	0.00
Agent		Gas + Tar + Char	
Steam	8.80	CO	4.10
N_2 purge	6.55	CO_2	6.10
O_2 Air 1	0.44	CH_4	0.77
N_2 Air 1	1.46	H_2	0.39
O_2 Air 2	1.86	N_2	14.14
N_2 Air 2	6.14	H_2O	6.91
Total	25.25	NH_3	0.01
		Benzene	0.02
		Phenol	0.00
		Naphthalene	0.00
		Char	0.77
		Ash	0.04
Total (Biomass + Agent)	33.25	Total	33.25